University of Glasgow

Use of Synthetic mRNA Transfection Encoding Telomerase to Improve the *In-Vitro* Lifespan of Dental Pulp Stem Cells.

Fatoumata Kinteh BSc, PGD

Submitted in fulfilment of the requirements for the Degree of Master of Science by Research (MScR) in Biochemistry and Biotechnology.

School of Medicine, Dentistry and Nursing, College of Medical, Veterinary & Life Sciences

University of Glasgow.

October 2024

1 ABSTRACT

Dental pulp stem cells (DPSCs), like most stem cells, have the potential to be used in regenerative medicine. However, one of the limitations to the usage of DPSCs is their inability to maintain a long term, *in-vitro* lifespan due to replicative senescence. A key contributing factor to this senescence is telomere erosion.

Our research aimed to generate and use a synthetic messenger RNA (mRNA) encoding the human telomerase, a key protein responsible for telomere maintenance. mRNA was chosen instead of reprogramming cells using DNA constructs as the latter carries the risk of unwanted genomic integrations. Successes with the highly effective COVID-19 vaccines and other RNA drugs, such as small interfering RNA (siRNA) drugs, has driven substantial improvements in RNA delivery technologies and greatly increased the potential of mRNA approaches.

After correcting a mutation found in the telomerase mRNA sequence, we synthesised telomerase mRNA from the corrected plasmid using CleanCapAG™ to add cap1 structure to the 5' end, substituting the normal uridine triphosphate (UTP) with the N1-methylpseudouridine triphosphate and polyadenylating the final product. We used eGFP-encoding mRNA made the same way as a transfection control. We showed that both DPSCs and a control cancer cell line, TR146, could be transfected with enhanced green fluorescent protein (eGFP) mRNA at high efficiency with a simple procedure and an inexpensive commercially available RNA transfection reagent.

Telomere lengths (TL) in DPSCs (both wild type and transfected) were quantified as a relative measurement using the quantitative polymerase chain reaction (q-PCR) method originally designed by Richard Cawthon and later modified by O'Callaghan and Fenech. We found that, indeed, telomere erosion occurs in DPSCs as the cells age by increasing passage numbers. However, DPSCs with shorter telomere lengths transfected with the telomerase mRNA showed no sign of telomere extension.

In contrast, TR146 cancer cells which had shorter telomeres than DPSCs had their telomeres significantly extended after transfection with the same synthetic

telomerase mRNA indicating the mRNA was functional. It is possible that the synthetic telomerase mRNA is not translated in DPSCs, and Western blot evaluation is needed to test this. Initial experiments suggested other genes required for telomere extension were transcribed in DPSCs. However further works is also needed to test if these are expressed strongly enough.

Keywords: DPSCs, synthetic mRNA, telomeres, telomerase, q-PCR

2 TABLE OF CONTENTS

3 TABLES

4 FIGURES

5 ACCOMPANYING MATERIAL

Appendices

a) PCR Oligonucleotides (Primers).
b) q-PCR Oligonucleotides (Standards and Primers).
c) PCR (cDNA) Oligonucleotides.
d) Composition of Buffers and Reagents.

6 ACKNOWLEGEMENT

This Thesis would not have been possible without the invaluable and selfless efforts of my Supervisors Dr Andrew Hamilton and Dr Jean Quinn. I would like to extend my unwavering appreciation to them for all the support. Andy thank you for not only being an outstanding supervisor but for being an amazing teacher and for believing in me. You have been supportive, understanding, patient and motivative. I had learned so much from you, your mentorship, invaluable insights, and direction will go a long way in paving the way for any future research I will be undertaking.

I would like to express my sincere appreciation to Professor Andrea Sheriff, Convener Glasgow Dental School for her immense support during my Programme, and to all the Staff and students of the GDHS, who in one way or the other contributed to the success of this degree and making the GDHS a wonderful environment for learning and research.

I would like to acknowledge the invaluable support of my amazing colleague and Lab partner, Othman Baradhwan, for his support and involvement in providing me with the DPSCs used in this research, and Dr Jennifer Malcolm GDHS for the TR146 cells. I am grateful to Mrs Janette McBride, administrator SOMDN for her support and friendship, Mrs Zayneb Makki for the help and counsel amidst all the challenges. I wish to express my sincere gratitude to Dr Tomoko Iwata and all the support staff of the SOMDN for their immense help and support. I wish to thank my friend and former work colleague Bubacarr JB Touray, University of Wisconsin-Madison, for his support and contributions during the research.

I am indebted to my parents and siblings for their constant encouragement and unwavering support all through the Programme.

Finally, to my other half ML Drammeh and my daughter Labeeqa Mbia, you made this Thesis unique. Labeeqa, thank you for accompanying me all through the journey, from the libraries, parks, and to all the meetings with Andrew. ML Drammeh, thank you for being patient and understanding. I dedicate this to you.

7 AUTHOR'S DECLARATION

I declare that the work described in this Thesis under the title, **"Use of Synthetic mRNA Transfection Encoding Telomerase to Improve the *In-Vitro* Lifespan of Human Dental Pulp Stem Cells"**, embodies an authentic and original record of my work under the supervision of Dr Andrew Hamilton, unless otherwise acknowledged or cited.

I further declare that this Thesis has not been submitted by me or any known person as work forming part of a Thesis presented for any other degree at the University of Glasgow or any other Institution.

Fatoumata Kinteh

8 ABBREVIATIONS

ARCA	Anti-reverse cap analogs
ATP	Adenosine triphosphate
bp	Base pairs
BSA	Bovine serum albumin
BGH	Bovine growth hormone
BMSC	Bone marrow stromal cell
cDNA	Complementary DNA
CIB	Clustered isolation buffer
CIB-S	Clustered isolation buffer - without sucrose
CTP	Cytidine triphosphate
diF	Deionised formamide
DKC	Dyskeratosis congenita
DMEM	Dulbecco's modified eagle's medium
dNTPs	Deoxynucleotide triphosphates
DPSCs	Dental pulp stem cells
dsRNA	Double stranded RNA
EDTA	Ethylenediaminetetraacetic acid
EdU	Ethynyl deoxyuridine
eIF	Eukaryotic translational initiation factor
ESCs	Embryonic stem cells
FISH	Fluorescence *in-situ* hybridisation
gDNA	Genomic DNA
GOI	Gene of interest

GTP	Guanosine triphosphate
HF	High fidelity
HKG	Housekeeping gene
hTERC	Human telomerase non-coding RNA component
hTERT	Human telomerase reverse transcriptase
IL	Interleukin
IFN	Interferons
IVT	*In-vitro* transcription
kb	Kilobases
LNA	Locked nucleic acid
LNP	Lipid nanoparticles
MDA-5	Melanoma differentiated associated-5
miRNA	Micro RNA
MSCs	Mesenchymal stem cells
NAD	Nicotinamide adenine dinucleotide
NLS	Nuclear localisation signal
nts	Nucleotides
ORF	Open reading frame
PBS	Phosphate buffered saline
PKR	RNA-dependent protein kinase
q-PCR	Quantitative polymerase chain reaction
RT	Room temperature
RBP	RNA binding protein
RIG1	Retinoic-acid Inducible Gene 1

RT-PCR	Reverse transcription PCR
SCG	Single copy gene
SCs	Stem cells
snRNA	Small nuclear RNA
snoRNA	Small nucleolar RNA
STELA	Single telomere length analysis
TBE	Tris-borate EDTA
TFX	Transfection
TL	Telomere length
TLR	Toll like receptors
tRNA	Transfer RNA
TRF	Telomere restriction fragment
UTP	Uridine triphosphate
UTR	Untranslated region

9 INTRODUCTION

9.1 Background History

DNA transfection has been a highly effective tool in the biological engineering of cells to alter the expression of genes (BasiouniFuhrmann and Schumann, 2012). This method had been used for years to express proteins in mammalian cells, and more recently for SARS COV2 vaccines (Barajas Galindo et al., 2022), by the introduction of a foreign DNA. However, at the same time, there have been concerns raised especially over the viral-based vectors used for introducing foreign DNA into cells about integration or causing adverse effects on the host genome despite their effectiveness (Martinez-Negro et al., 2018): What if this transfection method causes an irreversible mutation or unwanted consequences such as the activation of oncogenes, which may lead to the development of cancerous cells or insertion mutagenesis leading to the expression of altered proteins with negative effects for patients? Studies conducted following the trials of treating X linked severe combined immunodeficiency (X1-SCID) mice with the conventional gamma retroviral vectors resulted in the occurrence of acute lymphoblastic leukaemia in patients (Hacein-Bey-Abina et al., 2003, Howe et al., 2008). This malignancy development years after the gene therapy treatment was believed to be related to insertional mutagenesis of the retrovirus amongst other factors.

However, DNA is not the only nucleic acid that may be used in the transfection of mammalian cells or in the formulation of vaccines and drugs. Recently, synthetic messenger RNA (mRNA) was found to be a highly effective way of engineering expression of SARS-CoV2 proteins for immunisation (Mulligan et al., 2021, Patel et al., 2022). mRNA had been described in the early 1950s as an important pillar in the passing down of genetic information. Crick initially described the key role of mRNA in the flow of genetic information in his writing “Central dogma of Molecular Biology” (Kim, 2022). mRNA transfection does not result in genome disruption, but it was not until recently that mRNA was used as a valuable tool in biological engineering and gene expression, and its recent approval (2020 – 2021) to be used in the formulation of emergency vaccines. Why has this other nucleic acid not been used until recently? We will begin with a brief review of natural mRNA

synthesis and structure, to provide a better understanding of the various components of mRNA and its function, before discussing use of synthetic mRNA in general and for this project.

9.2 Normal Generation of mRNA from Transcription, Translation and Degradation

DNA does not directly encode proteins. Instead, mRNA carries the genetic code from DNA via transcription into the cytosol, where it is translated into proteins with the help of other RNAs such as the ribosomal RNA (rRNA) and transfer RNA (tRNA), at the protein synthesis sites which are the ribosomes (Lemonnier and Lemonnier, 2023). Catalytic enzymes called RNA polymerases are responsible for DNA transcription to form phosphodiester bonds which link the ribonucleotides together in a single chain to generate RNA (Henderson et al., 2021). The reaction is extended one nucleotide at a time from the 5' to the 3' direction off a single strand DNA template unwound from the DNA of the gene. The nucleotides (nts) in a single strand DNA are matched with incoming nts to produce a complementary nucleotide sequence of the RNA, hence copying the genetic code. RNA nts are made up of the four major bases (Adenine, Guanine, Cytosine and Uracil). However, there are a number of post-transcriptional modified nts present in natural RNA template (Helm, 2006), such as the N6-methyladenosine (Chan et al., 2024), 5-methylcytosine and pseudouridine (PetushkovEsyunina and Kulbachinskiy, 2023). These modifications play a part in the biology of RNA and its synthesis.

The RNA polymerase must recognise the part of the genome, where transcription will be initiated. The transcription initiation step is a vital step as it determines which, and how much, protein will be synthesised. In general, each mRNA encodes the synthesis of a single protein unless where alternative splicing occurs then it may synthesise several closely related proteins. The polymerase binds firmly to a promoter DNA to open the double helix, thereby exposing a short segment of single strand DNA for transcription to occur. The step does not require the adenosine triphosphate (ATP) energy for hydrolysis, due to the reversible structural changes that both the polymerase and the DNA undergo, which results into a formation of

an energetically stable state to support the reaction (MurakamiMasuda and Darst, 2002).

The RNA synthesis continues until the polymerase II (Pol II) is eventually released from the DNA template by the 5'-3' exonuclease Xrn2 in the nucleus (Jia and Qian, 2021). In what is referred to as the "torpedo" model of termination, cleavage of the nascent transcript occurs at AATAAA site also referred to as the Poly-A site, providing a 5' phosphate-entry point for the 5'-3' exonucleases that tracks down the nascent transcript "chasing" down the RNA Pol(II), catching it up and displacing it from the DNA template thus ending transcription (Cortazar et al., 2019, Lai et al., 2020, Eaton et al., 2020). This well supported model also implies that 3' untranslated regions (UTRs) are not actually "transcription terminator" sequences *per se,* even though they are often described as such on plasmid maps. Rather, these non-coding parts of an mRNA contain sequences required for initial cleavage and subsequent polyadenylation of the mRNA (Mischo and Proudfoot, 2013). 3'UTRs usually also have multiple docking sites for a range of *trans*-acting factors that generally serve to limit translation, such as micro-RNA (miRNA) and RNA binding proteins (RBP).

In most eukaryotic cells, during or after the transcription of mRNA by RNA Pol (II), the pre-mRNA undergoes three special processes: the 5' end capping, the RNA splicing to remove introns and finally the 3' cleavage and polyadenylation, after which the mature mRNA molecule is exported to the cytosol to be translated into the specific protein or similar proteins. We will review each of these as they are important considerations when designing effective synthetic mRNA.

9.2.1 Capping

During transcription, RNA Pol (II) products are capped with the addition of a methylated guanosine cap structure on the 5' terminus, which is linked through a 5' to 5' triphosphate bridge to the first transcribed nucleotide (Galloway and Cowling, 2019). This mRNA cap protects the pre-mRNA from decay and plays a crucial role in the cap dependent protein synthesis (i.e. stability and translational efficiency of the mRNA). In addition to its key role in the translation, it also protects from 5'-3' exonuclease cleavage of the mRNA and in recruiting proteins for pre-mRNA splicing, polyadenylation, and nuclear exports (RamanathanRobb

and Chan, 2016). The cap in mRNA is quite functional throughout the entire activities of the mRNA.

Several types of natural mRNA capping structures exist, but the predominant one is the 7-methylguanosine cap (CapG/m7G). The capping is catalysed co-transcriptionally by a few reactions and enzymes (triphosphatase, guanylyl transferase, and methyl transferase) (Lenasi and Barboric, 2013). The cap binds to cap-binding complexes and other ribosomal proteins, and can only be removed by specialised decapping enzymes. Thus, it protects the mRNA from 5'-3' cellular exonucleases which require a 5' terminal phosphate (Warminski et al., 2023) and hence, leading to premature degradation (Wojcik et al., 2021). Many capped mRNA have a methyl group on the N-7 position of the G terminal residue. Additionally, there is usually 2'-O-methylation on the ribose of the first transcribed nts which provides the basis for the nomenclature: The m^7GpppN (Cap 0), m^7GpppNm (Cap 1) and the m^7GpppNmpNm (Cap 2) (Furuichi, 2015). These important modifications are introduced co-transcriptionally in nature and can be included in structure of cap analogues used to make synthetic mRNA (https://www.trilinkbiotech.com/gmp-reagents). The 2'-O-methylation in synthetic mRNA enhances translational efficiency and prevents the activation of retinoic-acid inducible gene 1 (RIG1) and melanoma differentiated associated-5 (MDA-5) sensors that causes innate immune responses (Kim et al., 2021).

9.2.2 Splicing

RNA splicing is a very vital process, allows for the removal of introns in two ways, either alternative or constitutive splicing (van den HoogenhofPinto and Creemers, 2016). This particularly important post-transcriptional process allows for joining of exons together in diverse ways, to allow mRNA transcripts to express many different proteins (Rachez et al., 2021). The spliceosome, made up of proteins and small nuclear RNAs, assembles on the pre-mRNA to perform the splicing. When making synthetic mRNA, one cannot just transcribe genomic DNA because the splicing process cannot easily be done *in-vitro,* but the process is easily bypassed by using complementary DNA (cDNA) copies of properly spliced mRNA as templates for *in vitro* transcription. The figure below (***Figure 1***) shows the synthesis of mRNA from transcription to post transcription modifications (e.g. splicing).

Figure 1: mRNA processing from DNA showing the different processing and parts

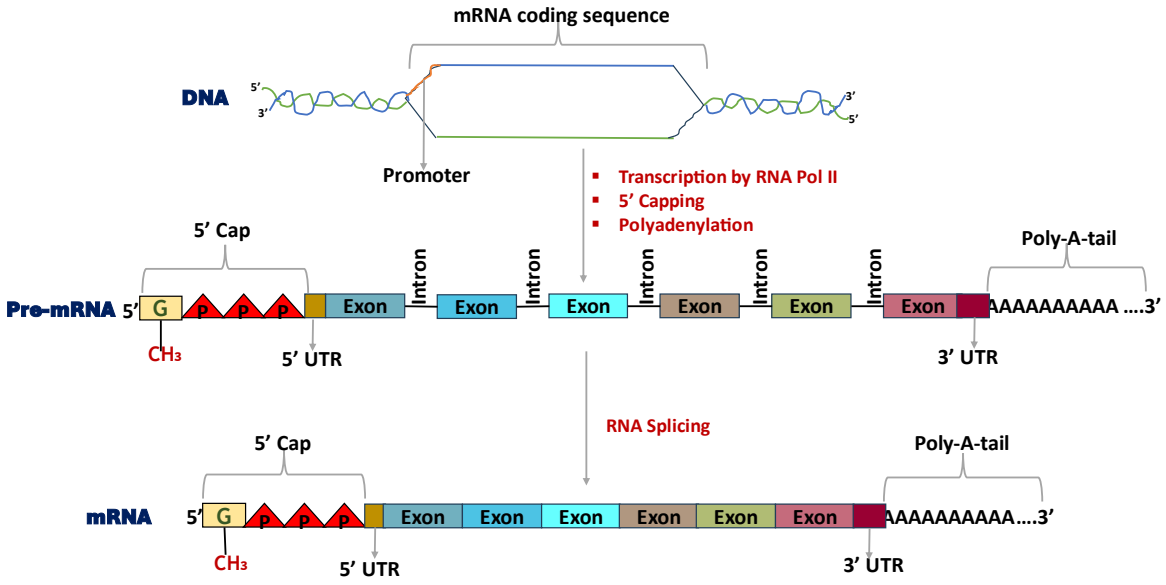

Fig 1: syntheses of mRNA from DNA showing the various processes from transcription to post transcription modification. The process shown in this figure is a representation of mRNA synthesis.

9.2.3 Polyadenylation

The polyadenylated tail is another key component of mRNA, added at the end of the 3' UTR it also plays a vital role in protein synthesis. The length of the poly-A tail usually varies between 20-250 nucleotides (nts), and, generally, the longer the length of the Poly-A tail, the more stable the mRNA (protecting it from degradation). Poly-A tail binds to proteins called the polyadenosyl-binding proteins, which interact with the N-terminus of eukaryotic initiation factor 4G (eIF4G), and then a further interaction with the 5'cap and eukaryotic translation initiation factor 2α (eIF2α). These interactions result in the formation of a closed loop mRNA structure (MazumderSeshadri and Fox, 2003), thereby increasing the stability by protecting it from nuclease degradation and increasing the translation efficiency by reutilising ribosomes (Oh and Kessler, 2018).

9.2.4 mRNA Degradation

A vital post-translational activity worth mentioning is the degradation of mRNA. Once the cell no longer needs expression of the mRNA, the mRNA is degraded in granular structures referred to as P-bodies in the cytoplasm (Braun and Young, 2014). This process first involves the deadenylation of the 3' end to remove the

poly-A tails and the 5’ cap end is also decapped which normally protects the mRNA from the exonucleases. This allows for the 3’ – 5’ exonucleases or the 5’ – 3’ exonucleases respectively to degrade the mRNA. This process can be triggered by interaction with *trans*-acting factors such as miRNA.

9.2.5 mRNA Feature that Affects its Translation

All mRNA processes from transcription to mRNA degradation are highly regulated resulting in individual mRNA levels that vary enormously within and between cells. This is important because the level of mRNA is a major factor for how much protein is produced. Additionally, *cis*-acting mRNA regions (e.g., the 3’ untranslated region) and *trans*-acting factors (e.g., miRNA), affect how much an mRNA is translated. These will be discussed further below in the context of synthetic mRNA. Key features that affect the regulation and stability of mRNA includes RNA sequence, secondary structures, structure, and length of the transcripts, and as well as trans-acting factors.

9.2.5.1 Sequence

The translation is initiated at the 5’ cap. The 5’ UTR allows the access of the 40S ribosome along with Met-tRNA and set of initiation factors moving linearly towards the first AUG codon (Kozak, 1991). The 5’ UTR may either facilitate or inhibit translation initiation when being traversed by the pre-initiation complex as it scans it towards the initiation site, but the rules are not clear. The sequence around the first AUG codon also affects translation (Kozak, 2002). Weak Kozak sequences or strong Kozak sequences form unique functional groups with differentially regulated translation in cells (Acevedo et al., 2018). For optimal translation, GCC**R**CCAUGG (**R** = A/G) is the best context of AUG initiation for a cultured mammalian cell, and for maximum translational effects the most preferable is a purine, with A at -3 and G at +4 (Kozak, 1991).

Another crucial factor in modulating translation and elongation rates is codon usage, which varies between individual mRNAs (Presnyak et al., 2015). Apart from methionine and tryptophan, a single amino acid is encoded by multiple synonymous codons due to degeneracy in genetic code, resulting in codon optimality which favours common codons (optimal for gene expression) to rare codons (sub-optimal for gene expression) in a gene. Codon frequency depends on

the abundance of the corresponding tRNA in a cell and codon favouritism in the transcriptome (codon bias) (Hanson and Coller, 2018). Codon usage is positively related to mRNA stability and associated to the regulation and degradation of mRNA (Harigaya and Parker, 2016). Different organisms have different codon preferences which then affects how mRNAs are expressed outside of their native organism.

9.2.5.2 Secondary Structures

mRNA folds on itself to form multiple hairpin structures and other sophisticated structures giving rise to secondary and tertiary structures in mRNA (Gaspar et al., 2013), and these secondary structures play a vital role in protein synthesis. Secondary structures are considered essential for the function of coding mRNA in relation to stability (LiaoDong and Somero, 2021), regulation, translation, elongation rates, and degradation (Del Campo et al., 2015). Secondary structures are also known for their roles in the function of non-coding RNAs, which includes small nuclear RNA (snRNA) (especially the U6 snRNA that plays a key role in mRNA spliceosome assembly) (Wassarman and Steitz, 1993, Dunn and Rader, 2010), tRNA (which requires a specific folding to enable its function), miRNA (key player in the variation of translational processes) (Hasler and Meister, 2016) and small nucleolar RNA (snoRNA) that plays a primary role in post transcriptional modifications, and directs chemical changes in rRNA (WajahatBracken and Orang, 2021). Notably, the presence of secondary structures located in the UTRs affects the translational efficiency and output of some mRNA (Song et al., 2016).

9.2.5.3 Transcript Structure

The mRNA structural design also regulates the translation and degradation. ***Figure 2*** is a cartoon representation of a mature mRNA showing the various parts of the body and their functions. A capped mRNA provides stability and promotes translation, whereas uncapped mRNA triggers innate immune responses by the activation toll-like receptors (TLRs) and production of interferons (Smietanski et al., 2014). 5’ and 3’ untranslated regions are non-coding regions that do not directly take part in the translation process, but strongly influence levels of translation (LytleYario and Steitz, 2007). The role of the 5’ UTR is quite crucial and important for translation efficiency, as it contains the site for the binding of

the preinitiation complex (Asrani et al., 2018). In mammalian eukaryotic mRNAs, the 5' UTR is usually short with a length of 53-218 nts (LeppekDas and Barna, 2018) (the longest being in humans, ≈218 nts), compared to 3'UTR which can be quite long in mammals (about 700 nts in mouse and 1100 nts in human) and subjected to lots of variation in length, which can affect translation of the mRNA. The variations in the 3' UTR length in most transcripts is generated by the usage of the different polyadenylation sites (Li et al., 2023). In principle, the general relationship between the length of 3' UTR and mRNA stability and translation is inversely related (Matoulkova et al., 2012). A wide range of the human genome is known to have alternative polyadenylation sites within the 3' UTR (Algama et al., 2014), which results into alternative docking sites for *cis*-acting (example AU rich elements) and *trans*-acting (example RBP) regulatory elements (Matoulkova et al., 2012).

Figure 2: Structure of the mature mRNA showing the different parts of the body and their functions

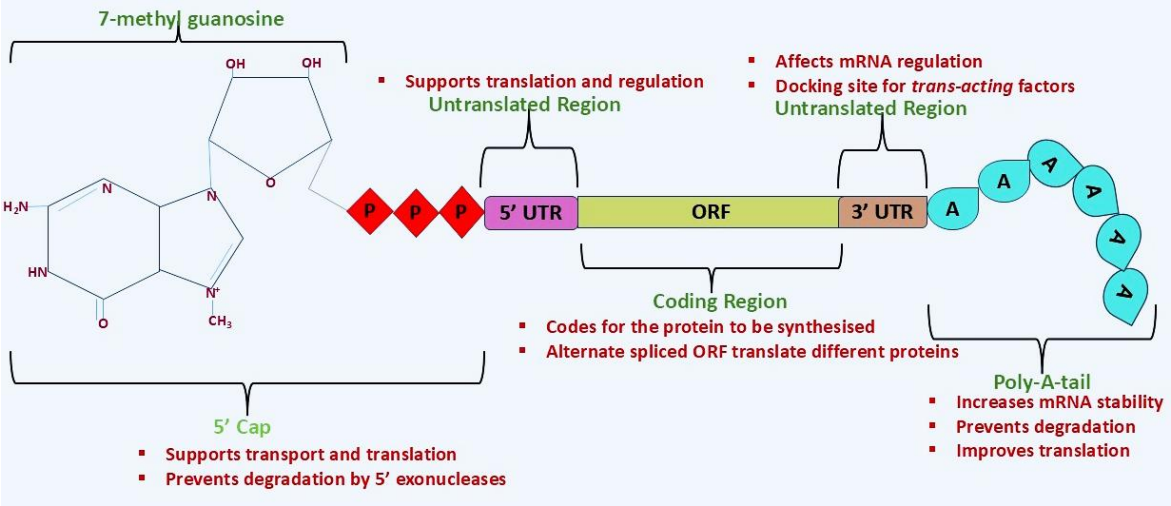

Fig 2: structure of a mature mRNA body showing the different parts and the functions of each part of the mRNA.

9.2.5.4 *Trans*-acting Factors

Alterations in mRNA expression are highly likely to occur during translation or post-translation in relation to the 3' untranslated region. miRNAs and RNA binding proteins usually target the 3' UTR leading to variations in the translation process. They infrequently appear within the 5' UTR and the open reading frame (ORF) and they are less effective in these regions (LytleYario and Steitz, 2007). This is likely

due to the binding of the ribosome that displaces these *trans*-acting factors out of the way from the 5' end all the way to the stop codon, and its disengagement at the stop codon prevents any further displacement of those on the 3' UTR. The presence of these *trans*-acting factors such as miRNA binding sites within the 3' UTR, results in changed functions, localisation, stability, and translation efficiency of the mRNA (Berkovits and Mayr, 2015, Feng et al., 2018). Effects of different 3' UTR can be studied e.g., by fusing these downstream of mRNA encoding reporter proteins, such as luciferase (Zhang et al., 2024) or green fluorescent protein (GFP).

9.3 Synthetic mRNA

9.3.1 Advantages of mRNA Transfection Over DNA

As already mentioned, transfection with DNA viral-based vectors involves, or at least risks, the genomic integration into the host (transfected) cell or insertional mutagenesis. With mRNA transfection on the other hand, only translation in the cytosol is involved. For this reason, there is no interference with the genetic material of the transfected cell. mRNA non-viral vector-based transfection of cells is not only safer as a protein expression technique, but it is also a simpler and faster technique than DNA based methods (Pardi et al., 2018). mRNA transfection also allows proteins to be produced in both mitotic and post-mitotic cells (Oh and Kessler, 2018). DNA transfection, which requires nucleus entry, takes place in mitotic (dividing) cells, since they have no nuclear membrane which allows the DNA nuclear access for transcription to take place. In post-mitotic cells, the chromosomes are now always bounded by a nuclear membrane, thus preventing the foreign DNA from entering the nucleus of the cell. Unlike, DNA transfection mRNA transfection does not require nucleus entry, thus making it also a good method to transfect non-dividing cells. An additional merit of mRNA over DNA, is its ability to achieve controlled expression of multiple proteins through the combination of multiple mRNA in distinct ratios (Kwon et al., 2018), with lesser risk of unintended edits, whereas this is technically exceedingly difficult to achieve with multigene DNA transgene constructs.

The success of the COVID-19 (Pfizer, Moderna) mRNA vaccines in the year 2020 are key examples of the efficacy of synthetic RNA in modern day biomedical science (Sahin et al., 2020). The success of these followed the less well-known examples of RNA drugs, such as patisiran, mipomersen, givoseran, which are based on small interfering RNA (siRNA). These have led to a huge interest in mRNA in the field of therapeutics as an agent with enormous potential for the development of vaccines, treatment of diseases through temporary genetic reprogramming enabled by mRNA drugs administered through intravenous and subcutaneous injections. But what caused the delay in the use of mRNA as biomedical tool and what could possibly have changed to allow researchers to utilize mRNA as an essential tool recently?

9.3.2 Structure of the Synthetic mRNA

Synthetic mRNA like endogenous (normal) mRNA is made up of the Cap, 5' UTR, Coding region, 3' UTR and the Poly-A tail. Co-transcriptional capping is the most common method of introducing a cap structure on synthetic mRNA, wherein developed dinucleotide cap analogues are used as capping reagents during *in-vitro* transcription (Ohno et al., 2023), but these methods have only recently been developed. The 5'-Cap can be optimised in synthetic mRNA by using the anti-reverse cap analogues (ARCAs), or the CleanCap™. ARCA is an old capping technology (compared to the CleanCap). mRNA capped with ARCA have a higher *in-vitro* translational property, as compared to the conventional *mCAP* (m^7Gp_3G) capped mRNAs (Grudzien-Nogalska et al., 2007, ShanmugasundaramSenthilvelan and Kore, 2022). But *in-vitro* measurements do not assess problems associated with activation of innate immune response. According to the Trilink company, ARCA has about 70% capping efficiency, with about 30% of the transcript containing a 5' phosphorylated end because the GTP in the transcription reaction (necessary for the transcription of the mRNA body) competes with ARCA for incorporation as the first nucleotide (Inagaki et al., 2023). These phosphorylated mRNA (uncapped mRNA) trigger the activation of immune responses in cells. Although they can be removed, the procedure is time consuming and exposes the mRNA to exonucleases. The new capping method (CleanCap) not only adds a Cap1 structure to the 5' ends of the mRNA but also has greater than 95% capping efficiency because when using this, the first transcribed nucleotide is A. ATP is

very poorly incorporated as the first nucleotide by T7 RNA polymerase, but the dinucleotide AG is very efficiently incorporated. CleanCap is an AG dinucleotide with a 5 – 5 link to the methylated G and is also very efficiently incorporated because the G stabilises the ternary transcription initiation complex. So, as long as the first two nts downstream of the T7 promoter are AG, the T7 incorporates CleanCap far more efficiently than incorporation of A as the first nucleotide leading to a very high proportion of properly capped transcripts relative to 5'-triphosphorylated RNAs.

9.3.3 Instability of Synthetic mRNA

Doubts about the stability of synthetic mRNA had led to a delay in its use in biological engineering. An unprotected single-stranded mRNA is highly unstable and is prone to nuclease degradation (Wang et al., 2021). The instability of mRNA is a result of the 2' hydroxyl group (Fang et al., 2023), one of the chemical structures which distinguish mRNA from the DNA structure. In mRNA, the single-stranded nature of the molecule made it quite easy for the 2' hydroxyl group to reach the phosphodiester backbone and make a cut to the chain and this is promoted by alkaline conditions and cations, such as Mg^{2+}. Double-stranded regions of RNAs (such as are found frequently in tRNA and rRNA) have higher stability, as compared to mRNA, due to the 2'hydroxyl groups being restricted (somewhat) from reaching the phosphates.

Even more important than this chemical instability is that mRNA is also very susceptible to degradation by ribonucleases (Mino and Takeuchi, 2021), which are a class of enzymes quite common in biological materials. This problem is made much worse by the fact that it is quite difficult to completely get rid of these ribonucleases. Moreover, the fact of the matter is that ribonucleases are very stable and robust enzymes that are used in a wide range of processes in molecular biology, for example in DNA or plasmid preparations. As a result, they are one of the most common surface contaminants in the laboratories and are quite active in variable conditions. Thus, doubts and challenges associated with handling unstable mRNA is a probable contribution to the limited exploration of its use as a cellular reprogramming tool.

Being a large and negatively charged molecule, mRNA cannot easily pass through the cellular membrane passively and so delivery methods involving lipid encapsulation have been developed to get it into the cytosol (KaczmarekKowalski and Anderson, 2017). It is extremely fortunate that these also turned out to protect the mRNA from nuclease degradation, and this has been critical for the use of synthetic mRNA in practical *in-vivo* applications. Although, the lipid encapsulation technology was pioneered for the *in-vivo* delivery of siRNA, it was rapidly and successfully repurposed and retargeted for longer RNA to combat COVID (Tenchov et al., 2021, Conte et al., 2023).

9.3.4 Lipid Encapsulation of mRNA

The major limitation in the broad application of mRNA in therapeutics is the intracellular delivery of the molecule (Kowalski et al., 2019). In facilitating the cellular entry of mRNA, delivery mechanisms are utilised and some of the methods (cationic lipid encapsulation) have the secondary, but vital property of being able to protect the RNA from being attacked by exonucleases.

Encapsulation of mRNA using lipid nanoparticle (LNP) is a widely used method (Balmayor, 2022), as it was the very first method used in delivering the nucleic acid as compared to the physical methods of delivery, such as electroporation, which is the most recent (Kim and Eberwine, 2010). A major drawback of electroporation is its inability to be used on a large area and difficulty to adapt to *in-vivo* (as it requires surgical intervention to enable transfer to internal organs) (Sokolowska and Blachnio-Zabielska, 2019). Lipid encapsulation allows for the negatively charged nucleic acid to be surrounded (encapsulated) by the positively charged cationic lipid forming a vesicle around the mRNA which floats within it and hence, forms a chemical complex that can actively pass through the cellular membrane. The lipid encapsulation of mRNA delivery method is not the most efficient, but it does have quite a lot of advantages as compared to the other methods. Importantly, the encapsulation of mRNA by lipid nanoparticles (LNPs) promotes the stability of the nucleic acid and protects it from ribonuclease digestion and immediate degradation, whereas in the case of electroporation, it only successfully delivers the naked mRNA and therefore, does not protect it from any form of degradation or ribonuclease digestion.

9.3.5 Immunogenicity of Synthetic mRNA

Another factor that delayed use of synthetic mRNA is its immunogenicity. Transfection of RNA into mammalian cell causes immune responses triggered by receptors such as the TLRs and MDA-5 that recognises foreign RNA (Drzeniek et al., 2024), and can sense the LNPs used for transfection. These trigger the inflammatory pathways responsible for the induction of the interleukin (IL) family which in turn trigger inflammatory cytokine production. In the context of using mRNA as vaccines, some responses can be advantageous e.g., adjuvant properties of LNPs are vital in antigen immune responses that causes reactogenicity of mRNA. It is relevant to note that my research is not to develop a vaccine, hence the positive immunogenicity of mRNA is not of any relevance to my work, which is to express telomerase in stem cells. However, the inhibition of protein translation or synthesis by the interferon pathway and the degradation by ribonucleases is relevant, as these would suppress the expression of the telomerase in the cells which will compromise the research. Hence, consideration must be made in the design of the mRNA to minimise the above problems. mRNA generated by the cell is recognised as self by the cell and does not trigger any immune responses, on the other hand, the introduced synthetic mRNA during transfection is recognised by receptors as non-self or as an invasion thereby triggering immune responses (Drzeniek et al., 2024). How are these mRNA perceived differently by the cell? It is partly because natural mRNA never transits through endosomes, where RNA receptors are, whereas uptake of encapsulated synthetic mRNA does. Synthetic mRNA (*in-vitro* transcribed mRNA) can activate receptors, such as the TLR3, 7 and 8, RIG1, and the RNA- dependent protein kinase (PKR). These TLRs that recognises synthetic mRNA are located in endosomes. TLR 3 recognises double stranded mRNA that transits through endosomes, while TLR 7 and 8 recognises U-rich or GU-rich single stranded mRNA (WilliamsSim and Wolin, 2025). RIG1, MDA-5 and PKR recognises synthetic mRNA because of the presence of; double stranded mRNA, residual triphosphates at their 5’ ends (i.e. uncapped mRNAs) and the absence of the 2’O-methylation of the 5’ cap structure or 5’ terminal nucleotide. Due to <100% efficiency of the 5’ capping during *in-vitro* transcription, these receptors can be activated, thus RIG1 and MDA-5 activates the expression of interferons (IFN-α and IFN-ß) encoded genes, which causes an immune response (Andreev et

al., 2016). The accidental formation of double stranded RNAs during *in-vitro* transcription (Cui et al., 2023), are also known to play a crucial part in the activation of interferons (IFN), thus shut down protein syntheses.

9.4 Dental Pulp Stem Cells (DPSCs)

Stem cells are one of the most important type of cells in biomedical engineering and regenerative medicine today. They are extensively used in therapeutics for various medical and beauty purposes. These cells are well known for their capability to develop and differentiate into several cell lineages (pluripotent), and they are also known to have clonogenic and self-renewing ability (Korbling and Estrov, 2003). Embryonic stem cells (ESCs) have been explored in great deal in the field of regenerative medicine, but their use is considered unethical by certain cultural groups and to avoid conflicting with these, they have not been widely used for clinical purpose. The controversy related to their usage is the destruction of embryos to source them. Among the clinical concerns and problems related to the clinical uses of ESCs, is that they can potentially cause tumours due their inherent capacity to proliferate rapidly and accumulate mutations and chromosomal aberrations in culture (Prentice, 2019). Unlike ESCs, adult stem cells do not have limitations due to ethical reasons as they can be isolated from adult patients from whom informed consent can be obtained. Autologous adult stem cells have a reduced risk of immunological rejection (Centeno et al., 2016, Centeno et al., 2018), and the risks associated with ESCs with regards to tumours forming is reduced in that of adult stem cells (Hombach-Klonisch et al., 2008).

Dental pulp stem cells (DPSCs) are adult mesenchymal-like stem cells (MSCs), and like many stem cells they are self-renewing with a high proliferation capability, lower immunogenicity, and the ability to differentiate into multilineage cells (Wang et al., 2022).

9.4.1 Characteristics of DPSCs (Origin, Niche and Heterogeneity)

Formation of tertiary mineralised matrix from odontoblast-like connecting tissues that protects the dental pulp following dentine damage either by mechanical or diseases like trauma, led Gronthos *et al* (2000) to speculate that the source of these cells might be the dental pulp cavity itself. The very first population of

DPSCs were then isolated and characterised from the pulp cavity of an adult molar teeth (Gronthos et al., 2000). They demonstrated that DPSCs share *in-vitro* similarities to bone marrow stromal cells (BMSCs) related to protein expression, however, DPSCs unlike BMSCs possess a significant ability in terms of proliferation and development.

DPSCs derived from the embryonic ectodermal layer are thought to originate from migrating neural crest cells during embryonic development (Thesleff and Aberg, 1999, Chai et al., 2000). Neural crest cells disperse and migrate through different regions of the embryo, differentiating into several cell lineages, including the mesenchyme of the head and the neck (Pisciotta et al., 2020). In the tooth, these stem cells form a connective tissue which is surrounded by the dentine, and its external layer comprised of the odontoblasts which produces an extracellular matrix which has a vital role in the growth of tissues, remodelling, and maintenance (Zhang et al., 2017). Gronthos *et al* (2000) demonstrated that DPSCs like mesenchymal cells exhibited a fibroblast-like morphology that adheres to plastic surfaces to form colonies.

They can be easily harvested from either shed teeth or extracted molars and premolars of adult patients, and are found in distinct niches of the pulp cavity. Expression of the various stem cell markers of DPSCs was used to localise the DPSC niches within the pulp cavity. Two (STRO-1+ and CD146+) subpopulations of heterogeneous DPSCs represent two populations in the vasculature, and STRO-1+ is also expressed in the neurosheath layer (Yu et al., 2015), i.e. non-vascular DPSC niches. Expression of OCT4 and CXCR4 according to Yu *et al*. (2015), also characterise the DPSC niche. Expression of OCT4 was detected in either vascular or non-vascular niches of human deciduous teeth, while the receptor for SDF-1, CXCR4 was strongly expressed in inflamed pulp in the non-vascular niche and weakly expressed in the blood vessel walls. The expression of these stem cell markers including ALDH1, which was expressed in isolated in DPSCs are indicative that DPSCs resides in the vicinity of perivascular blood vessel and nerve fibres (Machado et al., 2016). Recent studies in mouse models also suggest the existence of more than one distinct niche of stem cells in DPSCs (NagataOno and Ono, 2021). DPSCs niches within the pulp cavity, which is a sealed environment, potentially

housing several stem cells (Laino et al., 2006), could result in the inconsistent biochemical properties of isolated DPSCs because the microenvironment contributes to the heterogeneity of DPSCs.

There are no specific biomarkers available for DPSCs that distinguishes them from other adult stem cells, however, they express the following mesenchymal markers Stro-1, CD29, CD44, CD73, CD90, CD105, CD146, CD166, and CD271, hematopoietic markers CD34 and CD117, and stemness markers OCT4 and NANOG. It had been demonstrated that different DPSCs isolates do not all express all of these markers, and the ratio at which they express them differs (Kawashima, 2012).

DPSCs have been known to differentiate *in-vitro*, into cell lineages, such as odontoblast-like cells, myogenic, adipogenic, chrondogenic, osteogenic and neurogenic (Lei et al., 2014, Marrelli et al., 2018, Wang et al., 2022).

Gronthos et al. (2000) used enzymatic digestion method to isolate DPSCs from the pulp in their initial work. The dental pulp was digested with a collagenase, following which the cell suspension was then seeded into Dulbecco's modified eagle's medium (DMEM) supplemented with nutrients and additives such as fetal calf serum, L-glutamine, and penicillin streptomycin. Single cell suspensions were isolated by passing cells through a Falcon strainer. Post two weeks cell cultures were then fixed with formalin and then strained with 0.1% toluidine blue as means to assess colony forming efficiency. About 50 cells aggregates were then stored as colonies.

According to Gronthos et al. *(2002),* a very small population of DPSCs derived from a single colony proliferate extensively *in-vitro*, that is over 20 population doublings, while the majority (80%) of the colony have a lesser proliferation *in-vitro* (Nel et al., 2022). Hence, one of the postulates of Gronthos et al. is the existence of a hierarchy of progenitors in the adult pulp cavity, where only a minor fraction of DPSCs population are highly proliferative *in-vitro* and exhibit self-renewal and multipotent stem cell properties (Gronthos et al., 2002). Hence, stem cell populations in DPSCs are now identified to be heterogeneous population with variation in certain biological characteristics including telomere length, suggesting the presence of sub-populations within the stem cell pool with superior regenerative potential (Alraies et al., 2017). According to Alraies et al. (2017),

DPSCs that exhibit multipotency, high proliferative and self-renewal capabilities have longer telomeres ranging between 18 - 20 kilobase (kb), however, the length of telomere equivalent for low proliferative populations ranges between 5 – 13 kb. The low proliferative sub populations of DPSCs showed positive expression for CD271 (low affinity nerve growth factor) and senescence marker p53, p21 and p16.

Prolonged *in-vitro* expansion affects DPSCs biological properties. DPSCs with longer telomeres (approximately 20 kb) had their telomeres reduced to approximately 6 kb after 55 population doublings (Alraies et al., 2017). DPSCs population that exhibit osteogenic and chrondogenic differentiation capabilities was greatly reduced or impaired after several population doublings (Alraies et al., 2017, Alaidaroos et al., 2021). Senescent DPSCs cells also showed increased ß-galactosidase activity, and changes in the morphology of the cells: They were larger, flattened, multinucleated (stress fibres) and vacuolated (Alraies et al., 2017, de Farias et al., 2024).

DPSCs ability of high proliferation, self-renewal and differentiation into several cell lineages including odontoblast-like cells (Gronthos et al., 2002), showed that there is a great potential for its usage in regenerative dental therapies. In DPSCs sub-population, the superior colony-forming efficient DPSC population expressing high $CD90^{+}$, multilineage potential, low CD271, and enhanced *in-vivo* bone formation capabilities (Alraies et al., 2017), could be utilised for regenerative medicine. Another very important property of DPSCs is their ability to survive cryopreservation. DPSCs remain viable and proliferate efficiently after long-term uncontrolled cryopreservation in the -80 ℃ (Raik et al., 2020).

9.4.2 Limitations in DPSC Usage for Therapeutic Purposes

Recent pilot studies and phase (I) clinical trials in humans have been reported to demonstrate and support claims that transplantation of mobilised human DPSCs is a safe and efficient therapeutic approach (Orimoto et al., 2020) in the regeneration of damaged pulp and dentine in the root canal space. However, there are challenges faced with the clinical application of DPSCs.

One important limitation related to the clinical application of DPSCs is the inconsistent differentiation potential of DPSCs observed between *in-vitro* and *in-vivo* studies (Gronthos et al., 2002). Hence, discrepancies in the reported

differentiation potential and regenerative capacity of DPSCs between *ex-vivo* and *in-vivo* studies is a major challenge in the translation of research to clinical practice.

DPSCs are only present in very low density in the pulp (Pilbauerova et al., 2021b), thus, the number of cells required for regenerative clinical procedures becomes limited. The expansion of these cells *in-vitro* to meet the required amount needed for therapeutics is limited as DPSCs become senescent and loses their differentiation potential following several population doublings. Like all MSCs, DPSCs have limited proliferative capacity both *in-vivo* and *in-vitro*, due to cellular senescence, thus limiting their biomedical applications. Cell replicative senescence and aging in *in-vitro* human cells are associated with several factors, the activation of accelerated telomere erosion, increased levels of reactive oxidation species that causes an increased level of oxidative DNA damage, mitochondrial dysfunction, and the increased levels of expressed cell cycle regulators such as cytokine dependent kinase (Aan et al., 2013, Haj et al., 2023). The other key factors and activities that promotes cellular senescence is the activation of the growth promoting mammalian target of rapamycin pathways (Antonioli et al., 2019). Due to the limited duration of this project, the work presented here will focus on only one of these factors: Telomeres.

9.5 Telomerase and Telomeres

Telomeres are heterochromatic structures that protect the end of chromosomes formed by short repeatable (TTAGGG) DNA and are bounded by specialised proteins (shelterins) (Trybek et al., 2020). The shelterin complex (see ***Figure 3***) binds to telomeres by forming a loop (T-loop). This T-loop prevents chromosomal end to end fusion and degradation (Li et al., 2021). Telomere lengths (TL) shorten during cell replication due to the end replication problem. During duplication, DNA polymerase is unable to fully replicate the lagging strand (3’ end of the linear chromosomes), removal of RNA primers that provides the OH groups for addition of dNTPS by the DNA polymerase causing shortening of the synthesized DNA as compared to the other template strand (Bar and Blasco, 2016). Hence, as cell division continues, the TL progressively shorten, and this is the hallmark for cell

aging (Tedone et al., 2019), and results in limiting the maximum number of cell division.

In continuously proliferating cells, such as immortal ESCs and in many human cancer cells, this telomere erosion problem is solved by the expression of the enzyme telomerase (hTERT), which is a reverse transcriptase enzyme that uses an RNA template (the non-coding RNA TERC), to synthesise short TTAGG repeats that are added to the ends of chromosomes. This extends TL in cells and as a result solves the end replication problem during cell division. Thus, cells that express this enzyme have an extended lifespan. Telomeres are susceptible to oxidative damage due to being guanine rich structures (Remot et al., 2022).

When telomeres reach a critical length, they become dysfunctional, and cells lose their proliferating capacity, this results in cellular replicative senescence or a permanent replication arrest (Cheng et al., 2013). However, continual overexpression of this protein may cause the cell to be tumorigenic in certain cases. Previous studies show that the human telomerase reverse transcriptase (hTERT) plays a vital role in tumorigenesis, cell growth, and migration (Vahidi and Samadani, 2021).

Most healthy adult human stem cells are known to have their telomeres between 7–13 kb, while cancer cells maintain their TL between 2–6 kb (Kelland, 2005). The TL in cancer cells is critically short (dysfunctional) but evades the checkpoint for apoptosis. Tumour cells evade apoptosis through several ways including but not limited to: defect in apoptotic pathways, by upregulating anti-apoptotic proteins such as Bcl-2 family, downregulation of pro-apoptotic proteins (Bax, Caspase-8), and activation of proteins (NF-κB) that interferes with apoptosis signalling (Debatin and Krammer, 2004, Fulda, 2013). hTERT activity was found to be absent in most normal human somatic cells, but present in more than 90% of cancerous cells and other *in-vitro* immortalised cells (Zhu et al., 2008) despite the short telomere length. Presumably, the rapid division rate of cancer cells and consequent telomere erosion is too much to be fully compensated by increased telomerase expression.

Human healthy chromosomes of somatic cells have TL between 10–15 kb, and TL is reduced by 20–50 bp after every cell replication cycle (BarnesFouquerel and

Opresko, 2019). Replicative senescence occurs when telomeres are critically shortened, and dependent on *p53* and retinoblastoma as part of DNA damaged response pathways (Nassour et al., 2023). However, the exact mechanism by which extensively shortened telomeres trigger induction of DNA damaged sensing machineries and activation of immune signalling pathways required for cell death remains unclear.

TERT activity is dependent on a non-coding RNA, hTERC, and other telomerase activity associated proteins (see ***Figure 3***). Examples of which includes but not limited to the following, TEP1, NHP2, NOP10, Dyskerin, GAR1, WRAP53, TCAB1 (Nagpal et al., 2020). Some of these proteins interact with the hTERC to enhance the stability of the RNA. The catalytic subunit, hTERT, interacts independently with the non-coding RNA, hTERC which is thought to be constitutively expressed in most cells. The interaction between these two major subunits has been identified in hTERT activity (Nishio et al., 2007).

Figure 3: Structure of the telomerase and shelterin complex at the end of chromosomes

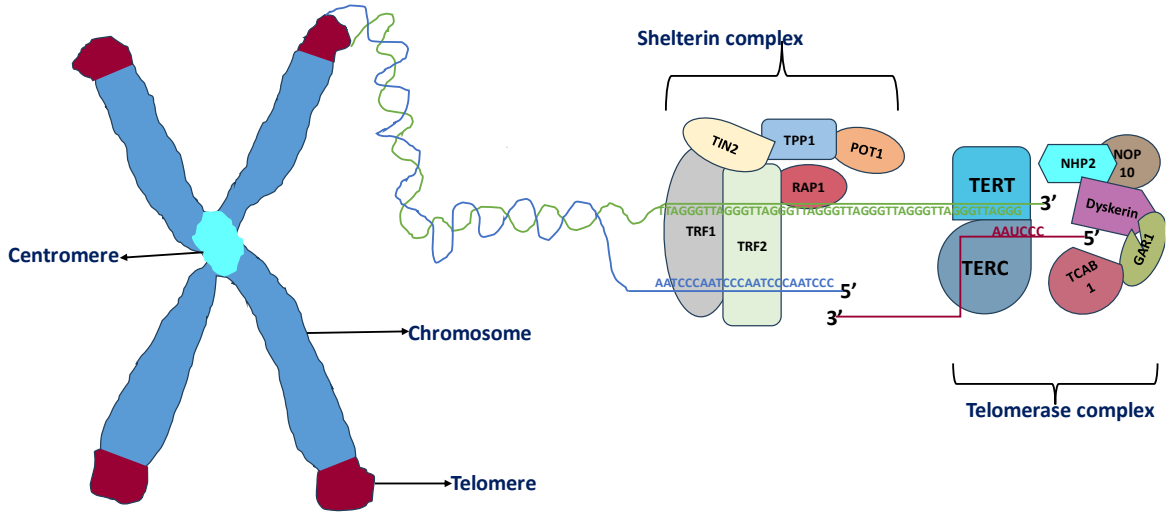

Fig 3: structure of a chromosome highlighting the ends of the chromosome to show the shelterin complex and the telomere complex. The various genes that make up the complexes are shown in the figure above. The TERC (telomerase RNA component) serves as a template to synthesise the complementary strand.

DPSCs have been successfully immortalised in previous studies by introducing mutant genes that create a chromosomal condition necessary for the expression of cell cycle regulators, and the immortalised cells were not tumorigenic but in

fact were able to differentiate into several functional tissues including neurons, as well as osteogenic and adipogenic differentiations (Wilson et al., 2015, Orimoto et al., 2020). Orimoto et al. had reported their success in the efficient immortalization of several species of cells including DPSCs by the co-expression of three genes, namely the R24C mutant cyclin-dependent kinase 4, cyclin D1 and TERT. Their results showed that successful immortalised cells show no changes in cell morphology and no indication of cellular senescence. However, they were also certain that the expression of the individual genes alone is not sufficient to immortalise the DPSCs and that only a combined expression of the K4DT genes could achieve the said immortalization. In a clinical setting, immortalisation is usually undesirable. Rather, a stimulation of proliferation to achieve sufficient cell numbers followed by quiescence or differentiation is desirable. Orimoto et al. used retroviral plasmids (transduction), which as well as carrying the risk of unwanted genome disruption (discussed above) makes it difficult to stop expression. In contrast, synthetic mRNA is intrinsically self-limited as it is not renewed and has a finite cellular lifespan. Our initial question was whether we could achieve hTERT expression and extension of telomeres while using the synthetic mRNA on DPSCs. The first step to achieving this focused on mRNA encoding the human telomerase gene.

Why mRNA transfection encoding human telomerase gene? This is vital to test the importance of telomerase expression in the maintenance of proliferation and differentiation capacity of human DPSCs. If telomerase expression shows positive effects on the proliferation and or differentiation capabilities of DPSCs, then it could be part of an approach to make enough DPSCs that can differentiate into several cell lineages for clinical and biomedical uses.

It would be advantageous to extend the lifespan of DPSCs beyond what we have now. It is not clear how long telomerase needs to be expressed in DPSCs to maintain a long-term proliferation in these cells, however, continuous expression of telomerase could risk malignancy in cells. Thus, the self-limiting nature of synthetic mRNA expression is an advantage in a clinical setting. If conventional synthetic mRNA formulations provide insufficient mRNA lifespan, other

modifications such as formation of circular mRNA or other chemical modifications that resist exonuclease mRNA decay could be envisaged in the future.

Another alternative is to do multiple serial transfections of DPSCs with the telomerase mRNA. Human cells were efficiently reprogrammed using this method in the past: Somatic cells were reprogrammed to pluripotency (induced pluripotent stem cells) by sequentially transfecting the cells with modified mRNA (Warren et al., 2010). This method should be efficient and applicable to a wide range of human cell reprogramming using synthetic mRNA.

9.6 Considerations in Synthetic mRNA Design for this Project

Recent improvements in modifications in structure of synthetic mRNA have enhanced translatability and reduced immunogenicity. These include modified cap analogues, such as CleanCap™, that greatly decrease the proportion of uncapped transcripts and substituting the natural UTP with a modified N1-methyl pseudouridine triphosphate (PhuaLeong and Nair, 2013). The N1-methylpseudouridine triphosphate minimises immune responses by minimising the activation of endosomal TLRs that are responsible for the induction of innate immune receptors, such as cytokines and interferons, while improving and promoting gene expression (Wang et al., 2024) In synthetic mRNA, the modified nts are observed to have a positive effect on the overall expression of proteins as compared to non-modified nts. These nts, for example N1-methyl pseudouridine triphosphate, are thought to reduce the activation of immune response activities, such as the activation of PKR and phosphorylation of eIF2α (Svitkin et al., 2017, SvitkinGingras and Sonenberg, 2022), hence improving both translation and stability of the mRNA.

Therefore, modification of the various parts of the mRNA construct during its design is essential for its protection and of course stability. Thus, in the design of our synthetic mRNA, we will optimise the *in-vitro* transcription (IVT) of the mRNA construct by using the CleanCap AG™ to optimise the 5'-Cap, thereby increasing the capped mRNA and reducing the 5'-triphosphorylated mRNA produced. The CleanCap AG™ will be added co-transcriptionally to the 5' end of the RNA transcript (https://www.trilinkbiotech.com/gmp-reagents). An additional advantage of this cap structure is to prevent nonintentional immune responses

caused by the recognition of innate immune sensors of viral RNA (ChaudharyWeissman and Whitehead, 2021).

Codon optimality is vital, however, in the case of our design we will be using the hTERT plasmid therefore, it does not require any recoding since it is a human gene we are confident that most of its sequences should be optimal enough for the research. We will be optimising our mRNA by substituting the natural UTP with N1-methylpseudouridine triphosphate, this is intended to enhance stability and expression, and minimise the activation of PKR (Anderson et al., 2010) and TLRs in endosomes (Andries et al., 2015). Finally, we will polyadenylate the mRNA transcripts in a separate step using the yeast poly(A) polymerase, the interaction of the poly-A tail with *cis*-acting factors promotes mRNA stability (Torabi et al., 2021). The Lipofectamine MessengerMax™ will be used as the transfection reagent in this research, for the safe delivery of the mRNA into the cells and improved transfection efficiency.

9.7 TL Measurement

The methods used to measure telomere lengths are diverse. The selection of which method to use is dependent on a few factors including but not limited to the following: Sensitivity of the method, time, cost, and amount of the sample. In our study we aimed only to measure relative change in TL to see if expression of telomerase will make any difference. We will try these two methods listed below.

9.7.1 Fluorescence *In-Situ* Hybridisation (FISH)

Quantification of TL by FISH is a direct approach, which can be used to measure absolute length. Its advantage is that FISH does not require large amount of DNA sample to analyse TL or relative length of telomeres in cells. The use of confocal microscope with good resolution, individual telomeres can be measured but this was not readily available for this project and besides, only a relative measurement is necessary to test the effectiveness of telomerase mRNA expression. The method uses a specific telomere probe complementary to 8 units of the telomere repat to hybridise to the telomeres of intact chromosomes within immobilised (fixed) cells (Lansdorp et al., 1996). In principle, the total amount of fluorescence measured in any given cell is directly proportional to the sum of all TL within that cell and

so, total fluorescence can be used to compare different fixed cells (e.g. wild type DPSCs samples to telomerase mRNA transfected DPSCs sample). In practice however, variability of target access, probe penetration, fluorescence quenching and background fluorescence means that the method can have problems. The method is not sensitive for the measurement of TL in senescent cells due to background fluorescence which can be challenging for this project.

9.7.2 Quantitative Polymerase Chain Reaction (q-PCR)

q-PCR is a far more sensitive measurement than FISH because of the massive amplification signal from PCR. However, it usually looks at the whole populations of DNA rather than individual cells. Still, it can be used to measure absolute amounts of DNA or differences in amounts between DNA samples of cultured cells. Absolute quantifications need preparation of a standard curve of the same amplicon, but relative quantification does not. Relative quantification of telomere DNA by amplifying the telomeric DNA was originally designed by Richard Cawthon (2002). It uses a single copy gene (36B4) as its reference non telomeric gene (Cawthon, 2002) to control variation in DNA input amounts. Like FISH, q-PCR is suitable for small sample sizes.

PCR amplification of tandem repeats such as telomeres is quite challenging. Any primers that perfectly match the tandem repeats are inevitably at least partially complementary to each other resulting in the annealing of the two primers to each other instead of annealing to the template DNA. This results in poor DNA amplification of the target and strong accumulation of primer “dimers.” Cawthon et al. *(2002)* and O’Callaghan & French (2011) solved this problem for telomeres by designing forward and reverse PCR primers for these repeats with a base mismatch (to the telomere repeat sequence) on every sixth base (that is following every five bases) and the mismatch being different on the forward and reverse primers. This reduces the hybridisation of the two primers to each other. To compensate for the reduced complementarity to the telomere repeat, the primers are also much longer than conventional PCR primers which enhances the annealing of the primers to the target DNA template for efficient PCR (Cawthon, 2002, O'Callaghan and Fenech, 2011).

10 OBJECTIVES

The ultimate aim of the project is to express hTERT in DPSCs to try to increase the useful lifespan of this type of adult stem cell. Specific sub-aims were:

10.1 Create an *In-Vitro*-Transcribable DNA Template for Telomerase

The plasmid with the human TERT cDNA (phTERT-mRNA) will be used as a template for polymerase chain reaction (PCR). A proof-reading thermostable DNA polymerase Phusion and hTERT primers will be used to amplify the hTERT ORF, following which we will insert the hTERT sequence into a plasmid that has T7 promoter and a 3' UTR to create a DNA template for transcription.

10.2 Test if DPSCs can be Successfully and Efficiently Transfected to Express Synthetic mRNA

DPSCs will be transfected with *eGFP*-mRNA as a transfection control in developing an efficient assay using Lipofectamine MessengerMax™ as the transfection reagent. The successful assay will then be used in the transfection of DPSCs with the *hTERT*-mRNA.

10.3 Test Different Methods for Measuring TL in DPSC

We will test the different methods of measuring telomere levels in DPSCs. There are different methods of measuring the TL, such as the quantitative polymerase chain reaction method which has the advantage of using smaller amounts of DNA. An alternative method would be the use of quantitative fluorescence *in-situ* hybridisation with fluorescent telomere nucleic acid probes, which is a more direct approach.

10.4 Measure Natural Levels of Telomeres in DPSCs

We will measure the relative levels of telomeres in non-transfected DPSCs (wild types), to compare the natural levels between the different passage numbers, that is, between early passages and late passages. We will also compare those levels of telomeres to that of human cancer cell lines we have in the Hamilton labs.

10.5 Test Effect of Expression of Synthetic Telomerase mRNA on Length of Telomeres

We will use one of the methods for measuring TL in DPSCs to test the effect of expression of the synthetic mRNA. The comparison of the relative TL between the hTERT-mRNA transfected samples and a control (non-transfected samples), will give us an idea as to how efficient and translated the synthetic mRNA in DPSCs.

Figure 4: Flow chart illustrating design and steps involved in the research.

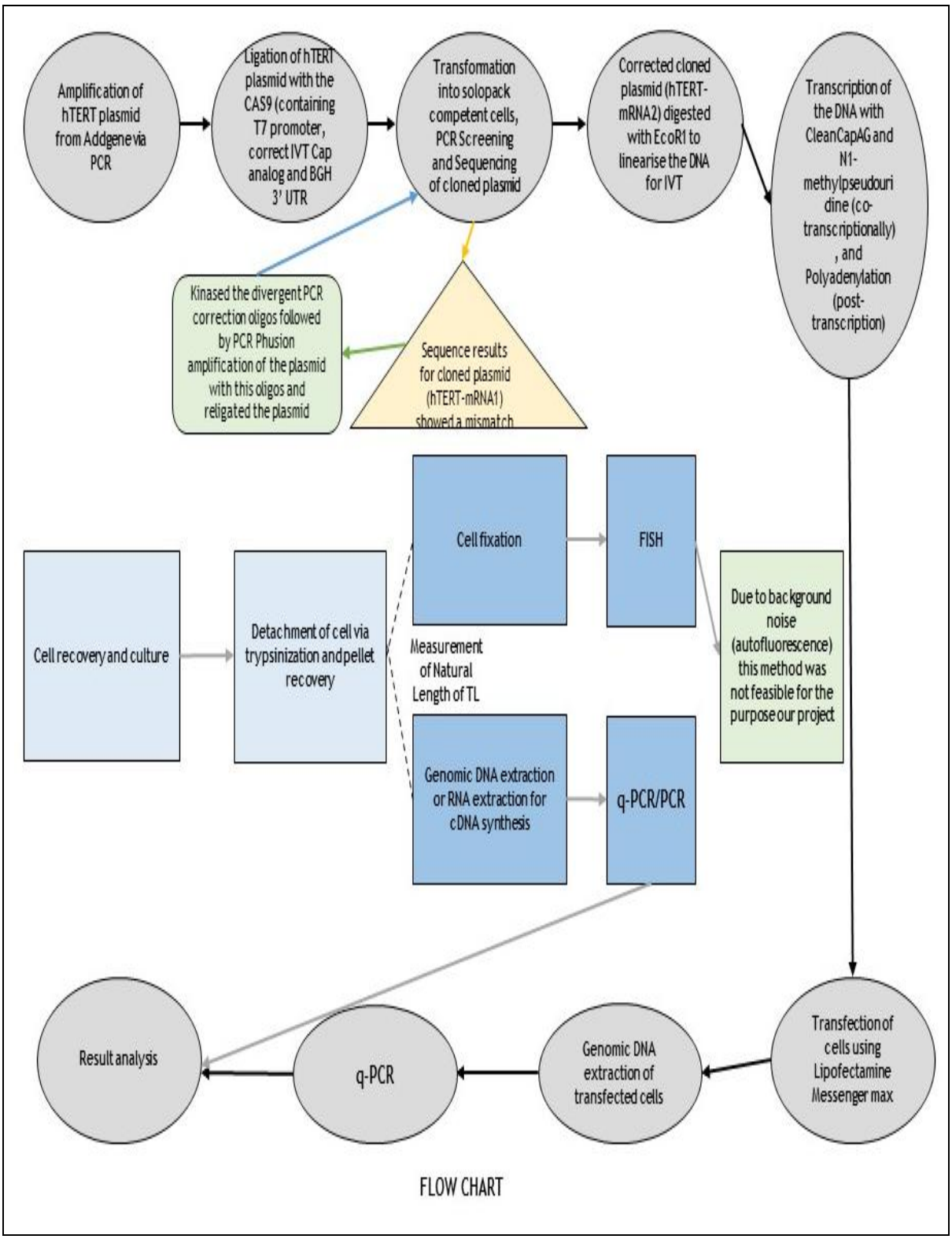

11 MATERIALS AND METHODS

All materials were supplied from Sigma-Aldrich/Merck unless stated otherwise.

11.1 Molecular Cloning.

11.1.1 *E. coli* Establishment and Growth

*E. coli (*Strain: "NEB Stable") obtained from Addgene as a stab culture was streaked on an LB agar plate containing 100 $\mu g.mL^{-1}$ ampicillin and incubated at 37 ℃ overnight to obtain distinct individual colonies. A single colony was picked and inoculated into 50 mL of LB broth with 100 $\mu g.mL^{-1}$ ampicillin in a conical flask and incubated in a shaking incubator at a speed of 180 rpm overnight at 37 ℃.

11.1.2 Plasmid Extraction and Quantification

Bacterial cells were pelleted by centrifugation at 5000 × g for 10 min at room temperature (RT). The plasmid was extracted using the Qiagen Column Midiprep Kit according to manufacturer's instructions (alkaline lysis, followed by ion exchange chromatography and isopropanol precipitation) and quantified for quantity and purity by UV spectrophotometry (freedom from other nucleic acid contamination), gauged by gel electrophoresis.

11.1.3 Gel Electrophoresis

DNA and RNA were routinely analysed for quality and quantity by agarose gel electrophoresis. Between 20–200 ng of the DNA or RNA (the latter in 50% deionised formamide) were mixed with ≥1/5 volume of 6 x loading dye and samples were separated by electrophoresis on 0.8%-2% (w/v) agarose gels in 0.5 × TBE buffer at 150 V for approximately 30 min. Size standards were the 1 kb Plus Ladder (Invitrogen/Thermo Fisher Scientific). DNA or RNA were then visualised by staining of the gel in a 1 $\mu g.mL^{-1}$ solution of ethidium bromide for 15 min and the fluorescence visualised on FUJI FLA-5000 Fluorescent Image Scanner at an excitation wavelength of 532 nm.

11.1.4 PCR Amplification of Plasmids with Phusion DNA Polymerase and Purification

A total volume of 100 µL was made for the PCR reaction prepared on ice, containing 20 µL of the 5× Phusion™ HF buffer (Thermo Fisher Scientific), 2 µL of 10 mM (each) dNTPs (NEB), 5 µL of 10 µM of both the forward and reverse primers (see ***Appendix A*** for sequences), 3 µL of DMSO, 1 µL (~0.4 ng) of 1000-fold diluted plasmid DNA template, 1 unit of Phusion™ high fidelity DNA polymerase (Thermo Fisher Scientific) and 63.5 µL of purified water. 30 cycles of PCR were run on a T3000 Thermocycler (Biometra) on the following program: denaturation for 10 s at 99.0 ℃, annealing for 10-15 s at 50.0-60.0 ℃, extension for 30-60 s at 72.0 ℃ for 30 cycles, and 5 min final extension reaction at 72.0 ℃. After completion, the amplified DNA was purified using the Purelink™ PCR Purification Kit (Thermo Fisher Scientific) as per the manufacturer's instruction and 5 µL of the sample was run on a gel to ascertain recovery.

11.1.5 Restriction Enzyme Digestion

DNA was digested with 10-20 units of enzyme in 1x of the enzyme manufacturer's buffer provided for at least 1 h at the appropriate temperature for that enzyme (37 ℃ or 55 ℃). Reactions were terminated by heating to 65 ℃ for 10 min to kill the enzyme. For sequential digestion with buffer-incompatible enzymes, the second digestion was carried out with the enzyme which required a higher salt concentration after the addition of the appropriate amount of supplemental sodium chloride.

11.1.6 Gel purification of DNA

After electrophoresis and staining, the gel was placed on a transilluminator, UV light switched on and, using a clean scalpel blade, bands corresponding to the DNA of interest were excised. DNA was purified from the gel slice using the Purelink Quick Gel Extraction Kit as per the manufacturer's instructions. Successful DNA isolation was verified by gel electrophoresis and DNA quantified by comparative UV fluorescence using known amounts of ladder DNA as reference quantities.

11.1.7 Ligation of Plasmid Vectors with Insert

DNA was ligated in a PCR tube containing 3:1 (molar ratio) inserts and vector DNA, respectively. 5-10 units of the T4 ligase enzyme was used per 10 µL reaction in 1×

ligase-manufacturer's buffer with 1 mM of ATP and incubation at RT (~18 ℃) for between 1-18 h.

11.1.8 Transformation of *E. coli* with Recombinant DNA

An aliquot of the Strataclone Solo Pack™ competent cells was thawed on ice and 2 µL of the DNA ligation was then added to the cells and gently mixed. The mixture was incubated on ice for about 20 min and then gently placed in a water bath at 42 ℃ for 45 s, to deliver a heat pulse before the addition of 42 ℃ preheated SOC medium. The mixture was incubated in the tube for an hour at 37 ℃ to allow expression of antibiotic resistance in transformed bacterial cells before being spread on a freshly prepared LB agar plate with appropriate antibiotics and incubated overnight at 37 ℃. All plasmids used encoded ampicillin resistance, so this was used at 100 µg.mL^{-1}.

11.1.9 PCR Screening of *E. coli* Colonies with GoTaq™ Master Mix

Colonies were labelled by writing directly underneath the colony on the petri dish, then selected from the incubated plate by separately touching with a clean pipette tip and then touching some of that transferred colony to the bottom of a PCR tube for screening. Sufficient master mix containing 200 nM of each PCR primer (see ***Appendix A*** for sequences) and 1 x GoTaq™ PCR mix (hot start formulation) for 20 µL per colony to be screened was prepared. To each tube containing the colonies, 20 µL of the prepared master mix was added and the PCR reaction was set. The PCR was run on a T3000 Thermocycler (Biometra) on the following program: a single initial cell lysis/Taq activation for 2 min at 99.0 ℃, followed by 30 cycles of denaturation for 10 s at 99.0 ℃, annealing for 10-15 s at 50.0-60.0 ℃, and extension for 30-60 s at 72.0 ℃. The samples were then run on a gel, stained, and imaged to determine if any recombinant-specific band had been amplified and the colonies that passed PCR screening were selected and inoculated in 5 mL LB broth containing 100 µg.mL^{-1} ampicillin and incubated overnight at 37 ℃.

11.1.10 Mini Prep Plasmid Extraction

This method used solutions P1, P2 and P3 from a Qiagen Plasmid Midi Kit but not the columns. The inoculated bacterial cultures were spun at 5000 × g at RT for 10 min and the supernatant was discarded. Pellets were resuspended in 400 µL of P1

buffer (containing RNase), and then 400 µL of the P2 lysis buffer was added and gently mixed by inversion (×3) within 5 min. Then 400 µL P3 buffer was added and vigorously mixed to form a precipitate. The mixture was then centrifuged at 5000 × g for 10 min at RT. The solution was removed avoiding any white precipitate at the bottom or floating on top, placed into a fresh tube and polyethylene glycol (MW ~8000) to a final concentration of 10% (w/v) added to the solution. The mixture was vortexed and placed on ice for 30 min to precipitate the plasmid before it was spun at ≈16000 x g for 20 min. The plasmid pellet obtained after discarding the supernatant was washed with 85% ethanol and re-spun at maximum speed for 1 min and supernatant was discarded, the pellet allowed to air dry and re-dissolved in 50 µL dH_2O then run on a gel to confirm recovery and quality.

11.1.11 Sanger Sequencing of phTERT-mRNA

Plasmid samples were sent to Eurofins Genomics for Sanger sequencing and results were obtained in multiple file formats including *.abi* files and, using Serial Cloner version 2.6.1, aligned with the electronically created sequence files of the desired recombinant to determine if cloning had worked.

11.2 *In-Vitro* Transcription of Synthetic mRNA

mRNA was synthesized from linearised plasmid templates generated by restriction enzyme digestion or PCR amplification and purified using ion exchange (Qiagen) or silica columns to ensure elimination of any contaminating proteins. A typical 20 µL reaction contained the following concentration of reagents added in the order shown: 1 × manufacturer's transcription buffer, 5 mM each nucleotide mix (ATP, cytidine triphosphate (CTP), guanosine triphosphate (GTP), and N1-methylpseudouridine triphosphate), 50 mM of magnesium acetate, 10 mM of CleanCap AG™, 5 mM of dithiothreitol (DTT), 20 units of RNase inhibitor, 600 ng-1 µg of DNA template and 80 Units T7 RNA Polymerase enzyme (Thermo Fisher Scientific). The reaction was incubated at 37 ℃ for about 3 h (until reaction turns cloudy; this is a precipitate of pyrophosphate and is a reliable indicator that substantial transcription has taken place). We then added 2 Units of RQ-DNase (Promega) and incubated again at 37 ℃ for another 15 min. RNA was then purified by two sequential precipitations in 2 M lithium chloride each at -20 ℃ for an 1 h

to eliminate any double-stranded RNA followed by extraction with phenol/chloroform and precipitation with 0.3 mM sodium acetate and an equal volume of isopropanol, washing with 70% ethanol and redissolving the RNA pellet in sterile water.

1 µL of the *in-vitro* transcribed mRNA before the polyadenylation was collected and saved up to be used as a non-polyadenylated reference control, the rest of the mRNA was then polyadenylated with 6 units of yeast poly-A polymerase in a 1 × E- pap buffer supplied by the manufacturer (Thermo Fisher Scientific), 1 mM of ATP, and 2.5 mM of manganese (II) chloride and incubated at 37 ℃ for 20 min. The RNA was columned purified using a Purelink™ PCR Column Purification Kit as per manufacturer's instruction (choosing buffer B2), and then mixed with an equal volume of deionised formamide, heated to 60 ℃ and run on a gel alongside the non-polyadenylated control to check the polyadenylation had worked.

This purified, polyadenylated mRNA was quantified by UV spectrophotometry and stored as aliquots of 10 µL in the -80 ℃.

Additional notes: Plasmid templates must (as for e.g. the phTERT-mRNA2) have the transcription initiation nts immediately downstream of the T7 promoter configured correctly to allow incorporation of the CleanCapAG™ cap analogue. CleanCap AG™ was used to ensure a high proportion of the transcripts had a Cap1 structure at the 5 'end and minimal 5'triphosphate. N1-methylpseudouridine triphosphate was used in place of UTP to minimise activation of TLRs in endosomes.

11.3 Cell Culture

The human DPSCs were obtained (via another student in this laboratory, (Othman Baradhwan) from Lonza, Cambridge UK (PT-5025), who recommended a seeding density of 5000-6000 cells/cm^2, i.e. between 125000-150000 cells per T25 flask.

These cells were cultured in Knockout DMEM™ (Invitrogen/Thermo Fisher Scientific), supplemented with 10% (v/v) heat inactivated foetal bovine serum (Invitrogen/Thermo Fisher Scientific), 1% (v/v) penicillin-streptomycin solution (Invitrogen/Thermo Fisher Scientific), and 2 mM L-glutamine at 37 ℃ in 5% CO_2 –

95% air. The medium in the flask was changed twice a week. The cells were passaged and sub-cultured by trypsinization (see below), at 90% confluency which was typically 10-14 days after initial seeding.

11.3.1 Initial Seeding of DPSCs

The frozen cells in cryovials (~1×10^6 cells/mL) from different passage numbers were thawed out on a water bath set at 37 ℃, for not more than 2 min. The ethanol/isopropanol cleaned cryovials, were opened in a sterile cell culture hood and cell suspensions were transferred into a sterile universal tube and approximately 10 mL of fresh media was added. The cells were then centrifuged at 300 × g for 5 min at RT, before being resuspended in fresh growth media, and then evenly distributed in three separate T25 flask and then we add appropriate volumes of media to each flask to a total volume of 5 mL.

11.3.2 Subculture or Passage of DPSCs

Cells were sub-cultured or passaged at a cell confluency of ≥90% for each flask. In a sterile field, we aspirated and discarded the media from the flask, washed off remaining media in the flask with sterile Phosphate Buffered Saline (PBS, Gibco). Cells were detached with 0.25–0.5 % w/v trypsin-EDTA. Successfully detachment of cells was monitored using an inverted brightfield microscope and trypsin was then neutralised by adding 6 mL of fresh media. The cells were then transferred into a sterile 15 mL centrifuge tube, centrifuged at 300 × g for 5 min at RT, and the pellets washed in sterile PBS, centrifuged again at 300 × g for 5 min at RT. Cell pellets were either resuspended in fresh media and seeded into a new flask or in cell recovery medium in cryovials for storage.

TR146 cells and C2C12 cells were obtained from ATCC via Dr Andrew Hamilton and Dr Jennifer Malcolm (Oral Science, School of Medicine, Dentistry and Nursing, Glasgow University) and cultured in DMEM™ (Invitrogen/Thermo Fisher Scientific) with 4500 mg/L glucose, sodium pyruvate and sodium bicarbonate, supplemented with 10% (v/v) non-heat inactivated foetal bovine serum (Invitrogen/Thermo Fisher Scientific), 1% (v/v) penicillin-streptomycin solution (Invitrogen/Thermo Fisher Scientific), and 2 mM L-glutamine at 37 ℃ in 5% CO_2 – 95% air.

11.4 Methods of Measuring TL

11.4.1 Fluorescence *In-Situ* Hybridisation (FISH)

Cell fixing: Cells (C2C12 or DPSC) were detached from the flask/plate via trypsinization and washed with PBS and centrifuged at 1000 × g for 3 min at RT, using clean Eppendorf tubes. Cell pellets were resuspended in 1 mL of CIB buffer (10 mM HEPES/potassium hydroxide, pH 7.5), 10 mM sodium chloride, 5 mM magnesium chloride and 300 mM sucrose) and then bovine serum albumen (BSA, to mitigate clumping of cells), Triton X-100 (to permeabilise cells) and EDTA (to remove cytoplasmic RNA, and swell nuclei) were added to 0.1% w/v, 0.1% v/v and 15 mM, respectively. The suspension was gently mixed and incubated on ice for 5 min and centrifuged at 1000 × g for 3 min at 4 ℃. Supernatant was aspirated and discarded, and the pellet of nuclei taken up in 1 mL of CIB-S (10 mM HEPES/potassium hydroxide pH 7.5), 10 mM sodium chloride, and 5 Mm magnesium chloride) containing 0.1% BSA and fixed by addition of 1/10 volume of freshly prepared 40% (w/v) formaldehyde (see ***Appendix D*** for sequences) at RT for 15 min. The fixed nuclei were spun down at 1000 × g for 3 min at RT, the supernatant discarded, pellet washed in water, resuspended in an appropriate volume of PBS, and stored at 4 ℃ until use.

FISH: On a clean microscope slide, about 2 µL of the fixed nuclei were dropped within hydrophobic barrier circles drawn with an Immedge™ pen and spun down at 1000 × g for a few seconds to flatten nuclei. 0.1 µM Telomere ×5 cy3 probe in FISH buffer (see ***Appendix D*** for sequences), was added on to the dried cells and the slide was set on a PCR block and the following programme carried out: 99 ℃ for 10 min, then to 45 ℃ for 30 min at a temperature change rate of 0.10 ℃ per s. This hybridisation solution was washed off with PBS at 45 ℃, DAPi (0.1 µg.mL^{-1} in PBS) stained for 5 min, and examined microscopically using Olympus IX51 Inverted Fluorescence Microscope with Olympus U-LH100HG Light source and Retiga R1 CCD camera, 40X objective lens (Olympus Japan, aperture 0.6 with adjustable focus ring). Images were taken with excitation filter Olympus U-MNV2 for DAPI fluorescence in blue (excitation 360-370 nm, emission 420 nm) and Olympus Fluorescence narrow red for Cy3 fluorophore (Olympus Japan, U-MN1GA3) excitation 540-550 nm / emission 575-625 nm using Micromanager Open-source Image capture software. Images were opened and colourised in ImageJ

(with FIJI release plug-ins) and scale bars calculated based on known size of full-sized images for each lens. Comparable images have the same exposure times, and brightness or contrast settings consistency unless otherwise stated in the legends.

11.4.2 Quantitative Polymerase Chain Reaction (q-PCR)

Genomic DNA (gDNA) extraction: Detached cells via trypsinization were resuspended in 200 µL of PBS and gDNA was extracted using the Purelink™ Genomic DNA Mini Kit as per manufacturer's instructions. The gDNA in 50 µL elution buffer was quantified using the Nanodrop 1000 Spectrophotometer and examined by gel electrophoresis to ascertain recovery and purification quality, and stored at -20 ℃ until use.

Oligomers (PCR Primers and Standards): The oligomers used for the q-PCR were the telomere forward and reverse primers, Cawthon Telomere forward and reverse primers, 36B4 forward and reverse primers, TEL standard, and the 36B4 standards (see ***Appendix B*** for sequences). 10 µM concentration of all the oligonucleotides were prepared using ultrapure water and stored at -20 ℃. All primers and standards for telomere q-PCR were HPLC purified.

q-PCR: All samples were run on an AB Step-One Plus Real-Time PCR System, version 2.3. Sufficient Master Mix solution was prepared (see ***Table 1***) for samples, standards, and no template control (NTC) to be run in triplicate with an additional 3% for pipetting errors, mixed and centrifuged briefly.

Table 1: Representation of master mix solution preparation

Reagents	Volume (µL) for one sample	Final Concentration
2× SyGreen Hi-ROX	10 µL	1×
Forward Primer (10µM)	0.2 µL	0.1 µM
Reverse Primer (10µM)	0.2 µL	0.1 µM
H_2O	4.6 µL	

In a 96 well plate, 15 µL of the Master Mix solution was added to 5 µL of each sample DNA/standard/NTC (≥20 ng total DNA), sealed the plates with flat

MicroAmp© 8-cap strip and centrifuged briefly at 1200 rpm at 4 ℃, and stored at 4 ℃ if not used immediately.

Cycling conditions used were: 10 min at 95 ℃, followed by 40 cycles of 95 ℃ for 15 s, 60 ℃ for 1 min, and then a melt curve.

Analysis: The analyses of the results were done using the $\Delta\Delta C_T$ method (Livak Method, (Livak and Schmittgen, 2001)), to compare the relative fold change between samples, this is similar to Cawthon's T/S (Telomere / Single copy) method with slight modification (Cawthon, 2002).

T/S ratio (T/S of one sample relative to another sample) = $2^{-(\Delta Ct_1 - \Delta Ct_2)} = 2^{-\Delta\Delta Ct}$, where $\Delta Ct = Ct_{\text{telomere}} - Ct_{\text{single copy gene}}$.

11.5 Transfection of Cultured DPSCs or TR146 Cells

Cells were plated at a density between 3-5 × 10^4 cells/well and at a confluency of 50–70%, before they were transfected with eGFP-mRNA and the hTERT-mRNA in Lipofectamine™ MessengerMax™.

The Lipofectamine™ MessengerMax™ (Thermo Fisher Scientific) transfection reagent was diluted in Optimem (Gibco/Thermo Fisher Scientific) serum-free medium at a 6% (v/v) concentration 10 min before mixing with mRNA (also diluted in Optimem, but only immediately prior to mixing with diluted transfection reagent). Cells were transfected with either *eGFP*-mRNA alone or that plus *hTERT*-mRNA or the latter alone. *hTERT*-mRNA was mixed with *eGFP*-mRNA at a 9:1 ratio (by mass) (see ***Table 2***). Typically, there was one well of *eGFP*-mRNA TFX, two wells of *hTERT*-mRNA co-TFX, and two wells of *hTERT*-mRNA co-TFX ×2 (double transfection).

Table 2: Representation of amount of RNA used during transfection per well of a standard 24-well TC plate.

Gene	RNA	Mass (ng)
GFP (control)	*eGFP*-mRNA	500
TERT	*hTERT*-mRNA	450
	eGFP-mRNA	50

Wells that were transfected twice (double transfection) were done a day (24 h) apart between the two transfections.

11.6 RNA Extraction from DPSCs

Media was discarded, and cells were washed with PBS. 1 mL of TRI reagent™ (Sigma) was added to the cells and the homogenate then transferred to a clean tube, then 1/10 volume of 1-bromo-3-chloropropane was added to the tube and vortexed to allow for an even mixing. The mixture was centrifuged at 16,000 x g until the aqueous layer was distinctly clear from the organic and the insoluble interface. The aqueous solution containing the soluble RNA was then aspirated into a new tube. An equal volume of isopropanol was added to the tube and gently mixed and incubated overnight at -20 ℃ to precipitate the RNA which was then pelleted by centrifugation at 16,000 x g for 15 min at RT and washed with 70% ethanol. The pellet was redissolved in 200 µL of deionised water and 5 µL run on a gel to ascertain recovery and purity. If RNA contained any remnant gDNA, it was then treated with 10–20 units of DNase enzyme, followed by phenol chloroform extraction, then run on a gel to ascertain recovery and quantified using the Nanodrop Spectrophotometer. Purified RNA was stored at -80 ℃, until use.

11.7 Complementary DNA (cDNA) Synthesis by RT-PCR

cDNA was synthesised using approximately 200 ng of RNA, 200 units of the SuperScript™ IV reverse transcriptase, 5× SSIV buffer, 5 mM of DTT, 10 units of ribonuclease inhibitor, 50 ng of random hexamers, and 0.5 mM of dNTPs. Synthesis was performed as per manufacturers instruction for RT+ and RT- reaction. The cDNA was stored at -80 ℃, until its use as a template for PCR.

12 RESULTS

12.1 Preparation of Synthetic mRNA

12.1.1 Preparation of a Plasmid for *In-Vitro* Transcription of a Synthetic mRNA Encoding the hTERT Gene (phTERT-mRNA2)

Plasmid pHage2-EF1a-TERT-IRES-Puro was obtained from Addgene and used as template for PCR to amplify the hTERT coding sequence with oligos hTERT 5.1 and hTERT 3.1 (see ***Appendix A***), using proof-reading thermostable DNA polymerase Phusion to reduce the likelihood of errors in the sequence arising. DNA of the expected size was observed after gel electrophoresis. The DNA was purified and digested with BsmBI and EcoRI restriction enzymes, purified with silica columns again and ligated with the 3 kb vector fragment of EcoR1 + EcoRV + Nco1 – cut peCas9-mRNA that contains the T7 promoter with the correct transcription initiation context for subsequent *in vitro* transcription with CleanCap™ Cap analogue and the BGH 3' UTR (see graphical map on ***Figure 5***). The EcoRV was included to reduce the size of the Cas9 ORF-containing fragment making it easier to gel purify the vector fragment. The ligation mix of that vector with the hTERT PCR DNA was transformed into *E. coli* (XL1 blue) and colonies screened by PCR with primers hTERT 5.1 and hTERT 3.1. One positive colony was grown, and plasmid extracted with Qiagen Plasmid Midi Prep Kit. The putative structure of this plasmid (phTERT-mRNA) is shown in ***Figure 6***, and was sequenced with primers hTERT seq1, hTERT seq2, hTERT seq3 and hTERT seq4 (see ***Appendix A***).

Figure 5: An illustration of the map of the circular peCAS9-mRNA

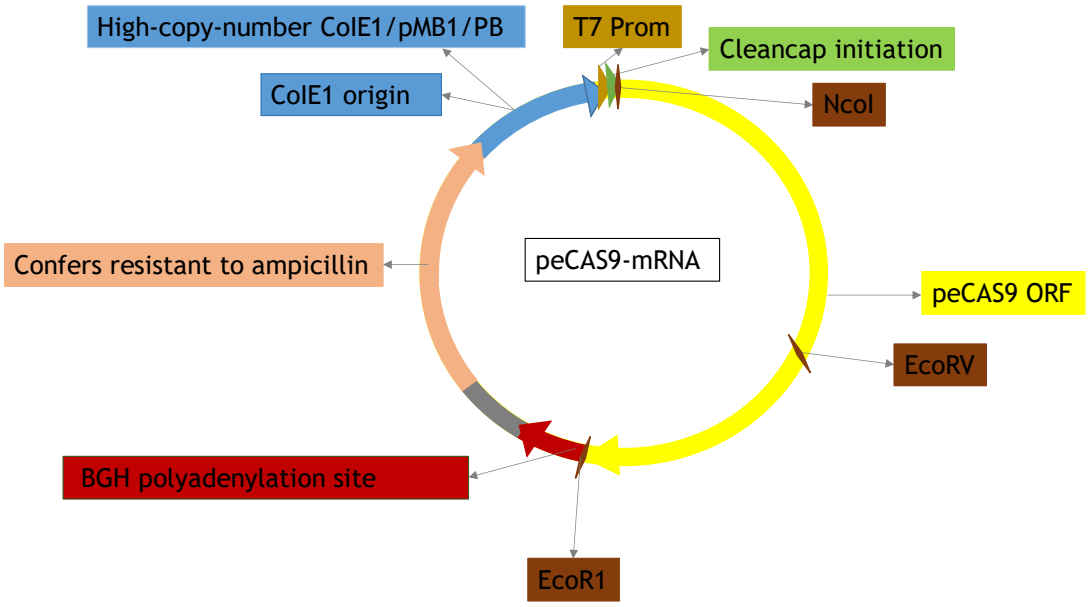

Fig 5: circular graphical map of the peCAS9-mRNA showing the relevant features such as the T7 prom and particular restriction enzyme sites.

The hTERT gene sequence from the Genome browser was compared against our cloned plasmid using the open-source DNA analysis software "Serial cloner." The comparison showed that the hTERT mRNA sequence had been successfully cloned but that there was a mismatch in a single base pair at a conserved RNA binding region between the sequence originating from the Addgene plasmid and the genome browser sequence. The base pair was in a codon for the amino acid, aspartic acid, that is well-conserved in all primates and other recently diverged groups such as rodents indicating positive selection as shown in ***Figure 7***. The difference in sequence changes this aspartic acid to glycine in our cloned sequence, thereby affecting the local charge in this RNA binding domain. Since protein-RNA interactions rely extensively on electrostatic interactions, this was a concern and therefore, site correction oligos were obtained to correct the plasmid.

Figure 6: An illustration of the map of the circular *hTERT*-mRNA

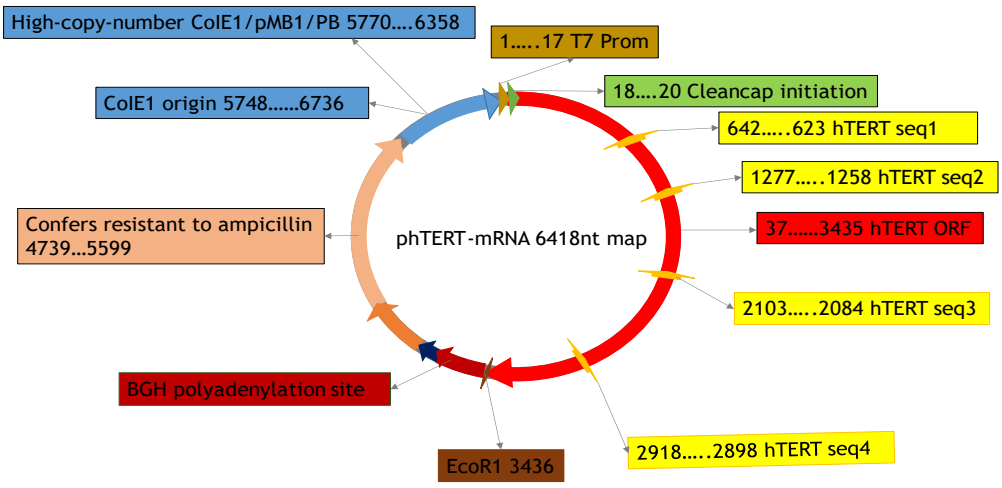

Fig 6. map of the phTERT-mRNA2 showing notable features such as the primer sequences, relevant restriction enzyme sites (BSMBI and EcoRI), T7 prom and the hTERT ORF.

Interestingly, the hTERT gene sequence in the plasmid (pHage2-EF1a-TERT-IRES-Puro) we obtained from Addgene, showed the same difference to the genome database hTERT sequence. Although this plasmid is cited in several publications, no mention is made of this potentially significant difference.

Figure 7: A UCSC Genome browser image showing the conserved region of the mutation in various primates and mammals

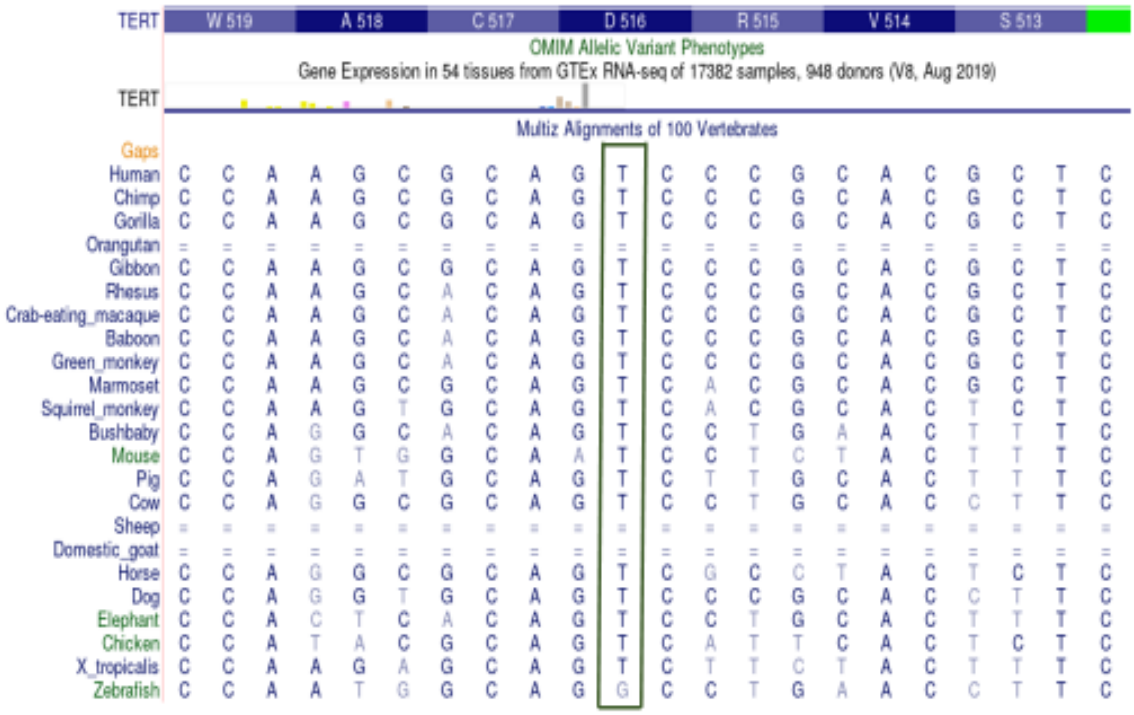

Fig 7. A UCSC genome browser generated snipped image of the hTERT gene **showing** the conserved region of the aspartate in some primates and other vertebrates. The highlighted area shows the exact codon in which the mismatched occurred, the right base for most primates is a T, and the plasmid from Addgene had a C in that region.

Two oligos made for divergent PCR shown in ***Figure 8*** (hTERTcorrect5 and hTERTcorrect3; see ***Appendix A***), were used with Phusion PCR to amplify the whole plasmid, fragment gel purified (as there were some non-specific smaller bands), phosphorylated, religated and transformed back into Agilent Solo Pack cells. There were no colonies found on the control (no ligase) and approximately 50 on the ligase. Six of these colonies were mini-prepped and they all showed a positive restriction enzyme pattern consistent with retention of the hTERT ORF, these colonies were amplified via PCR with the GoTaq Master Mix. The PCR products were then run on a gel against a DNA ladder and bands were observed, which show clear and distinct sizes that match the phTERT-mRNA product. We sent three out of the six for sequencing with the hTERT Seq3 primer which should go through the region with polymorphism.

Figure 8: An illustration of the PCR construct and the site correction of the polymorphism (phTERT-mRNA1 to phTERT-mRNA2)

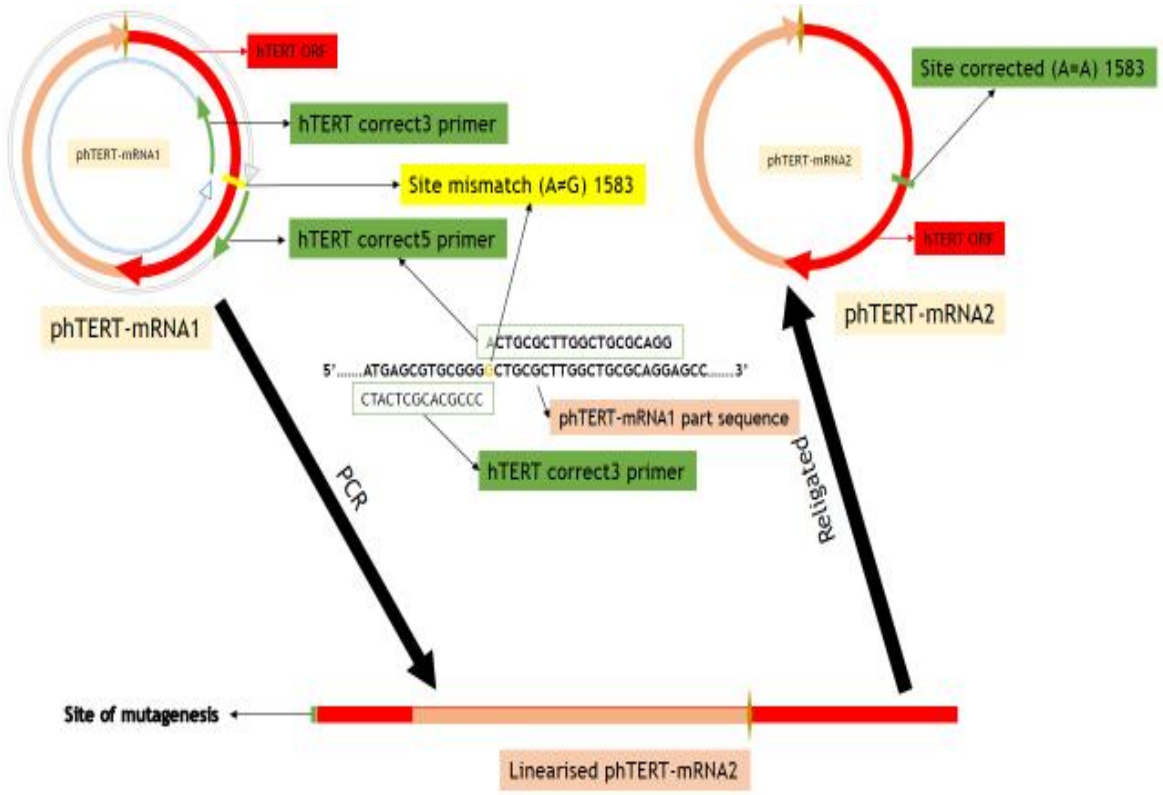

Fig 8: a cartoon image showing the process involved to correct the polymorphism by the divergent PCR oligos. Images shows the different phase of the correction, from the circular plasmid to the linearised PCR phase and the religation to a circular plasmid.

One of the sequencing runs failed, but the other two worked and showed that the site correction with the already mentioned oligos was efficient (***Figure 9***). We used the leftover mini prep broth to inoculate for Midi Prep processing of one of the corrected positive colonies from the Sanger Sequence results. The Midi Prep plasmid DNA was then sequenced off BGHrev and hTERTseq 1, 2, and 4 (see ***Appendix A***), which all showed the hTERT sequence had been perfectly maintained. No sequencing was done with hTERTseq3 again, we assumed it was unchanged from the sequencing of the mini-prepped plasmid. The corrected clone was named phTERT-mRNA2 and the original with the uncorrected sequence as phTERT-mRNA1.

The corrected phTERT-mRNA2 was further digested with the *Eco*RI enzyme which cuts immediately downstream of the hTERT ORF to prepare linear DNA as a template for in vitro transcription, and then deproteinised by phenol/chloroform

extraction. The BGH 3' UTR was not included because it had been found that a 3'UTR was not necessary to make a functional mRNA, since polyadenylation was carried out *in-vitro*. The purified plasmid was precipitated by isopropanol/sodium acetate precipitation, washed with 85% ethanol, air dried and redissolved in ultrapure water at a concentration of 165 ng.μL^{-1}

Figure 9: hTERT sequence obtained from UCSC Genome browser against the sequence results of the cloned plasmid phTERT-mRNA1 and the corrected phTERTmRNA2

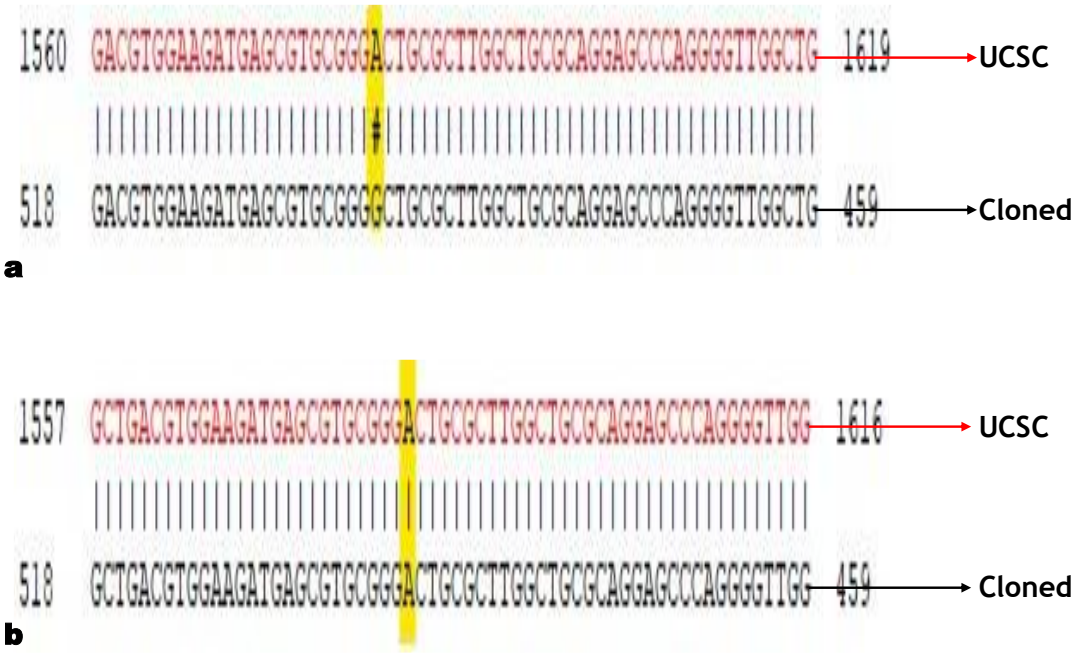

Fig 9. (a) the phTERT-mRNA gene sequence result compared against the hTERT gene sequence from Genome browser showing the mismatch (A≠G) at the RNA binding site. **(b)** the corrected hTERT-mRNA gene sequence result against the hTERT gene sequence from the Genome browser, indicating the correction of the mismatch (A=A). the lanes labelled **(UCSC)** the phTERT-mRNA sequence from the UCSC genome browser and lane (**Cloned**) phTERT-mRNA sequence result post transformation.

Thus, the aim of preparing an *in-vitro* transcribable DNA template encoding the human telomerase reverse transcriptase gene was achieved, and the DNA template was named phTERT-mRNA2.

12.1.2 *In-vitro* Transcribed *hTERT*-mRNA

The linearised phTERT-mRNA2 digested with the EcoRI restriction enzyme was successfully transcribed by the T7 RNA polymerase, and the CleanCapAG™, which adds a Cap1 structure initiation site to the 5' end to a high proportion of the

transcripts and ensures the reduction of uncapped 5' triphosphate formation of the transcript. The uridine in the dNTPS used was N1-methylpseudouridine triphosphate instead of the normal UTP. This was to improve mRNA stability, reduce innate immune responses, and minimise the activation of the TLRs in the endosomes.

Figure 10: Gel image showing the *in-vitro* transcribed non-polyadenylated mRNA against a DNA ladder

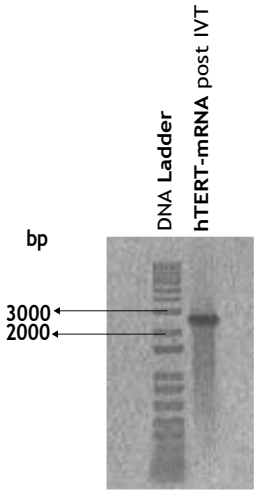

Fig 10. A gel image of the hTERT-mRNA2 against a 1kb+ DNA marker showing the perfect clean and clear single band of the RNA after an *in-vitro* transcription without polyadenylation.

Following the *in-vitro* transcription of the phTERT-mRNA2, the product was then purified by silica column purification. The success of this was tested by running the product on a standard non-denaturing gel, to see if a strong single band was observed. A single strong band was observed indicating efficient production of the mRNA. The hTERT-mRNA expected size is about 3.3 kb, it was not expected to be sized exactly by DNA size markers as these are double stranded, but were a convenient approximation (***Figure 10***). The RNA was then polyadenylated and the success of that step was determined by looking for a size shift between the non-polyadenylated mRNA and the polyadenylated mRNA (***Figure 11***), by gel electrophoresis.

The synthetic *hTERT*-mRNA was generated by me and Dr Andrew Hamilton.

Figure 11: Gel image showing the *in-vitro* transcribed phTERT-mRNA2, before and after polyadenylation against a DNA ladder

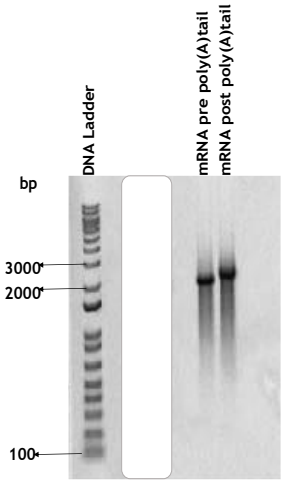

Fig 11. A gel image showing the *in-vitro* transcribed phTERT-mRNA2 before polyadenylation on the left and the polyadenylated transcribed phTERT-mRNA2 on the right, the shift in the sizes is an indication of the addition of As to the RNA after polyadenylation.

The quantified column purified mRNA was then stored as aliquots of 10 µL into clean PCR tubes and stored in the -80 ℃, named as ψUhTERT-mRNA with a concentration of 266 ng/µL.

12.2 Measurement of TL

One of the most important aspects of the project was the measurement of the TL in DPSCs. The first approach we tried was to use the fluorescence *in-situ* hybridisation method (FISH), which was a more direct approach to quantifying TL before we considered an alternative method, which is the quantitative polymerase chain reaction (q-PCR), after we failed to develop an efficient assay for the FISH due to background signal.

12.2.1 Fluorescence *In-Situ* Hybridisation (FISH)

To determine the relative lengths of telomeres in DPSCs, we originally intended to use an assay for FISH to quantify their lengths. This assay was to make use of cell nuclei fixed by formaldehyde in PBS spread out on a glass slide and treated with the cyanine3-labelled Telomere ex5 probe (see ***Appendix D*** for sequence). The mounted glass slides were run on a TELFISH program (see ***Section 9.4.1***), washed with PBS and DAPi stained.

12.2.1.1 Immortal Mouse Myoblast Cells (C2C12)

First, the telomere FISH assay was tested on the mouse myoblast cell line, C2C12, following cell fixation and at a Telomere ×5 probe concentration of 0.1 µM. Microscopic images of the C2C12 cells on ***Figure 12***, show strong punctate nuclear signal intensity with little cytoplasmic signal, as would be expected for a positive telomere signal. The CY3 images are shown in green colour, instead of the orange for a better eye resolution. Several aspects of the assay were adjusted to optimise signal:noise ratio: Different concentration levels of the Telomere ×5 probe, different temperatures in the TELFISH running program, and different cell fixation times. We realised that the best results were obtained for the conditions with a 0.1 µM concentration of Telomere ex5 probe, and the running temperature of 45 ℃, but the various cell nuclei fixation time had no significant effect.

Figure 12: Fluorescence microscope images showing the results following cell fixation and FISH for C2C12 cells

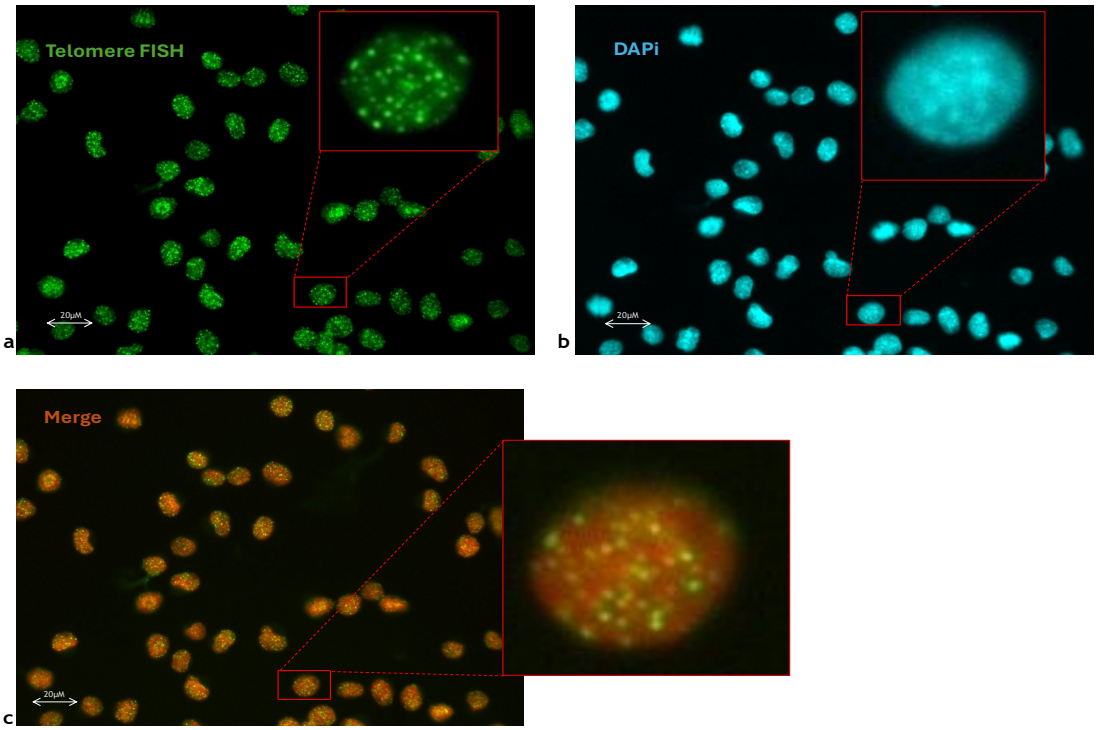

Fig 12: Telomere FISH in C2C12 cells. Image (a) showing the CY3 image at 1000 ms exposure and the image (b) is the DAPi image of the same cells at 200 ms exposure time, and (c) the merge image of the CY3 and DAPi showing no fluorescence signal outside of the nuclei of C2C12 cells and showing DAPi in red for a better colour contrast.

12.2.1.2 Dental Pulp Stem Cells (DPSCs)

The same optimised telomere FISH assay tested on C2C12 cells was then applied to the DPSCs. The microscopic images taken and produced on (***Figure 13***), showed less clear punctate telomere signal intensity in the nuclei and a lot of background noises from the cells' cytoplasm. Thus, I could not be sure the green signal in the nucleus was from telomeres. It could also be from the same thing causing background in the cytoplasm. Therefore, the quality of these images was unsuitable for telomere length analysis and measurement.

Figure 13: Fluorescence microscope images showing the results following cell fixation and FISH for DPSCs

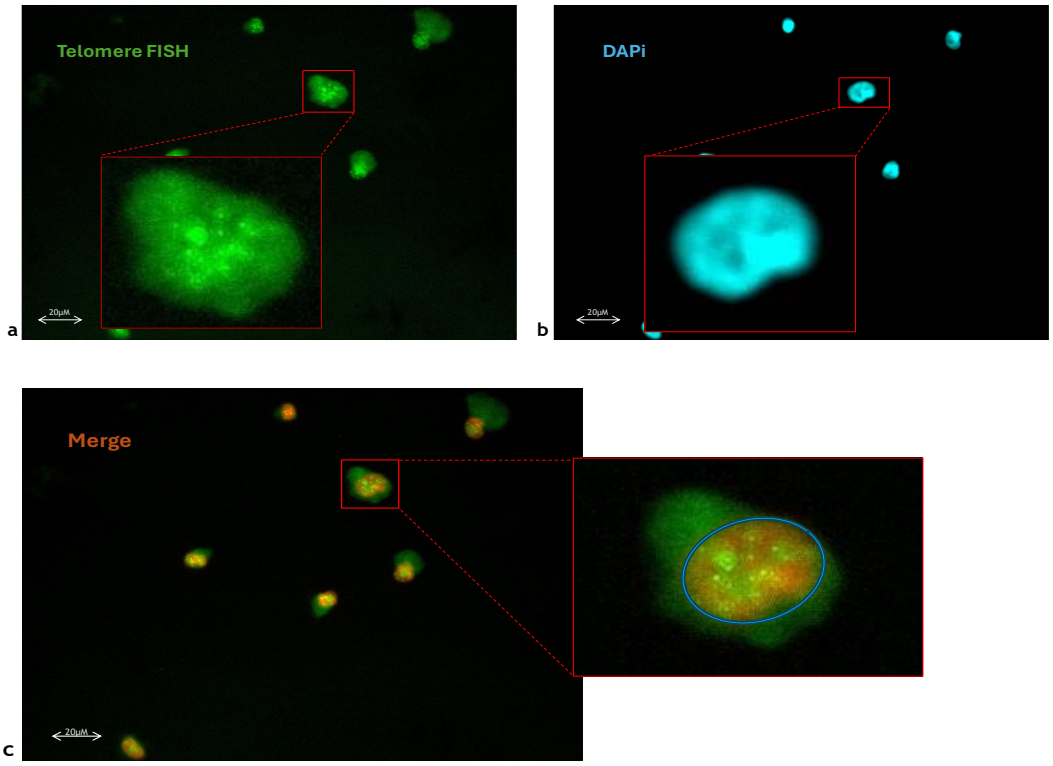

Fig 13: microscopy images of DAPi stained nuclei fixed cells for FISH in DPSCs. Image (a) showing the CY3 image at 1000 ms exposure and the image (b) is the DAPi image of the same cells at 200 ms exposure time, and (c) the merge image of the CY3 and DAPi showing the fluorescence signal outside of the nuclei of DPSCs and showing DAPi in red for a better colour contrast.

It is documented in various literatures that mouse cells are known to have longer telomeres, in comparison to human cells and are not susceptible to telomere-dependent senescence (Wang et al., 2009), hence, the stronger intensity of the signals in the mouse C2C12 cells was likely because of the cells' origin or the immortality or both. However, the presence of the cytoplasmic (and possibly

nuclear) background fluorescence from the DPSCs was of great concern and the need to outline and mitigate the cause(s) was necessary in the development of this assay.

The question raised was what was/were causing the strong background noise in the DPSCs? Could it be from the probe? Could it be because of autofluorescence, related to senescence or lipofuscin?

To answer the question with relation to autofluorescence, we used the same protocol on fixed DPSCs but without any fluorescence probe (Telomere ×5), just the buffer to see if we would observe any background noise. Strikingly, we did see similar background fluorescence, and not just in one wavelength but across all wavelengths. This suggest that the background noise is indicative of autofluorescence and changing the probe would likely have no effect on the results. How then do we fix this problem? Although cell fixing time is mostly associated with autofluorescence, we were able to conclude from our manipulations that neither the cell fixing time, nor the Telomere ×5 probe had any significant effect on the background fluorescence. A paper we had come across (Bertolo et al., 2019) stated that autofluorescence is seen in MSCs due to senescence and this is because of the presence of excited endogenous molecules with fluorophore-like properties being accumulated in the cytoplasm. Amongst these molecules is lipofuscin, an undegradable waste material which is also referred to as the age pigment, and it accumulates in the cytoplasm as cells age (Gray and Woulfe, 2005). DPSC are mortal cells, therefore, it is possible some of these cells undergoing cellular senescence, and hence, the autofluorescence.

According to Jenvey and Stabel (Jenvey and Stabel, 2017) an additional staining with Sudan black had shown an improved signal strength and a significant reduction of autofluorescence related to lipofuscin in their study, therefore we tested their idea and stained the DPSCs with Sudan black. However, we did not see any improvement in our results. This result of Sudan black stained cells shown in ***Figure 14***, was an indication that perhaps it was not lipofuscin at all, or that the assay was inappropriately carried out. Thus, we were not successful in confirming the effectiveness of the Sudan black technique in the reduction of fluorescence due to lipofuscin.

The argument remains, could a different probe provide strong signals? Well perhaps yes but since we had fluorescence signals from DPSCs treated without any probe and across all wavelengths, we had to save time and resources and therefore decided to try another method of measuring TL in DPSCs. The question of what causes the background noise in FISH images of DPSCs still remains.

Figure 14: Fluorescence microscope images showing the fluorescence in DPSC treated with buffer only and DPSC treated with Sudan black

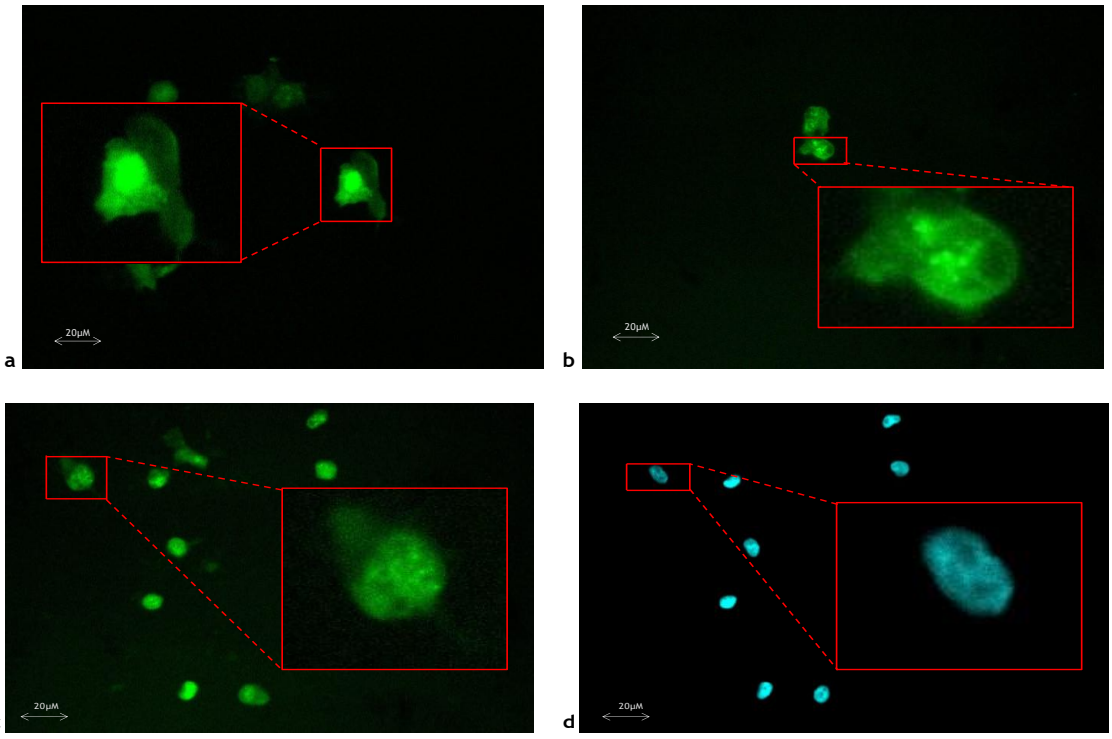

Fig 14: microscopy images of DAPi stained nuclei fixed cells in DPSCs. Image (a) showing the CY3 image of the buffer only treated cell, the image (b)showing the CY3 image of DPSC with the Telomere ×5 probe (c) is the CY3 image for FISH following Sudan black treatment at 1000 ms exposure and the image (d) is the DAPi image of the same Sudan black treated cells at 200 ms exposure time.

12.2.2 Quantitative (Real – Time) Polymerase Chain Reaction (q-PCR) to Quantify TL.

The initial aim was to use the q-PCR method of O'Callaghan and Fenech (O'Callaghan and Fenech, 2011), to determine absolute overall number of telomeres repeats per genome in a genomic DNA sample. Therefore, we purchased the telomere oligo standards described by Cawthon for absolute quantification. We realised that relative q-PCR would be enough for our immediate aims but

nevertheless used the oligo standards which served as good control when we were testing the relative q-PCR method.

Thus, a telomere standard curve was produced using the telomere standard oligos and primers (see ***Appendix B***), described in that paper to test the ability of the primers and PCR programme to amplify the telomere repeat sequence in our hands. The standards were prepared by serial dilution. The number of TTAGGG repeats in each standard dilution was calculated appropriately using the ratio of the molecular weight to the Avogadro's constant (O'Callaghan and Fenech, 2011) and plotted against Ct value (***Figure 15***) from dilutions 10^{-2} through 10^{-8} for the telomere standard, and 10^{-3} through 10^{-9} for the 36B4 SCG standard. The results of the graph generated from the q-PCR were plotted using spreadsheet, the slope and the value of the R^2 were calculated using MS Excel. The value obtained for the R^2 shows low variation in the spread (regression) for both the amplification of the telomere repeat and the house keeping gene (36B4 single copy gene), used by Cawthon and recently by O'Callaghan and Fenech (Cawthon, 2002, O'Callaghan and Fenech, 2011). The serial dilutions were used to produce ***Figure 16***, which shows the amplification of the NTC, and the Microsoft excel generated graph shown as (***Figure 15***) a logarithmic curve.

Figure 15: A Microsoft excel generated standard curve for the telomere and 36B4 primers

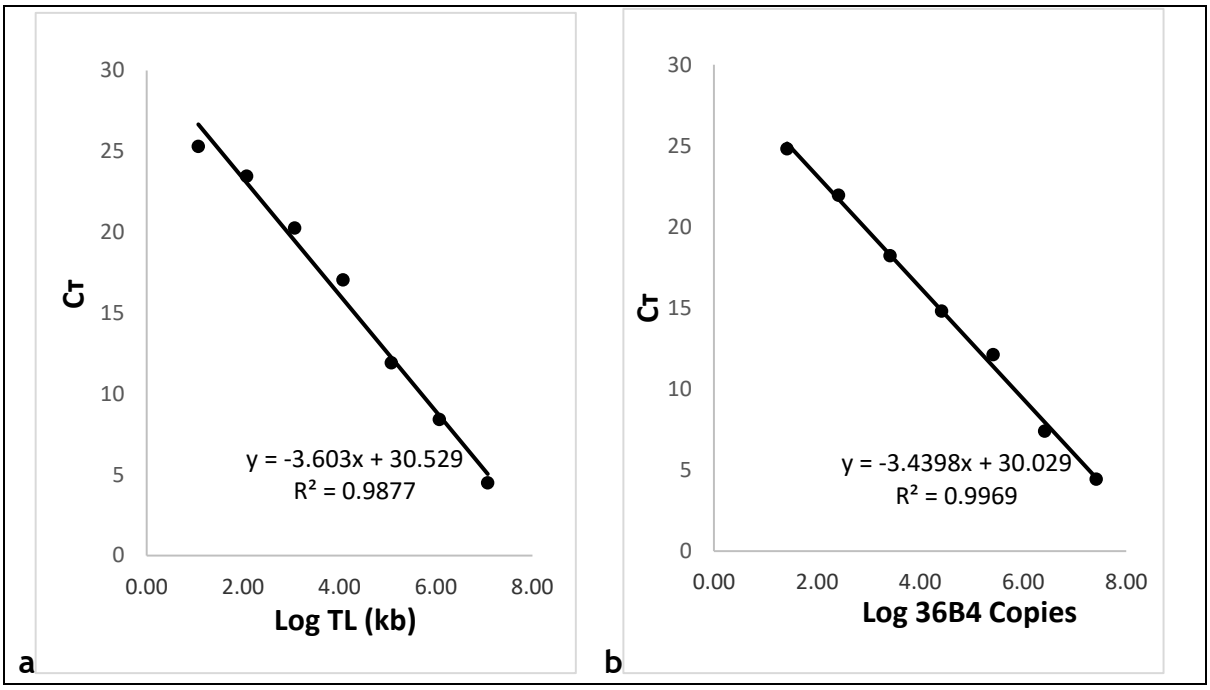

Fig 15: standard curve generated from the telomere and the single copy gene oligomers using SYBR green as the fluorescence Master Mix. Figure (a) shows the standard curve for calculating the absolute TL in kb per reaction tube, and figure (b) shows the standard curve for calculating the number of genome copies. The graph shown here represents the linear range of the PCR and it was used in determining the efficiency of our primers.

Although ***Figure 16*** indicates successful specific amplification of telomere repeats, at higher Ct values we saw the assay had signals in the NTC for both the telomere and the 36B4 amplifications. If whatever was responsible for the fluorescence increase in the NTC control was also occurring in our test samples, it would mean we could not be confident that the fluorescence in these samples was entirely due to amplification of telomere repeats and this would compromise quantification. The primers used had been HPLC purified, and therefore, the signals obtained in the NTC are highly unlikely to be related primer contamination. We tried different methods of troubleshooting; we used various sources of deionised (ultrapure) water to rule out contamination of the water. We still received NTC signals for all water sources and the implication was that the signals detected in the NTC were not because of water contamination either. We also tested different annealing temperatures and times, but even at the highest possible (72 ℃) temperature, there were still amplifications in the NTCs. Similarly,

adding 3% DMSO to the PCR reaction mix was futile as the amplifications in the NTC were still persistent.

Figure 16: A graphical illustration showing the CT mean and standard deviations of the serial dilutions of both standards

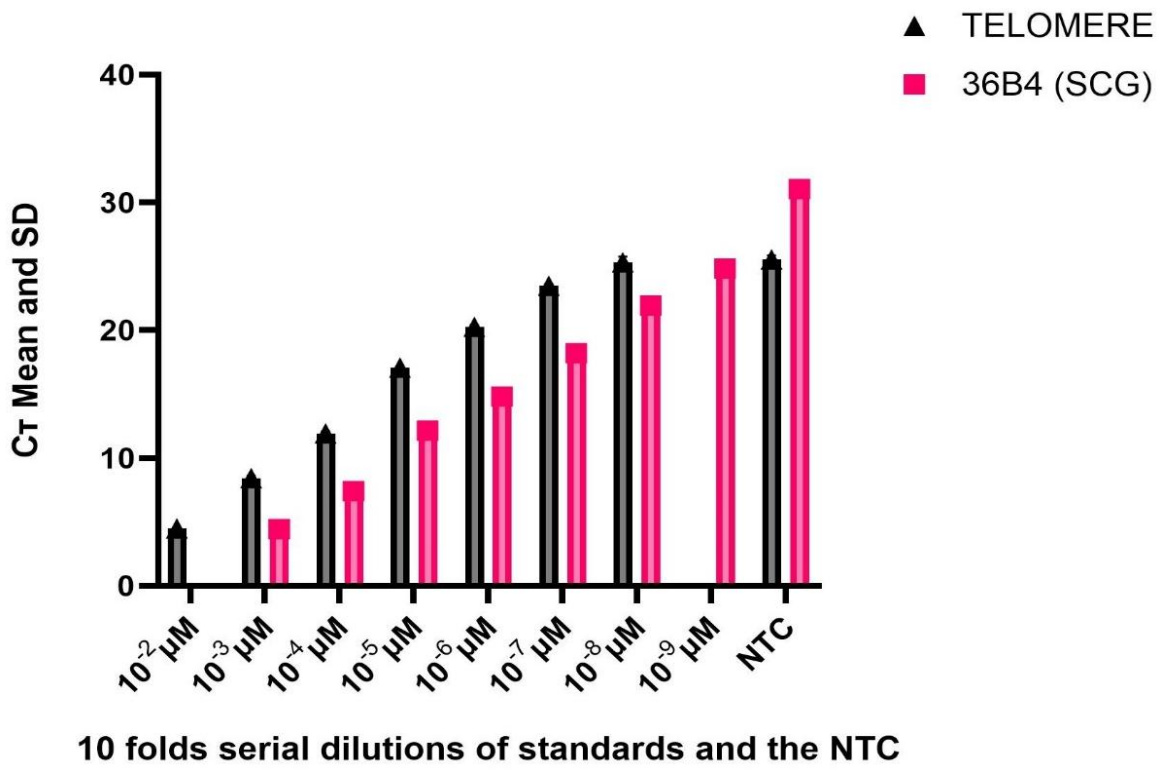

Fig 16: a graph showing the C_T mean and standard deviations for duplicate wells of the gene of interest (GOI), telomere and the house keeping gene (HKG), 36B4 for the standard dilutions and the NTC. The standards were diluted by 10folds from 10^{-}-10^{-9} (µM).

The assay used in this project was very similar to that of O'Callaghan and Fenech (2011), except for a slight difference in the Master Mix composition: O'Callaghan and Fenech used the Power SYBR I Master Mix (Applied Biosystems, #4367396); Contains AmpliTaq Gold DNA polymerase, dNTPs, SYBR I Green Dye, optimised buffers and passive reference dye (ROX) (O'Callaghan and Fenech, 2011), whereas we used SyGreen mix Hi-ROX (PCR Biosystems, PB012621-092-4) as this was the standard q-PCR Master Mix used in our laboratory for many other researchers assays and which performed well in these. O'Callaghan and Fenech reported some troubleshooting advice towards avoiding the amplification in the NTC. They have suggested that the dissociation curve could be used to determine whether it is either due to contamination or primer dimer formation, but we judged a gel would give better discriminative power. Regrettably, it was not reported by either paper

(Cawthon, 2002, O'Callaghan and Fenech, 2011), whether they had the amplification in the NTC or whether it affected analysis of their results.

To get more information, after completion of the q-PCR programme, we ran q-PCR products including the NTC on a gel to see the sizes of the products. ***Figure 17*** shows the band size of the NTC to be equal to the combined size of the primers, an indication that the NTC amplifications are primer dimer amplification.

Figure 17: Gel image showing the q-PCR products of the standards and NTC against a DNA ladder

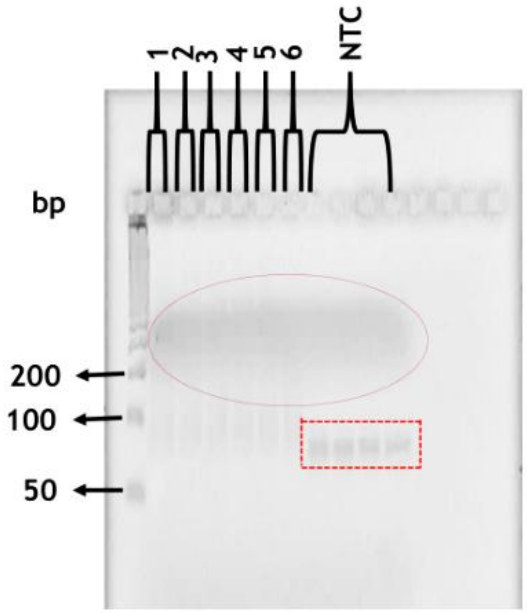

Fig 17: gel image of the q-PCR products for the telomere standard 10^{-8}µM (lane 1), DPSC genomic DNA (lane 2–6; control, TERT TFX1 24hr and 1week, and TERT TFX2 24 h and 1week respectively) and the NTC against a 50 bp DNA ladder. The four different NTC samples are from the different ultrapure water sources used in the q-PCR. The red box is an indication of the supposed primer dimer. The broad shadow indicated by the red oval is from fluorescence of xylene cyanol in the loading dye.

Importantly, the size of the amplicon in the NTC was completely different to those of the telomere standard and the sample genomic DNA. There was no sign of the primer dimers in these amplifications. Also, looking at the difference in the C_T values between the NTC and our samples, which was 5 C_Ts or more different we were comfortable to go on with the method given even though we had not eliminated the non-specific amplification coming from the NTCs.

12.3 Natural Relative Levels of Telomeres in Different Passages of DPSCs

We would expect the TL for cells from the early passage to have a greater length, as compared to those from the late passage due to cell aging (Mokry et al., 2010). To test this, the natural levels of telomeres were measured from the gDNA of early passage (P2) and late passage (P8). These (DPSC P2 and P8) cells had been resurrected from two separate cryovials prepared by previous students and therefore, were not a continuous passaging of cells from a single cryovial, this was done to save time. The results obtained from the technical replicates of the q-PCR for P2 and P8 showed a surprisingly low difference in TL as expressed in the T/S (telomere/single copy gene) ratio (see ***Section 9.4.2***). These results were consistent with the findings of Mokry *et al.* (2010), who have shown a large variation in the TL between the different passages (P2–P16). However, these results maybe a genuine representation of telomere attrition in DPSCs, or an inconsistency in the passaging of these cells. The difference in the relative fold change between the P2 and P8 was in fact less than 0.5, as illustrated in ***Figure 18***.

Figure 18: A graphical illustration of the relative natural TL expressed as 2^-ΔΔCT in DPSCs for P2 and P8

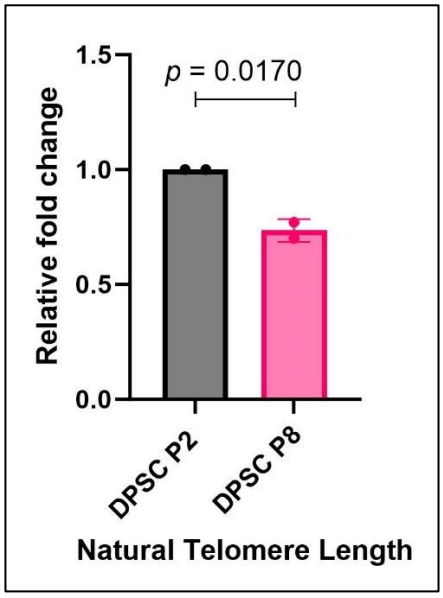

Fig 18: relative TL of DPSCs by q-PCR using a fold change method ($2^{-\Delta\Delta C_T}$) (Livak and Schmittgen, 2001). DPSCs resurrected from cryovials of passages 2 and 8 were used in this analysis. The two mean C_T of each sample were obtained from two separate q-PCR of the same DNA sample, hence technical (Tech.R) replicates. Data were analysed and plotted in GraphPad Prism and statistical differences calculated by paired t-test.

Genomic DNA was then extracted from different cryovials of two P2 and two P9 resurrected cells. These different samples from the same passage number were used to determine a correlation between biological replicates in both the early passages and late passages. The results obtained from these biological replicates were used in determining the level of variations between the replicates of the same passage number in our stock, and the difference in the relative TL between P2 and P9. As we had limited stocks of these DPSCs, and they were shared with other students we could not do more biological replicates.

Figure 19: A graphical illustration of the relative natural TL expressed as 2^-ΔΔCT in DPSCs for biological replicates of P2 and P9

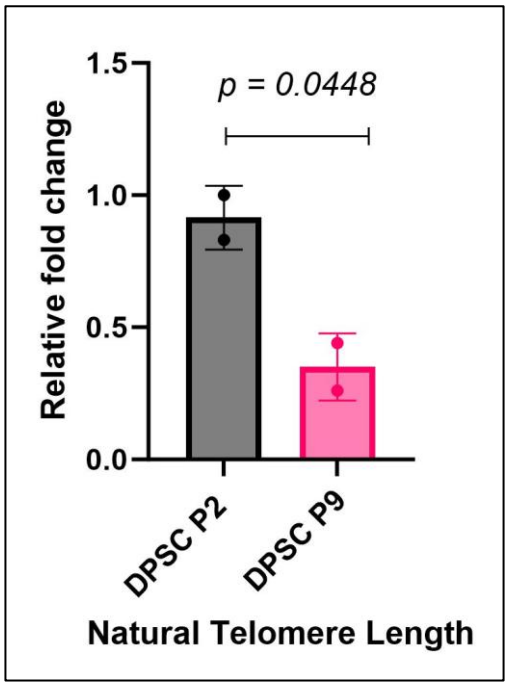

Fig 19: relative TL of DPSCs by q-PCR using a fold change method ($2^{-\Delta\Delta C_T}$) (Livak and Schmittgen, 2001). DPSCs resurrected from two different cryovials each of passages 2 and 9 were used in this analysis. The mean C_T were obtained from triplicate wells, and the data points are from two biological (Bio.R) replicates of passages 2 and 9. Data were analysed and plotted in GraphPad Prism and statistical differences calculated by paired t-test.

The relative fold difference between P2 and the P9 was quite large and not expected considering our initial finding of minor difference between the P2 and P8, but was consistent with the work of Mokry et al. *(2010)*. They *compared* relative TL, telomere to single copy gene ratio (T/S ratio) of DPSCs from P2–P16 cultured within a span of two months, and their results showed a statistically significant decline in TL as the cells age (increasing passages) *ex-vivo*. In that

study, the difference in the T/S ratio between P2 and P9 was more than 0.5, similar to that measured by us suggesting the P2-P9 finding (***Figure 19***) is genuine. Although only two biological replicates were available for each passage point, ***Figure 19*** shows a distinct decline in TL in the P9 cells, compared to P2, in contrast to cells from one of the P2 and a different cryovial of P8 (***Figure 18***). Passage number is only an approximation of the number of cell divisions, and it had not been recorded if the cells had been consistently grown in the same size and type of flask and to the same density for every passage and so, it is possible there was a greater real difference between the number of cell divisions than the single passage difference between P8 and P9 would suggest.

Since DPSCs are mortal cultured primary cells, we expected telomeres to be shortening even in early passage cells. In contrast cancer cell lines are immortal and this is partly due to overexpression of telomerase, an activity present in over 90% of cancer cells (Khattar et al., 2016, Taheri et al., 2022). So, we expected DPSC telomeres to be shorter than those found in cancer cell lines. To check this, we compared the TL of DPSCs from P2 (which was our reference sample in the analysis) and P8 to that of two human cancer cell lines, TR146 (human squamous cell (epithelial) carcinoma) and the HCT116 (human colon carcinoma). The comparative results obtained by q-PCR expressed as a fold difference ($2^{-\Delta\Delta C_T}$) is shown in ***Figure 20***. The DPSC P2 and P8 samples used in ***Figure 18*** and ***Figure 20*** are the same, however, the results were obtained from different q-PCR reactions. We have seen from the results obtained, that our expectations were far from the reality. Surprisingly, the DPSCs had longer TL than both cancer cell lines, and the difference was quite huge, when compared to the TR146 cells which had the shortest telomeres. It is possible that both TR146 and HCT116 are not typical of cancer cell lines and have unusually short telomeres but also possible that DPSC telomeres are much longer than we expected them to be.

Figure 20: A graphical illustration of the relative natural TL expressed as 2^-ΔΔCT in DPSCs and two other cancer cell lines

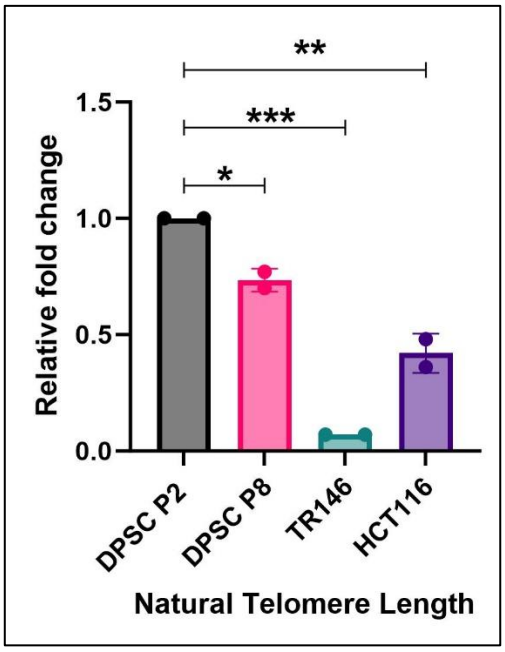

Fig 20: relative TL of DPSCs and two cancer cell lines (TR146 and HCT116) by q-PCR using a fold change method ($2^{-\Delta\Delta C_T}$) (Livak and Schmittgen, 2001). DPSCs from two different passages (P2 and P8) were used in this analysis as compared against two human cancer cell lines. The mean C_T were obtained from triplicate wells, and the data points are from two technical (Tech.R) replicates (two separate qPCR). Data were analysed and plotted in GraphPad Prism and statistical differences calculated by One-way ANOVA relative to DPSC P2. Asterisks indicate statistical significance, where *p < 0.01, **p < 0.001, and ***p < 0.0001.

12.4 Transfection

Now that we were more confident that there was clear telomere erosion in our DPSCs, we wanted to see if we could reverse this by expression of the synthetic telomerase mRNA. However, before that, we decided to test first if DPSCs could be successfully transfected in general with synthetic mRNA made by our procedure (see ***Section 5.1.12***). For this we used an eGFP-mRNA capped with the CleanCapAG™ reagent and made with complete N1-methylpseudouridine substitution of uridine as we had for the telomerase mRNA. DPSCs were transfected with either 500 ng *eGFP*-mRNA per transfection (*negative controls*), or 500 ng of a mixture (9:1 by mass) of *hTERT*-mRNA: *eGFP*-mRNA once for single transfected wells or twice for double transfected wells.

12.4.1 Transfection Efficiency

The fluorescence microscope (see description in ***Section 5.3.1***) was used to determine the efficiency of the transfection of the eGFP-only transfection. All microscopic images of transfected cells shown in this report were obtained 24 h

after transfection when the eGFP was clearly visible, although *eGFP* was actually visible after 1 h. The *eGFP*-mRNA transfected cells were used as the reference sample in measuring the efficiency of the transfection assay. However, the cells were not tagged with any intercalating fluorescent dye, such as DAPi or Hoechst, to avoid possible interference with subsequent q-PCR from DNA extracted from transfected cells. Instead, we relied on phase contrast illumination in combination with GFP fluorescence and overlayed these on Image J to measure the percentage of transfection.

The figure below (***Figure 21***), was used in determining the percentage of the transfection efficiency. In this *eGFP*-mRNA transfection of DPSCs from P9, we achieved more than 90% of transfected cells.

Figure 21: Fluorescence microscope images showing the expression of GFP in the transfected DPSCs and an overlay contrast image to determine the transfection efficiency

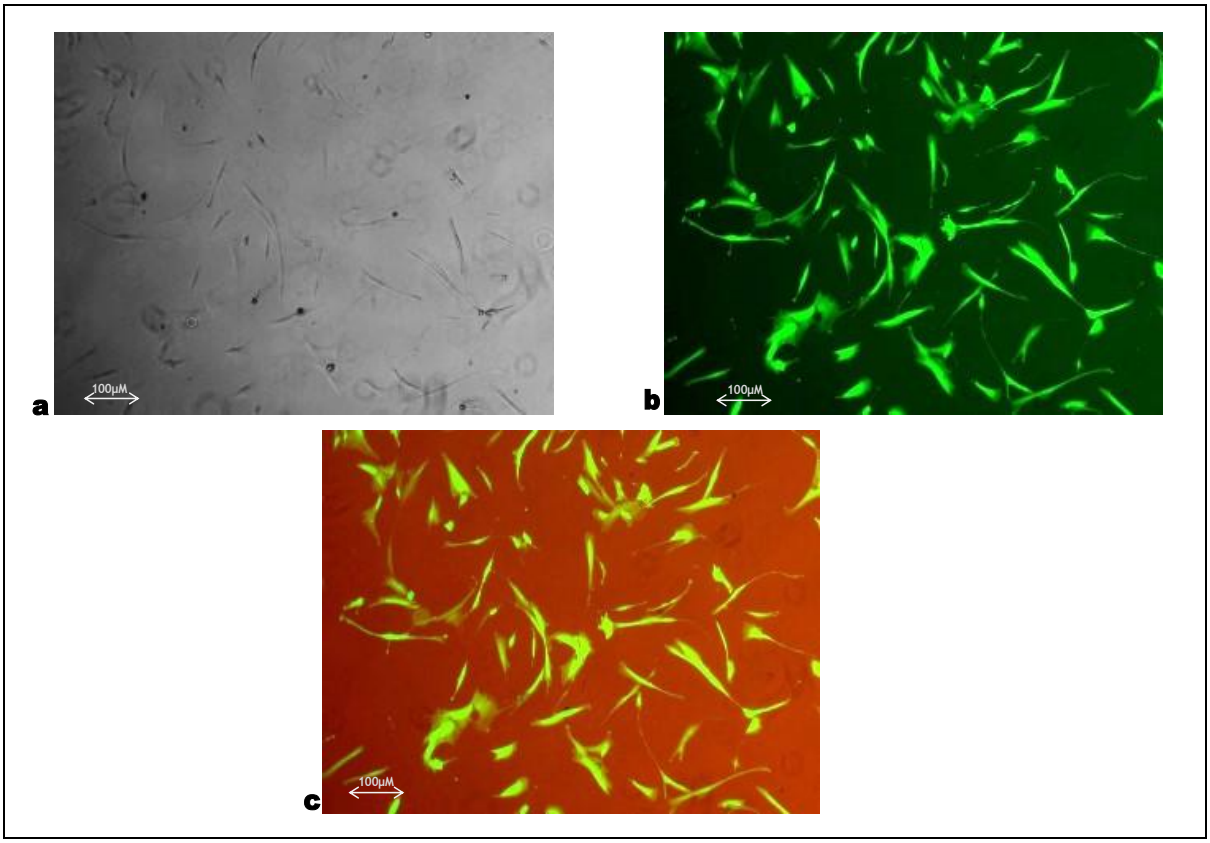

Fig 21: an image J produced image showing the DPSCs in figure (a) and the *GFP* transfected cells in (b). the overlay illustrated in image (c). The results obtained from all the cells transfected with the *eGFP*-mRNA shows a transfection efficiency ≥90%.

12.4.2 TL in Transfected DPSCs

Resurrected DPSCs from P6 cryovials were cultured and then seeded into a 24 well-plate. These DPSCs P6 were then transfected, as per the assay described in the section above (***Section 6.4.1***). The transfection of these cells was to test the effect of the *hTERT*-mRNA on the cells with some telomere attrition.

The fluorescent microscope images shown in ***Figure 22*** are the transfected wells of the *eGFP* only, and the *eGFP* + *hTERT* (1:9) at a 20X and 40X magnifications. Although the *eGFP* level is lower with the *eGFP* + *hTERT* transfection, the DPSCs still looked to have the same frequency of transfection. However, since the *hTERT* is not a fluorescent protein, we can only infer that we have a similar transfection efficiency with the co-packaged and co-transfected *hTERT*-mRNA.

Figure 22: Fluorescence microscope images showing the expression of GFP in the transfected DPSCs

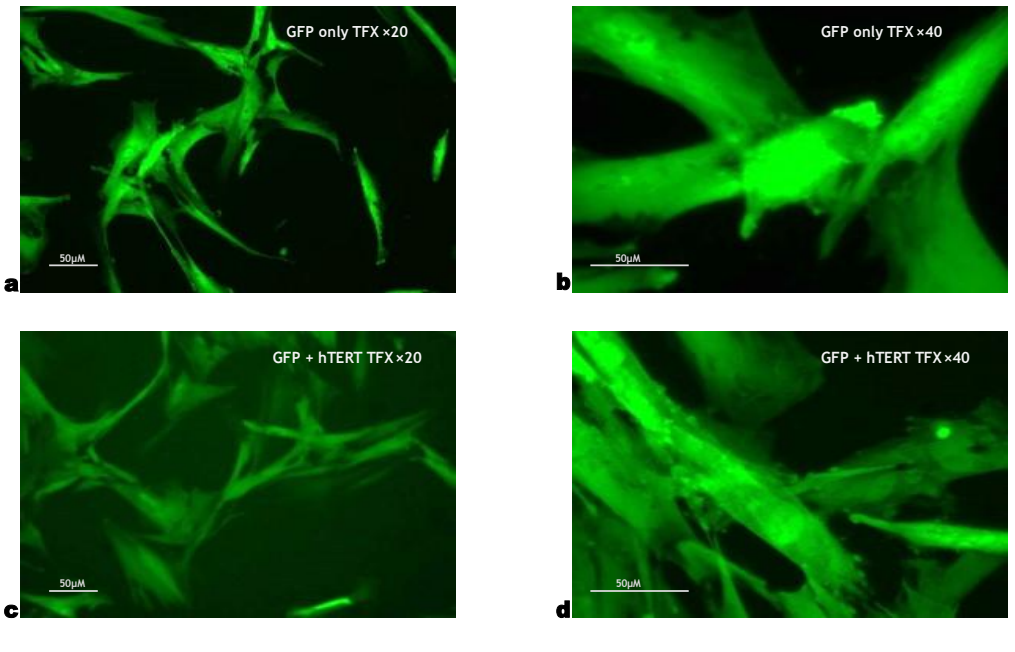

Fig 22: fluorescence microscope images showing the expression of the *eGFP*-mRNA in DPSC. Images (a) and (b) are the 500ng eGFP transfected cells at different magnifications, 20X and 40X magnification, respectively. Images (c) and (d) are the *hTERT*-mRNA co-transfected with *eGFP*-mRNA, at the two different magnifications.

The gDNA of transfected cells in each transfection well were then extracted at different time intervals (24 h and 1-week post transfection), and the relative TL were quantified by q-PCR. The data expressed as relative fold change by T/S ratio shows no relevant increase in the average TL between the negative control (*eGFP*-

only mRNA TFX) and the *hTERT*-mRNA transfected samples (*hTERT* + *eGFP* mRNA TFX) for DPSCs of P6. The q-PCR results (see graph on ***Figure 23***) for all the treatments, the single and the double transfection, as well as the post-24 h and post-1-week transfected cells showed no increase in the average TL, when compared to control.

Figure 23: A graphical illustration showing the q-PCR results for the transfection of DPSCs from Passage 6

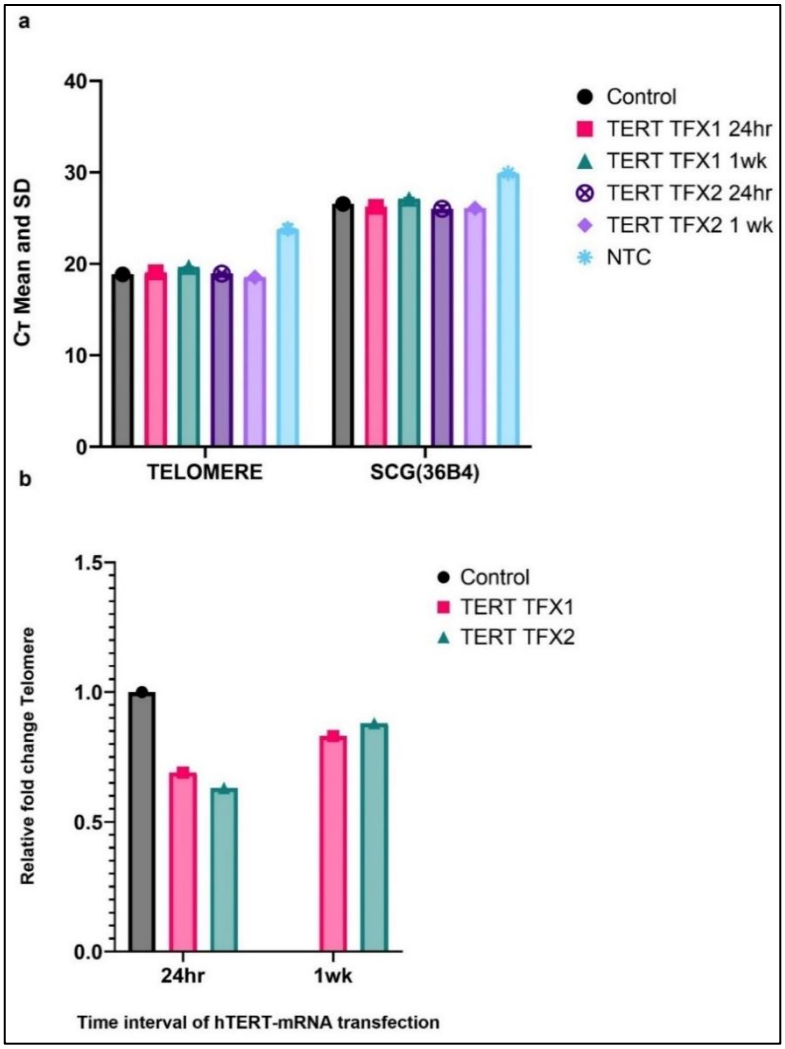

Fig 23: a graph showing the q-PCR results obtained from the different treatments of DPSCs P6. **(a)** the mean C_T and standard deviations from triplicates, showing the gene of interest (GOI), telomere and the house keeping gene (HKG) 36B4 SCG. The GFP transfected cells as the control, the *hTERT*-mRNA + GFP-mRNA (9:1) transfected cells as TERT TFX for the different time intervals and the number of times of transfection. **(b)** relative fold change ($2^{-\Delta\Delta C_T}$) as a relative measurement of TL for the different treatments under analysis.

The results obtained from q-PCR as shown in ***Figure 23*** are an indication that either the synthetic *hTERT*-mRNA does not work or that the relative TL in the DPSC P6 could not be extended for some other reason, such as they were already long

enough. One study conducted by a group in Czech Republic, were TL of DPSCs P2 and P7 isolated from different donors were measured by q-PCR. A lineage of DPSCs from one of the donors showed no telomere attrition with increasing passage number, while all other lineages showed decreasing TL with increasing passage number (Pilbauerova et al., 2021a). It is not known why this DPSC lineage differs from the rest of the DPSC populations, however, the authors suggested that it is important to study DPSC populations extracted from different teeth of the same donor for a wider range of results.

The sequence of the plasmid template for the synthetic mRNA encoding the *TERT* gene had been confirmed, and the mRNA size was as expected as determined by gel electrophoresis post IVT and polyadenylation (refer to ***Figure 11*** on ***Section 6.1.2***). However, we could not exclude some finer structure defect e.g. a failure in capping. We cannot rule out the possibility of the former unless we are able to see a positive effect of the *hTERT*-mRNA on a different passage for example P9 with the shortest telomeres or on a different cell line to rule that explanation out. This prompted the idea to test the effectiveness of the *hTERT*-mRNA on the TR146 cancer cell with the shortest TL. A successful extension of telomeres in the TR146 (cells with extremely low TL) would prove the effectiveness of the mRNA, thereby allowing us to test the effect it would have then on the DPSCs from P9 which shows large telomere attrition or erosion and have more confidence in any result.

To test the effectiveness of the synthetic *hTERT*-mRNA, we transfected the TR146 cells using the same assay with slight modifications (transfection images shown on ***Figure 24***). The modification involves an increase in the mRNA + lipofectamine mixture incubation time. mRNAs (both *eGFP* and *eGFP* + *hTERT*) and lipofectamine mixture were incubated for 25 min before the transfection of the TR146, as opposed to the previously used manufacturers-recommended time of 5 min. This was an alteration made following a dramatic improvement (increase from 25% to 65%) of gene knockout in DPSCs using CRISPR *CAS9*-mRNA by another student in the Hamilton labs after incubating the mRNA in Lipofectamine™ MessengerMax™ for 25 min, as compared to the 5 min. One of the explanations of increasing the incubation time from 5 min to 25 min was to allow sufficient time for the encapsulation of the large *CAS9*-mRNA by the lipofectamine. The manufacturers

recommendation of the 5 min incubation time had worked perfectly for a smaller mRNA such as the *eGFP*, and the increase in the incubation time to 25 min showed no sign of improvement in the percentage of transfected cells with the *eGFP*. Unlike the *eGFP*-mRNA, which is only about 700 bp, the sizes of the *CAS9*-mRNA and the *hTERT*-mRNA is over 3 kb and therefore, may require a longer incubation period to form the LNP + mRNA complex.

Figure 24: Fluorescence microscope images showing the expression of GFP in the transfected TR146

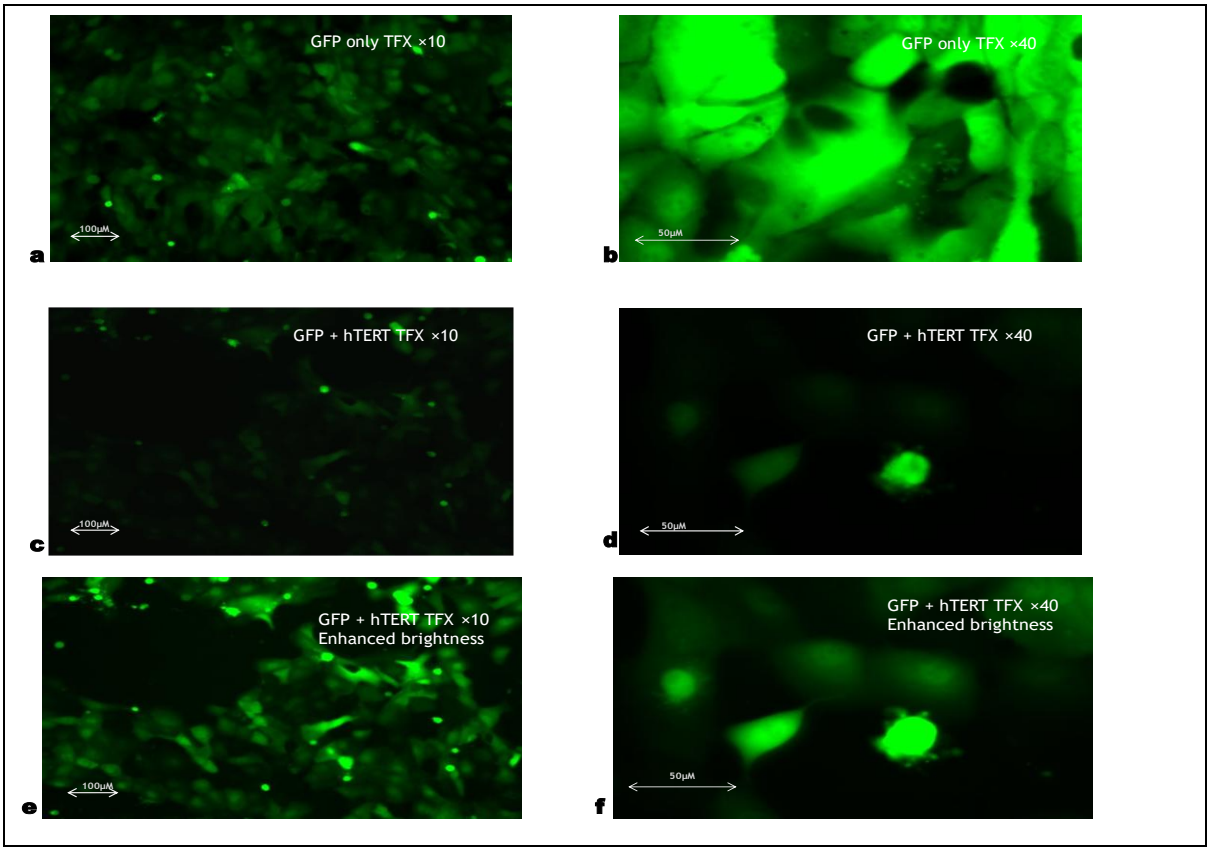

Fig 24: fluorescence microscope images showing the expression of the *eGFP*-mRNA in TR146. Images (a) and (b) are the 500ng eGFP transfected cells at different magnifications, 20X and 40X magnification, respectively whiles images (c) and (d) are the *hTERT*-mRNA co-transfected with eGFP-mRNA, at the two different magnifications. Images (a), (b), (c), and (d) are set at the same brightness and contrast, images (e) and (f) are enhanced brightness of the images (c) and (d).

The images shown in ***Figure 24*** (the transfected TR146 cells with *eGFP*, and *eGFP* + *hTERT*-mRNA), shows a high transfection rate with undiluted *eGFP*-mRNA similar to DPSCs (***Figure 23***), and lower *eGFP* expression where *eGFP*-mRNA was diluted 10-fold with *hTERT*-mRNA again similar to DPSCs.

Genomic DNA was extracted 24h and 1-week after transfection from the successfully transfected TR146 cells shown in ***Figure 24***, the TL were quantified using telomere to single copy gene ration ($2^{-\Delta\Delta C_T}$) by q-PCR and the results illustrated in ***Figure 25.*** This shows an interesting change in the average TL as manifested in the relative fold change difference between samples with the TL of the *hTERT*-mRNA transfected cells showing a great increase in their TL. The effects of the expression of the *hTERT*-mRNA were stronger in those cells that were transfected twice consecutively a day apart. The average relative TL in terms of the fold change was 2.58 times more than the control (*eGFP*-mRNA transfected) 1-week post-transfection.

Figure 25: A graphical illustration showing the q-PCR results for the transfection of TR146 cells

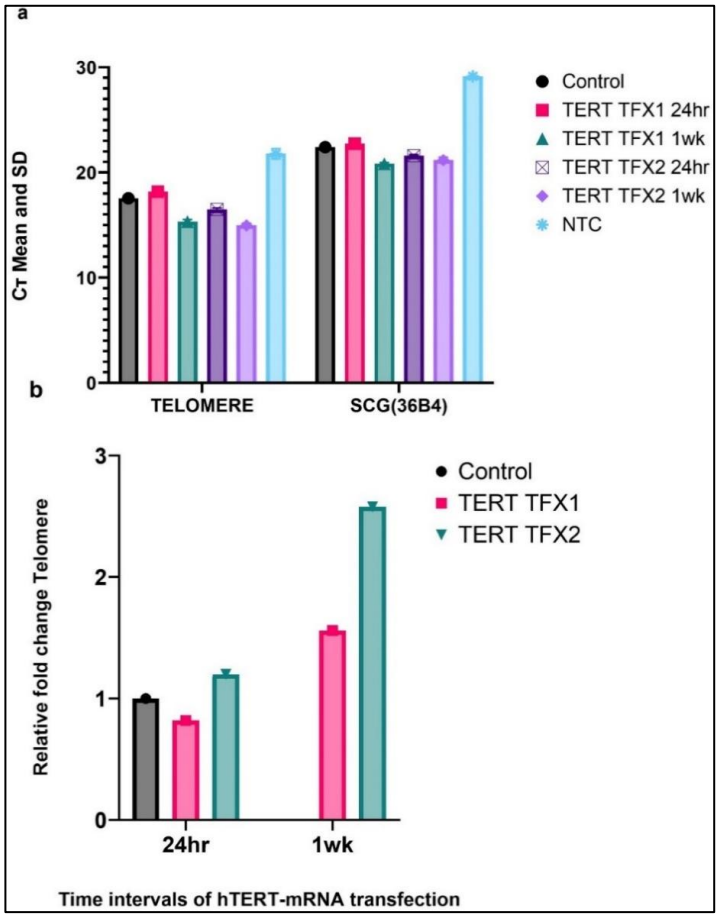

Fig 25: a graph showing the q-PCR results obtained from the different treatments of TR146. **(a)** the mean C_T and standard deviations from triplicates, showing the gene of interest (GOI), telomere and the house keeping gene (HKG) 36B4 SCG. The *eGFP* transfected cells as the control, the *hTERT*-mRNA + *eGFP*-mRNA (9:1) transfected cells as *TERT* TFX for the different time intervals and the number of times of transfection. **(b)** relative fold change ($2^{-\Delta\Delta C_T}$) as a relative measurement of TL for the different treatments analysed. Values shown as relative to eGFP-only TFX (24 hour).

Although, we were now certain of the effectiveness of the synthetic *hTERT*-mRNA from the results obtained in the TR146 cells, the question asked was whether the effectiveness in TR146 was due to the alteration in the mRNA-Lipofectamine MessengerMax™ incubation time, or because the average TL in these cells was extremely low compared to DPSCs?

Therefore, we then set up a new transfection with the DPSCs P9 which had shown the lowest average TL of all DPSCs we had tested, this time using a 25 min mRNA-Lipofectamine™ MessengerMax™ incubation time and using the same transfection protocol giving the best result in the TR146 cells i.e. the post-1-week double transfection of *eGFP* + *hTERT* (1:9).

However, following the second transfection and an incubation time of 1-week, there was much greater cell death than we had seen previously with just one TFX: approximately, 70% of the *hTERT*-mRNA transfected cells and close to 90% of the eGFP transfected cells appeared dead. This was assessed from the appearance of the cells under the microscope, which were rounded and floating. As a result, we were not able to successfully extract any gDNA from that transfection. The non-transfected cells (negative control) had less than 1% cell death. It is possible the double transfection protocol itself caused the toxicity, or it could be prolonged expression and toxicity of *eGFP* that killed the cells (Ansari et al., 2016).

Figure 26: A phase contrast microscopic image of the GFP-mRNA only and the hTERT-mRNA + GFP-mRNA (9:1) transfected cells of DPSC P9 post-1-week incubation

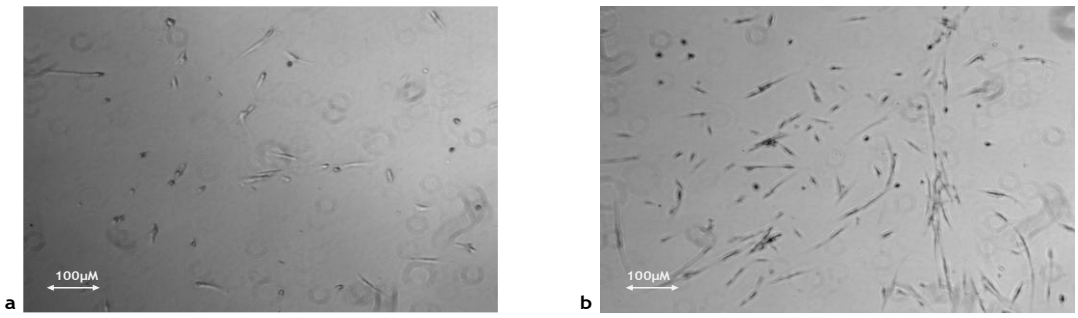

Fig 26: *GFP*-mRNA transfected cells (a) and the *hTERT*-mRNA + *eGFP*-mRNA (9:1) transfected cells (b) of DPSC P9 post 1-week incubation. The difference in cell population is an indication of higher cell death in *eGFP* only transfected cells than *hTERT*-mRNA + *eGFP*-mRNA (9:1) transfected cells.

We set up a new transfection again with DPSC P9, but this time around we only transfected the cells once but used the longer mRNA-Lipofectamine MessengerMax™ incubation time and incubated the transfected cells for 1-week before we extracted the genomic DNA. Although we had some cell death (see ***Figure 26***) it was not as bad as the double transfection and the gDNA yielded was enough for a single q-PCR reaction. The graph on ***Figure 27*** shows the relative fold change ($2^{-\Delta\Delta C_T}$) between the controls and the telomerase transfected DPSCs P9. The results were not different from the previously transfected DPSCs from P6, transfection of *hTERT*-mRNA did not measurably increase average relative TL.

Figure 27: A graphical illustration showing the q-PCR results for the transfection of DPSCs from Passage 9

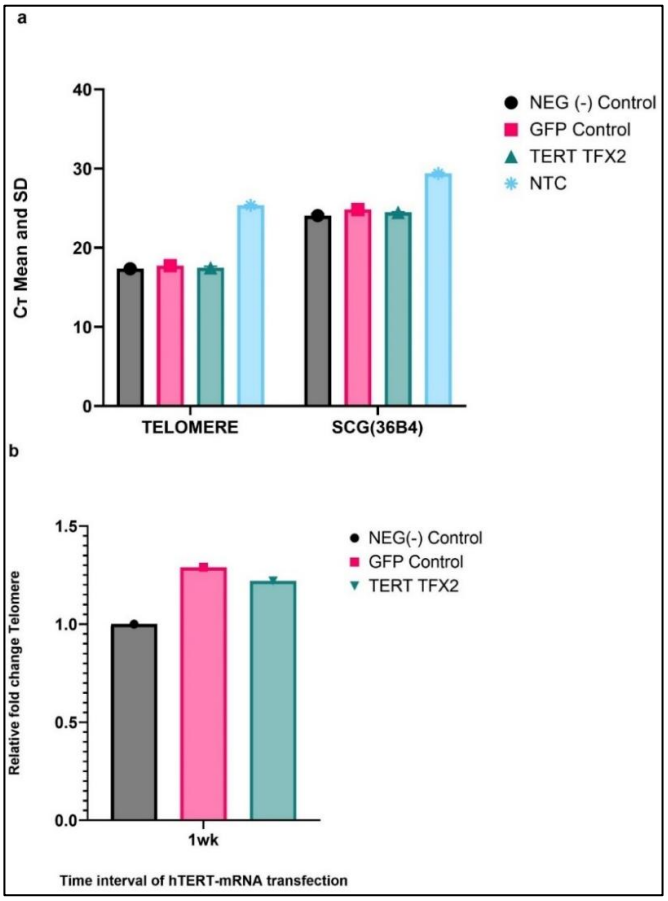

Fig 27: a graph showing the q-PCR results obtained from the different treatment conditions of DPSCs P9. (a) the mean C_T and standard deviations from triplicates, showing the gene of interest (GOI), telomere and the house keeping gene (HKG) 36B4 SCG. The negative control is a measure of the natural length of telomere in the said cells used as a control of the measurement, the *GFP* transfected cell as a control for the transfection and the *hTERT*-mRNA + GFP-mRNA (9:1) transfected shown as *TERT*. (b) relative fold change ($2^{-\Delta\Delta C_T}$) as a relative measurement of TL for the different conditions under analysis.

12.5 Test for Relevant Genes (mRNA) Expression in the DPSC cDNA

Why did we not see the *hTERT*-mRNA causing increased measurable TL in DPSCs? hTERT activity requires the activity of several other proteins for its stability and the stability of the TERC. It was possible that the failure of *hTERT*-mRNA to increase TL in DPSCs might be due to lack of expression of one or more if these in DPSCs therefore we began testing the cDNA from DPSCs for the expression of *NOP10, NHP2, WRAP53* (gene for Cajal body protein), *DKC1, TERC* and *hTERT* by end point PCR as a first step to assessing this (see ***Appendix C for primers***). Due to time constraints, we only had time to analyse early (P2) passage DPSCs. The expected amplicon size of each PCR is shown in ***Table 3***. Products of the RT- and RT+ PCR were run on a 2% gel and the results obtained are shown in ***Figure 29***.

The expected band sizes for each of the RNA products are as follows:

Table 3: Amplicon sizes of the RNA (genes) tested by PCR.

RNA (gene)	Amplicon size
DKC	1555 bp
NHP2	462 bp
NOP10	195 bp
TERC	451 bp
TERT	3399 bp
WRAP53	❖ 187 bp / 1127 bp / 707 bp

We have used three different pairs of primers for the *WRAP53* RNA; therefore, the different amplicon sizes are dependent on the sets of primer used (see ***Figure 28***). The gene diagram below (***Figure 28***) is a relevant guide to understanding the primers used in this part of the experiment and thus, give a better understanding of the primer combination of the *WRAP53* gene.

Figure 28: Cartoon representation of the genes tested for showing the primer locations, amplicon sizes and the length of the mRNA

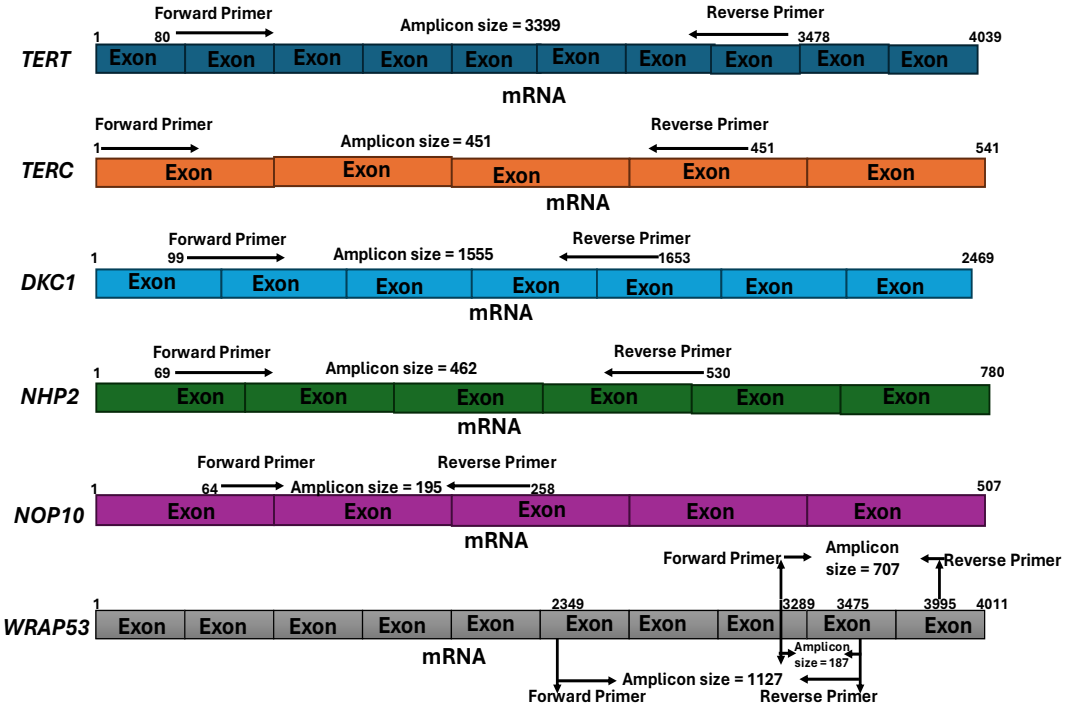

Fig 28: diagram of the different genes tested for with the position and amplicon size of the primers used.

All the genes tested for were expressed as shown from the bands and amplicon sizes on the gel image, except for *DKC* and *hTERT*. The primers are designed to amplify the ORF of the mRNA of the all the genes mentioned above.

Figure 29: Gel electrophoresis image of PCR products for RT+ and RT- showing the bands and sizes of relevant telomerase activity genes expressed in DPSCs

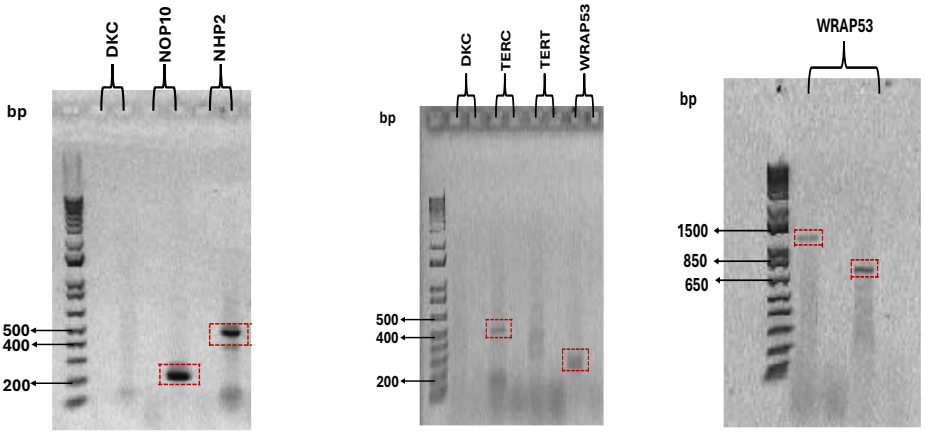

Fig 29: gel images of the RT-PCR products for *DKC*, *NHP2*, *NOP10*, *TERC*, *TERT* and *WRAP53* mRNA against 1 kb^{+} DNA Ladder.

The results obtained from the gel electrophoresis images shows the right amplification for the *NHP2*, *NOP10*, *TERC* and *WRAP53*. However, no true amplicon sizes were observed for the DKC and the hTERT genes. The test for *DKC1* gene which encodes the protein, dyskerin (Kanegane et al., 2005) is essential for the accumulation of the *TERC* in telomerase activity. Dyskerin forms a complex with *NOP10*, and *NHP2* to stabilise the *TERC* (Shukla et al., 2016), although our results showed no amplification of the *DKC* mRNA suggesting negligible expression in even early passage DPSCs. However, this would need to be confirmed with a cDNA from a positive control, such as hematopoietic stem cells (Elwood, 2004), male germ cells, and embryonic stem cells, which are known to have high level of telomerase activity (RoccaForesta and Ferlin, 2019).

13 GENERAL DISCUSSION

The basis for our studies was that stem cells including DPSCs, have a limitation in their potential usage in regenerative medicine due to the lack of long-term proliferation capacity *in-vitro* (finite expandable growth limit) (Hayflick and Moorhead, 1961, Wang et al., 2016), which is commonly associated with telomere shortening, an indication of cell aging. We aimed to see if a synthetic mRNA could be made for hTERT that would extend the lengths of telomeres in DPSCs.

13.1 Cloning of the Telomerase Sequence and Other Improvements to Consider in the Design of the Synthetic mRNA

The plasmid from Addgene we got that had the telomerase mRNA sequence was found to have a mutation within the coding region, resulting in the change of the amino acid from aspartic acid to glycine. This polymorphism was then corrected by site mutagenesis (see ***Figure 8***); however, the presence of this mutation is a significant finding as it affected a well conserved region of the gene. The sequence of the plasmid described by Addgene also had this mutation, so it did not occur after shipment and growth of the plasmid in our laboratory.

There had been reports of the identification of variants of the *TERT* gene (rare mutations) by a few papers, which were detected from next generation sequence results of patients with certain genetic disorders, such as aplastic anaemia and idiopathic pulmonary fibrosis (Selb et al., 2022, Virijevic et al., 2024). A list of known amino acid changes in *hTERT* and base changes in *hTERC* with the diseases associated with the mutations are published by (Hills and Lansdorp, 2009). However, all the mutations recorded in these papers are different from the one we found in our plasmid.

Following the correction of the polymorphism, the plasmid was successfully transcribed into an *hTERT*-mRNA, however, there is room for improvements in the design of the synthetic mRNA used in this research, most of which are achievable and cost effective. The *hTERT*-mRNA used was transcribed in a two-step method; transcription then followed by polyadenylation. This method was used in the preparation of most the mRNAs used in the Hamilton laboratories including *eGFP*, and that the addition of the poly-A tail was evident as observed in the shift in the

size of the mRNA before and after polyadenylation. This addition of the Poly-A tail usually varies, and ranges between 50–200 nts, although it had proven to be effective, an alternative method to this, involves the cloning and amplification of the plasmid containing the Poly-A tail before transcription in a one-step method. In this method, the polyadenylation of the mRNA is a co-transcriptional step and gives a more consistent length of poly-A tail in the mRNA produced. This method was used to successfully synthesize *eGFP*-mRNA designed in the Hamilton labs and was seen to have a better transfection efficiency, as compared to a different synthesised *eGFP*-mRNA done with the two-step method. However, it can be difficult to grow plasmids with such long homopolymeric regions.

Preparation of synthetic mRNA in our laboratory was improved by the optimisation of the coding region. We substituted the normal UTP with the N1-methyl pseudouridine triphosphate, and this had shown an improved transfection efficiency with the *eGFP*-mRNA. However, this could further be improved by substituting both uridine and cytidine with N1-methyl pseudouridine and 5-methyl cytidine, modifications done by another research group to improve the expression of tropoelastin (*TE*) (Golombek et al., 2023). The results presented by this research group explained that modified synthetic *TE*-mRNA with N1-methyl pseudouridine and 5-methyl cytidine showed the highest translation of the protein and simultaneously reduced immunogenicity, when compared to all other modifications including N1-methyl pseudouridine and normal cytidine.

Another useful consideration in the design of the synthetic mRNA is to utilize different 3’ UTRs to test the distinct levels of expression. The phTERT-mRNA used in this project was digested with EcoR1 restriction enzyme, that cuts immediately downstream of the *hTERT* ORF, thus cutting off the BGH 3’ UTR of the phTERT-mRNA before being successfully transcribed into the *hTERT*-mRNA. This approach had been successfully used in the lab for *eGFP* (Andrew Hamilton, *personal communication*). It was based on the idea that, apart from the Poly-A cleavage addition site, the sequences in 3’ UTRs mainly attract factors (e.g. miRNA) that lower translation. This approach is supported by the recent findings of Mamaghani *et al*. who also showed 3’ UTRs to be unnecessary for effective synthetic mRNA (Mamaghani et al., 2024). Nevertheless, a comparison of the expression of the

hTERT or *eGFP* (also prepared through in vitro transcription) tagged with different 3' UTRs could also be evaluated, with the level of expression to be measured in DPSCs as these are the target cells of interest. The different UTRs, such as the α-globin and ß-globin that expressed genes encoding proteins with greater half-life, as well as the hepatitis B virus and the bovine growth hormone (Jia and Qian, 2021) could also be tested.

13.2 Exploring FISH in DPSCs and Other Hybridisation methods.

The main objective of this research was to relatively measure the effects of telomerase mRNA in increasing TL transfected DPSCs as compared to wild type DPSCs, in which the FISH method would have been appropriate and more direct. The FISH technique had shown promising results in detecting the telomeres of C2C12 mouse cells (***Figure 12***); however, this was not the same for our DPSCs (***Figure 13***) due to background fluorescence. Our results for telomere measurement by FISH in DPSCs was limited by the background problem, which was not due to the Telomere ×5 probe, and therefore, other methods would be needed to resolve this problem should this approach be further investigated. Most studies that used FISH to quantify TL did not seem to have a background problem in their assay, although, many of them were TL analysis of cancerous and benign cells. Other probe types could increase signal strength which might overcome the background noise. One alternative method worthy of trying is the use of locked nucleic acids (LNA) probes which have been adapted recently rather than the DNA probes. The latter have been associated with low quality outputs such as sensitivity to nucleases, low target site accessibility, low hybridisation affinity and low cellular permeability, and these limitations are overcome by using the LNA FISH probes (Azevedo et al., 2019). Other literatures suggest the use of unlabelled nucleic acid probes as pre-treatment for so-called suppression hybridisation to overcome the non-specific background fluorescence (Frickmann et al., 2017). Most of the common notable optimisation for this type of assays such as the hybridisation time and temperature, probe concentrations and cell denaturation and fixing, which are necessary to produce desirable results were all tried but the background problem remained.

However, there are a variety of methods used to measure TL of different sample types and for various purposes other than the ones used in this research, each of them providing different information on TL, each having variable merits and demerits, ranging from cost, labour intensity, amount of sample, time, and constraints (difficulty) (Zanet et al., 2013, Lindrose et al., 2021, FerrerStephens and Kocher, 2023).

In a comparative study of the different methods of assessing telomere lengths in different laboratories, the results showed variations for both inter-laboratory and intra-laboratory technique (Martin-Ruiz et al., 2015). Martin-Ruiz *et al*. employed three different techniques; southern blotting, qPCR and single telomere length analysis (STELA), in which a very small number of the labs used Southern blotting or STELA. The coefficient of variations was larger in the qPCR technique, although this technique was performed by more than 50% of the laboratories.

Telomere restriction fragment (TRF) is a technique that requires substantial amount of DNA that quantifies TL by digesting the non- telomeric fragments and then separating the telomere fragments by size followed by southern blot or in-gel hybridisation and specific detection of telomere sequences using labelled complementary hybridisation probes (Baird, 2005). This technique would not have been useful for our research to measure TL of DPSC population because of the small amount of DNA available in our experimental workflow. The method also lacks the sensitivity to detect very short fragments and, hence, is unable to reliably quantify TL of senescent cells which might exist in our populations of DPSCs.

STELA technique uses telomere linkers (telorette) and primers to quantify TL of individual chromosomes rather than average lengths (FerrerStephens and Kocher, 2023). The method was more likely to give detail effects of the telomerase expression on specific chromosomes, however, like TRF the technique is both labour intensive (tedious) and time consuming. Hence, not entirely suitable for the duration of the research.

This work is preliminary research to test the effect of mRNA encoding telomerase gene on DPSCs, however, follow up research should consider using RT-PCR to test for senescent markers in DPSCs such as p53, p21, and p16 or senescence-

associated ß-galactosidase staining. The relationship between these biomarkers and TL as an alternative method to measure telomere erosion in DPSCs.

The most common method used in telomere measurement is the monoplex or singleplex q-PCR, a cost-effective method with the need for fewer resources (Verhulst et al., 2015, Martin et al., 2024).

13.3 q-PCR and New Developments in TL Measurement

The method used in this project is the monoplex q-PCR method originally designed by Richard Cawthon (2002), which was quite efficient except for the problem with the amplification in the NTC (***Figure 16***). The amplification in the NTC was investigated by running q-PCR products on a gel (***Figure 17***), and the problem was linked to primer dimer formation which was negligible in our gDNA samples. Although this problem was persistent throughout the experiment, we are confident that it will likely not influence the outcome of our results otherwise.

However, a recent and more advanced q-PCR method referred to as the monochrome multiplex q-PCR method also explained by Cawthon (2009), is designed to increase precision, and reduce the variability of T/S ratio (Martin et al., 2024). This method utilises a single reporter intercalating dye for both the reference and target signals within the same reaction tube. Unlike the singleplex method, this method is believed to be much more difficult. However, this new technique may not be the solution to the signals we have in the NTC.

Future work on q-PCR to measure TL may involve replacing the Sygreen Hi-ROX Master Mix (PCR Biosystems) used in this research to the Power SYBR I Master Mix (Applied Biosystems, #4367396); contains AmpliTaq Gold DNA polymerase, dNTPs, SYBR I Green Dye, optimised buffers and passive reference dye (ROX), used by O'Callaghan and Fenech (2011). A change in the q-PCR Master Mix could make all the difference regarding the signals in the NTC, since the ingredients in the two Master Mixes are most likely different.

13.4 TL in Wild Type DPSCs

A research paper (Mokry et al., 2010) reported that DPSCs, despite the ability to maintain their phenotypic and genotypic properties in extensive *in-vitro*

conditions, have a lower proliferation and prolonged doubling time following long-term *in-vitro* cultivation, due to telomere erosion.

From our data (***Figure 18***), the TL of wild type DPSCs from passage 2 and those of passage 8 showed a very narrow difference in their TL although, the DPSCs from passage 8 were shorter as expected. Our subsequent findings, however, indicated a large decrease in the natural TL of DPSCs from passage 2 to passage 9 (***Figure 19***), and the cell proliferation of these cells were quite slower, when compared to the cells from earlier passages including P8. We were only able to achieve about 50% confluence when we cultured these P9 cells *in-vitro* for 2 weeks (indicating a prolonged population doubling time). A few findings have reported an observed relationship between TL and passage number, and that TL of DPSCs decreases as the number of passages increases (Mokry et al., 2010, Pilbauerova et al., 2021). The data spread presented by Mokry *et al*. (2010), which showed the relationship between passage number versus TL, and passage number versus population doubling time, were similar to our findings. Their results showed a decline in TL as the number of passages (P2–P16) increases, but the decline was not very linear. Therefore, the difference in TL between our P8 or P9 could be a real reflection of a sudden decline in TL, but could also be by chance because we only looked at one sample of each.

We have mentioned in the introduction that DPSCs have shown variable biological properties including TL, associated with its niche and or heterogeneity. TL of DPSCs that exhibit multipotency, high proliferative and self-renewal capabilities range between 18-20 kb, while TL equivalent for low proliferative populations ranges between 5–13 kb (Alraies et al., 2017). The cells used in this research were isolated from heterogeneous population, therefore, the likelihood of individual cell chromosomes having high variation in TL is high. The q-PCR method used in this research, gives a relative TL measure of the entire cell population rather than the individual cell chromosome. In principle, any increase in total telomere amount should be detectable by this method irrespective of whether this is an extension of highly homogenous-lengthened telomeres or highly heterogenous-lengthened telomeres. It ought to be more sensitive to changes in TL where overall telomere amount is low (e.g. older DPSCs) compared to where overall TL is high

(e.g. already highly proliferative cells) as the proportional change caused by telomere expression would be smaller in the latter.

Physically isolating the different sub-population of heterogeneous DPSCs based on population doubling times to have a homogeneous sample population prior to transfection could improve the q-PCR measurement quality and reduce errors and biasness. It would allow us to test the effects of telomerase mRNA TFX on populations from low or high proliferative DPSCs sub-population (Alaidaroos et al., 2021). If these different populations were differently sensitive to mRNA TFX then this might allow differences in TL to be detected more easily.

In comparing the natural TL of the DPSCs to 2 other human cancer cell lines (TR146 and HCT116), the results (***Figure 20***) produced indicated that the TL of the DPSCs were longer than those of the cancer cells. Our results are in agreement with the research conducted by another group that compared the TL and telomerase activity of stem cells, including DPSCs, to 3 other cancer cell lines (Jeon et al., 2011). A notable feature of cancer cells is dysregulated proliferation and their resistance to programmed cell death.

Critically shortened TL in healthy human cells triggers activation of DNA damage pathways like the *p53,* leading to induced cell senescence or apoptosis once the telomere checkpoint mark is reached (Roth et al., 2007). However, cancer cells evade these checkpoints thus resulting in genomic instability and dysfunctional telomeres. Most cancer cells maintain their TL between 2–6 kb, whilst adult human stem cells are between 7–13 kb (Kelland, 2005). To sustain proliferation, tumour cells maintain the lengths of their telomeres to a certain degree, mostly by the reactivation of the telomerase gene (Kelland, 2005, Hills and Lansdorp, 2009).

13.5 mRNA Transfection in DPSCs

The transfection of DPSCs with the *eGFP*-mRNA showed a high efficiency, more than 90% of the cells were transfected. These results showed a promising approach for reprogramming of DPSCs using mRNA transfection for other traits besides telomerase, a technique worth exploring to enhance the uses of these cells because of all the advantages synthetic mRNA has over DNA based methods, as already discussed.

The phase contrast microscopic images shown in this report (see ***Figure 26***) had indicated toxicity of the transfection, although we had not shown the image of the non-transfected (negative control) cells which, in hindsight, should have been taken as a good reference. No assay was used at this point to measure cell death as we used the same cells for gDNA extraction and q-PCR hence, we avoided all forms of staining that could potentially affect our TL analysis. Thus, the judgement was based on physical observation of the cells (floating and round shape cells). mRNA transfection of DPSCs resulted in a large amount of cell death, after transfecting with double transfection and a longer incubation (1-week) and especially in later passages (DPSC P9). Those cells (DPSC P9) had an extremely low proliferation rate, hence, a very low density of the cells from P9 were used in the transfection to begin with, in comparison to DPSC P6 and TR146 cells. The reduction in transfected DPSC P9 cell population also seemed larger in *GFP*-only transfected DPSCs as compared to the *hTERT* + *GFP* transfected cells. Ansari *et al*. (2016) presented that cells expressing *GFP* are susceptible to death, due to several factors; including immunogenicity (Yang et al., 2014b), free radical oxygenation, and other mechanisms. The fluorescence of the protein achieved through excitation by photoactivation also results into the induction of phototoxic effects (Ansari et al., 2016). However, this cannot completely account for the post-TFX death. It is possible the cell death is also related to the mRNA quality. For example, trace amounts of dsRNA can be produced during *in-vitro* transcription reactions (Poynter and DeWitte-Orr, 2018, Son et al., 2024), which could trigger innate immune receptors and lead to death. In future, it would be wise to check mRNA for contaminating dsRNA for example by using the J2 antibody which recognises dsRNA. Finally, the lipofectamine may cause cytotoxicity to late passage DPSCs. Some toxicity of reagents used in the transfection of mRNA has been mentioned (Sakurai et al., 2022). Transfection with this reagent alone would be a good test and there are other RNA transfection reagents that could be tried if MessengerMax™ proved to be to toxic to late passage DPSCs. Also, future *hTERT*-mRNA transfection should test the effect of the *hTERT*-mRNA only transfection on DPSCs, as it is possible that eGFP toxicity might somehow have inhibited *hTERT* in DPSCs.

All *hTERT*-mRNA + *GFP*-mRNA (9:1) transfected DPSCs gDNA showed no sign of measurably increased TL with either DPSC from P9 or cells with slightly longer telomeres (DPSC P6) (***Figures 23*** **and** ***27***).

Findings reported by Alraies *et al.* (2017) discussed that wild type DPSCs show no expression or negligible expression for the *hTERT* gene (Alraies et al., 2017, Alaidaroos et al., 2021). Since hTERT activity requires other proteins to function, it is possible that these proteins are not efficiently expressed in DPSCs. This could be a plausible explanation as to why the synthetic *hTERT*-mRNA shows negative effect in DPSCs.

However, the transfection with the *hTERT*-mRNA + *GFP*-mRNA (9:1) worked perfectly on the TR146 human cancer cells (***Figure 25***), suggesting the mRNA was effective at encoding hTERT protein. This should be checked by Western blot for transfected DPSCs in future.

Cancer cells naturally reactivate telomerase to sustain cell proliferation (Kelland, 2005, Hills and Lansdorp, 2009), and Hills and Lansdorp (2009) have also mentioned overexpression of *hTERT, hTERC* and *DKC* in malignant cells. Thus, a sufficient expression of telomerase associated proteins in wild type cancer cells is a reasonable explanation for the successful transfection of TR146 with the synthetic *hTERT*-mRNA. However, telomeres and telomerase reverse transcriptase behaves differently in cancer cells for reasons not fully comprehended (Armstrong and Tomita, 2017).

Despite the anomaly in telomere and telomerase behaviour in cancer cells, the extension of TL in transfected TR146 cells presented in our results was not entirely due to natural telomere maintenance, but a positive response to the *hTERT*-mRNA. The differences in TL of the different treatments (***Figure 25***) strongly supports that claim. Our data for the relative TL expressed as fold difference between the single telomerase transfected cells and the double telomerase transfected cells was greater than 1 after 1-week of incubation.

The results presented in this research have shown no increase in the relative TL of the DPSC population post *hTERT*-mRNA transfection. This does not entirely prove that TL of individual cells within the sample population of DPSCs tested

were in fact not extended, this is due to inability of the said method to give details of measurement on the TL on a single chromosome/cell.

Telomerase activity is active during cell replication stage (s-phase), and cells in the M-phase (non-replicative stage) loses telomerase activity (Zhu et al., 1996). Therefore, transfected DPSCs in the M-phase will likely not have telomerase expression, thereby resulting in no measurably increased TL in those cells. However, it is unlikely that all the cells in the transfected sample to be in the same phase, and the mitotic phase is a short phase. It is not clear how long the cell cycle of DPSCs lasts or how long the telomerase mRNA last in these cells, as a result, we assess the transfected cells based on two different time points. We anticipated the different time points will contribute to the mRNA uptake and translation rate as well as the extent of cell proliferation.

An advanced new sequencing technique for TL measurement, next generation nanopore sequencing, is a promising alternative in measuring the TL of individual chromosomes and could provide a more detailed and better resolution of the effect of the *hTERT*-mRNA transfection on individual cells. Also, the biomarker for aging in most stem cells is a measure of the shortest telomere rather than the average TL (Tham et al., 2023). Therefore, the need to measure the absolute TL of individual cells is not only paramount to deduce the effect of the *hTERT*-mRNA transfection, but would provide a better understanding of the age-related senescence.

13.6 What Other Factors are Needed to Improve hTERT Expressions in DPSCs?

The hTERT activity as reported earlier requires other proteins for its success, maintenance, and stability. A few of these genes were tested by end point PCR of the cDNA to investigate their presence. However, not all of them were tested (other important genes such as *GAR1* and *TCAB1* were not tested for) and the *hTERT* and *DKC1* genes were negligible in DPSCs as shown in the results (***Figure 29***). A diverse set of primers for *DKC1* and the *hTERT* could have been used similar to those designed for the *WRAP53*, it could possibly have made a difference as sometimes certain primer combinations simply do not work. The large amplicon sizes of these genes, DKC1; amplicon size 1.5kb and hTERT; amplicon size 3.3kb, could result to the lack of detection. Hence, designing shorter amplicon sizes

within the ORF as accomplished for the WRAP53 is an approach worth trying for the DKC1 and the hTERT genes. The expression and activation of these genes is an important aspect of telomerase activity and telomere elongation. Therefore, the investigation of these proteins in DPSCs is required to widen our understanding of telomerase activity in DPSCs. Our experiment did not test for the proteins directly, rather we tested the genes using mRNA by RT-PCR, these were not a direct translation of the presence and expression of the said proteins and how much of each was present in the cells. Future work could further investigate the expression of all the proteins required to support telomerase activity in DPSCs by Western blots and determine the degree of their expression.

13.7 Future Work

Future work might involve co-expression of other factors from synthetic mRNA such as those described by Orimoto et al. (see ***Section 7.5***) (Orimoto et al., 2020), or the co-expression of mRNA encoding relevant genes required for telomerase activity such as *DKC* and the effect these will have on the cell proliferation using methods such as EdU (5-ethynyl-2-deoxyuridine) which detects and quantifies cell proliferation in live mammalian cells using a flow cytometry or fluorescence microscopy. The method measures the syntheses of DNA, where the proliferation capacity of the cell has a direct relationship with the amount of DNA synthesized.

Furthermore, checking the different lengths of telomere by q-PCR in different passages of DPSCs and comparing them to other stem cells in which telomerase activity is known to be active such as hematopoietic stem cells or embryonic stem cells, will help evaluate the level of telomere erosion and the effect on senescence and proliferation of DPSCs.

13.8 Conclusion

In summary we have confirmed:

- The successful synthesis of the phTERT-mRNA to a synthetic hTERT-mRNA.
- q-PCR was a useful method to estimate overall relative TL, but further optimisation to eliminate possible artefacts would be beneficial.
- The synthetic mRNA had a positive effect on transfected TR146 TL as measured by q-PCR.

- However, *hTERT*-mRNA had no effect on DPSCs, hence, TL were not measurably increased in those cells by the method used in this research.
- The need to further investigate other factors that could essentially support the expression of TERT in DPSCs is crucial and important to improve the *in-vitro* life span of the DPSCs to meet its potential usage in therapeutics and clinical trials.

14 APPENDICES

14.1 Appendix A: PCR Oligonucleotides (Primers)

Name of Oligo	Sequence (5' – 3')
hTERT 5.1	GAAACGTCTCACATGCCGCGCGCTCCCCGCTG
hTERT 3.1	GAAAGAATTCTCAGTCCAGGATGGTCTTGAAGTCT
hTERT seq1	GGCCCGTTCGCATCCCAGAC
hTERT seq2	GGGCAGTGCGTCTTGAGGAG
hTERT seq3	GGCCCTGTGGATATCGTCCA
hTERT seq4	TTGAAGGTGAGACTGGCTCTG
hTERT correct5	ACTGCGCTTGGCTGCGCAG
hTERT correct3	CCCGCACGCTCATCTTCCAC
T7prom CC	TAATACGACTCACTATAAGG
SAA mut chk	GCTTCTTTTCGTTCCTTGGC
BGHrev	TAGAAGGCACAGTCGAGG

14.2 Appendix B: q-PCR Oligonucleotides (Standards and Primers)

Name of Oligo	**Sequence (5' – 3')**
Tel Standard	TTAGGGTTAGGGTTAGGGTTAGGGTTAGGGTTAGGGTTAGGG TTAGGGTTAGGGTTAGGGTTAGGGTTAGGGTTAGGGTTAGGG
36B4 Standard	CAGCAAGTGGGAAGGTGTAATCCGTCTCCACAGACAAGGCCAG GACTCGTTTGTACCCGTTGATGATAGAATGGG
Telo F	CGGTTTGTTTGGGTTTGGGTTTGGGTTTGGGTTTGGGTT
Telo R	GGCTTGCCTTACCCTTACCCTTACCCTTACCCTTACCCT
Cawthon Tel1	CGTTTTTGAGGGTGAGGGTGAGGGTGAGGGT
Cawthon Tel2	TCCCGACTATCCCTATCCCTATCCCTATCCCTATCCCTA
36B4 F	CAGCAAGTGGGAAGGTGTAATCC
36B4 R	CCCATTCTATCATCAACGGGTACAA

14.3 Appendix C: RT-PCR Oligonucleotides (Primers)

hTERT 5.2	ATGCCGCGCGCTCCCCG
hTERT 3.2	TCAGTCCAGGATGGTCTTGAAGTCT
hTERC 5	GGGTTGCGGAGGGTGGG
hTERC 3	GCATGTGTGAGCCGAGTCCTGGG
DKC15	TAACATGGCGGATGCGGAAG
DKC13	CCTTCACTACTCAGAAACCAATTCTACCTCT
NHP25	ATGACCAAAATAAAGGCAGATCCCG
NHP23	TCATAGGGGTAGGGGCAGGGAC
NOP10 5	ATGTTTCTCCAGTATTACCTCAACGAGC
NOP10 3	TCAGAGGACAGGGCGCGGTT
WRAP53 5	ATGAAGACTTTGGAGACTCAACCGTTAGC
WRAP53 3	TTATATCAGCTCACCCACACCTCCCT
WRAP53 5.2	TCCGAGCCACATTTGCAAAA
WRAP53 3.2	TGAAAGCAGAGGTGGGTGAT

14.4 Appendix D: Composition of Buffers and Reagents

TBE (5×): 54 g of Tris base, 27.5 g of boric acid and 20 mL of EDTA

Formaldehyde: 300 – 400 mg of paraformaldehyde, 800 µL of ultra-pure water, 50 µL of NaOH, heat the mixture at 67 °C for 20 min.

FISH Buffer: 50% deionised formamide, 2× standard saline citrate buffer (SSC), 10% dextran sulphate, 20 µg. mL^{-1} tRNA from *E. coli*.

Telomerex5 probe: Sequence 5' – [Cyanine3] CCCTAACCCTAACCCTAACCCTAACCCTAA

15 REFERENCES

AAN, G. J., HAIRI, H. A., MAKPOL, S., RAHMAN, M. A. & KARSANI, S. A. 2013. Differences in protein changes between stress-induced premature senescence and replicative senescence states. *Electrophoresis,* 34**,** 2209-17.

ACEVEDO, J. M., HOERMANN, B., SCHLIMBACH, T. & TELEMAN, A. A. 2018. Changes in global translation elongation or initiation rates shape the proteome via the Kozak sequence. *Sci Rep,* 8**,** 4018.

ALAIDAROOS, N. Y. A., ALRAIES, A., WADDINGTON, R. J., SLOAN, A. J. & MOSELEY, R. 2021. Differential SOD2 and GSTZ1 profiles contribute to contrasting dental pulp stem cell susceptibilities to oxidative damage and premature senescence. *Stem Cell Res Ther,* 12**,** 142.

ALGAMA, M., OLDMEADOW, C., TASKER, E., MENGERSEN, K. & KEITH, J. M. 2014. Drosophila 3' UTRs are more complex than protein-coding sequences. *PLoS One,* 9**,** e97336.

ALRAIES, A., ALAIDAROOS, N. Y., WADDINGTON, R. J., MOSELEY, R. & SLOAN, A. J. 2017. Variation in human dental pulp stem cell ageing profiles reflect contrasting proliferative and regenerative capabilities. *BMC Cell Biol,* 18**,** 12.

ANDERSON, B. R., MURAMATSU, H., NALLAGATLA, S. R., BEVILACQUA, P. C., SANSING, L. H., WEISSMAN, D. & KARIKO, K. 2010. Incorporation of pseudouridine into mRNA enhances translation by diminishing PKR activation. *Nucleic Acids Res,* 38**,** 5884-92.

ANDREEV, D. E., TERENIN, I. M., DMITRIEV, S. E. & SHATSKY, I. N. 2016. Pros and cons of pDNA and mRNA transfection to study mRNA translation in mammalian cells. *Gene,* 578**,** 1-6.

ANDRIES, O., MC CAFFERTY, S., DE SMEDT, S. C., WEISS, R., SANDERS, N. N. & KITADA, T. 2015. N(1)-methylpseudouridine-incorporated mRNA outperforms pseudouridine-incorporated mRNA by providing enhanced protein expression and reduced immunogenicity in mammalian cell lines and mice. *J Control Release,* 217**,** 337-44.

ANSARI, A. M., AHMED, A. K., MATSANGOS, A. E., LAY, F., BORN, L. J., MARTI, G., HARMON, J. W. & SUN, Z. 2016. Cellular GFP Toxicity and Immunogenicity: Potential Confounders in in Vivo Cell Tracking Experiments. *Stem Cell Rev Rep,* 12**,** 553-559.

ANTONIOLI, E., TORRES, N., FERRETTI, M., PICCINATO, C. A. & SERTIE, A. L. 2019. Individual response to mTOR inhibition in delaying replicative senescence of mesenchymal stromal cells. *PLoS One,* 14**,** e0204784.

ARMSTRONG, C. A. & TOMITA, K. 2017. Fundamental mechanisms of telomerase action in yeasts and mammals: understanding telomeres and telomerase in cancer cells. *Open Biol,* 7.

ASRANI, K. H., FARELLI, J. D., STAHLEY, M. R., MILLER, R. L., CHENG, C. J., SUBRAMANIAN, R. R. & BROWN, J. M. 2018. Optimization of mRNA untranslated regions for improved expression of therapeutic mRNA. *RNA Biol,* 15**,** 756-762.

AZEVEDO, A. S., SOUSA, I. M., FERNANDES, R. M., AZEVEDO, N. F. & ALMEIDA, C. 2019. Optimizing locked nucleic acid/2'-O-methyl-RNA fluorescence in situ

hybridization (LNA/2'OMe-FISH) procedure for bacterial detection. *PLoS One,* 14**,** e0217689.

BALMAYOR, E. R. 2022. Synthetic mRNA - emerging new class of drug for tissue regeneration. *Curr Opin Biotechnol,* 74**,** 8-14.

BAR, C. & BLASCO, M. A. 2016. Telomeres and telomerase as therapeutic targets to prevent and treat age-related diseases. *F1000Res,* 5.

BARAJAS GALINDO, D. E., RAMOS BACHILLER, B., GONZALEZ ROZA, L., GARCIA RUIZ DE MORALES, J. M., SANCHEZ LASHERAS, F., GONZALEZ ARNAIZ, E., ARIADEL COBO, D., BALLESTEROS POMAR, M. D. & RODRIGUEZ, I. C. 2022. Increased incidence of Graves' disease during the SARS-CoV2 pandemic. *Clin Endocrinol (Oxf).*

BASIOUNI, S., FUHRMANN, H. & SCHUMANN, J. 2012. High-efficiency transfection of suspension cell lines. *Biotechniques,* 53.

BERKOVITS, B. D. & MAYR, C. 2015. Alternative 3' UTRs act as scaffolds to regulate membrane protein localization. *Nature,* 522**,** 363-7.

BERTOLO, A., BAUR, M., GUERRERO, J., POTZEL, T. & STOYANOV, J. 2019. Autofluorescence is a Reliable in vitro Marker of Cellular Senescence in Human Mesenchymal Stromal Cells. *Sci Rep,* 9**,** 2074.

BRAUN, K. A. & YOUNG, E. T. 2014. Coupling mRNA synthesis and decay. *Mol Cell Biol,* 34**,** 4078-87.

CAWTHON, R. M. 2002. Telomere measurement by quantitative PCR. *Nucleic Acids Res,* 30**,** e47.

CENTENO, C. J., AL-SAYEGH, H., FREEMAN, M. D., SMITH, J., MURRELL, W. D. & BUBNOV, R. 2016. A multi-center analysis of adverse events among two thousand, three hundred and seventy two adult patients undergoing adult autologous stem cell therapy for orthopaedic conditions. *Int Orthop,* 40**,** 1755-1765.

CENTENO, C. J., AL-SAYEGH, H., FREEMAN, M. D., SMITH, J., MURRELL, W. D. & BUBNOV, R. 2018. Correction to: A multi-center analysis of adverse events among two thousand, three hundred and seventy two adult patients undergoing adult autologous stem cell therapy for orthopaedic conditions. *Int Orthop,* 42**,** 223.

CHAN, A., NAARMANN-DE VRIES, I. S., SCHEITL, C. P. M., HOBARTNER, C. & DIETERICH, C. 2024. Detecting m(6)A at single-molecular resolution via direct RNA sequencing and realistic training data. *Nat Commun,* 15**,** 3323.

CHAUDHARY, N., WEISSMAN, D. & WHITEHEAD, K. A. 2021. mRNA vaccines for infectious diseases: principles, delivery and clinical translation. *Nat Rev Drug Discov,* 20**,** 817-838.

CHENG, G., KONG, F., LUAN, Y., SUN, C., WANG, J., ZHANG, L., JIANG, B., QI, T., ZHAO, J., ZHENG, C. & XU, D. 2013. Differential shortening rate of telomere length in the development of human fetus. *Biochem Biophys Res Commun,* 442**,** 112-5.

CONTE, M., CAROFIGLIO, M., ROSSO, G. & CAUDA, V. 2023. Lipidic Formulations Inspired by COVID Vaccines as Smart Coatings to Enhance Nanoparticle-Based Cancer Therapy. *Nanomaterials (Basel),* 13.

CORTAZAR, M. A., SHERIDAN, R. M., ERICKSON, B., FONG, N., GLOVER-CUTTER, K., BRANNAN, K. & BENTLEY, D. L. 2019. Control of RNA Pol II Speed by PNUTS-PP1 and Spt5 Dephosphorylation Facilitates Termination by a "Sitting Duck Torpedo" Mechanism. *Mol Cell,* 76**,** 896-908 e4.

CUI, T., FAKHFAKH, K., TURNEY, H., GULER-GANE, G., TOLOCZKO, A., HULLEY, M. & TURNER, R. 2023. Comprehensive studies on building a scalable downstream process for mRNAs to enable mRNA therapeutics. *Biotechnol Prog,* 39**,** e3301.

DEL CAMPO, C., BARTHOLOMAUS, A., FEDYUNIN, I. & IGNATOVA, Z. 2015. Secondary Structure across the Bacterial Transcriptome Reveals Versatile Roles in mRNA Regulation and Function. *PLoS Genet,* 11**,** e1005613.

DRZENIEK, N. M., KAHWAJI, N., PICHT, S., DIMITRIOU, I. M., SCHLICKEISER, S., MORADIAN, H., GEISSLER, S., SCHMUECK-HENNERESSE, M., GOSSEN, M. & VOLK, H. D. 2024. In Vitro Transcribed mRNA Immunogenicity Induces Chemokine-Mediated Lymphocyte Recruitment and Can Be Gradually Tailored by Uridine Modification. *Adv Sci (Weinh),* 11**,** e2308447.

DUNN, E. A. & RADER, S. D. 2010. Secondary structure of U6 small nuclear RNA: implications for spliceosome assembly. *Biochem Soc Trans,* 38**,** 1099-104.

EATON, J. D., FRANCIS, L., DAVIDSON, L. & WEST, S. 2020. A unified allosteric/torpedo mechanism for transcriptional termination on human protein-coding genes. *Genes Dev,* 34**,** 132-145.

ELWOOD, N. 2004. Telomere biology of human hematopoietic stem cells. *Cancer Control,* 11**,** 77-85.

FANG, L., XIAO, L., JUN, Y. W., ONISHI, Y. & KOOL, E. T. 2023. Reversible 2'-OH acylation enhances RNA stability. *Nat Chem,* 15**,** 1296-1305.

FENG, X., LI, L., WAGNER, E. J. & LI, W. 2018. TC3A: The Cancer 3' UTR Atlas. *Nucleic Acids Res,* 46**,** D1027-D1030.

FRICKMANN, H., ZAUTNER, A. E., MOTER, A., KIKHNEY, J., HAGEN, R. M., STENDER, H. & POPPERT, S. 2017. Fluorescence in situ hybridization (FISH) in the microbiological diagnostic routine laboratory: a review. *Crit Rev Microbiol,* 43**,** 263-293.

FURUICHI, Y. 2015. Discovery of m(7)G-cap in eukaryotic mRNAs. *Proc Jpn Acad Ser B Phys Biol Sci,* 91**,** 394-409.

GALLOWAY, A. & COWLING, V. H. 2019. mRNA cap regulation in mammalian cell function and fate. *Biochim Biophys Acta Gene Regul Mech,* 1862**,** 270-279.

GASPAR, P., MOURA, G., SANTOS, M. A. & OLIVEIRA, J. L. 2013. mRNA secondary structure optimization using a correlated stem-loop prediction. *Nucleic Acids Res,* 41**,** e73.

GOLOMBEK, S., HOFFMANN, T., HANN, L., MANDLER, M., SCHMIDHUBER, S., WEBER, J., CHANG, Y. T., MEHLING, R., LADINIG, A., KNECHT, C., LEYENS, J., SCHLENSAK, C., WENDEL, H. P., SCHNEEBERGER, A. & AVCI-ADALI, M. 2023. Improved tropoelastin synthesis in the skin by codon optimization and nucleotide modification of tropoelastin-encoding synthetic mRNA. *Mol Ther Nucleic Acids,* 33**,** 642-654.

GRAY, D. A. & WOULFE, J. 2005. Lipofuscin and aging: a matter of toxic waste. *Sci Aging Knowledge Environ,* 2005**,** re1.

HACEIN-BEY-ABINA, S., VON KALLE, C., SCHMIDT, M., MCCORMACK, M. P., WULFFRAAT, N., LEBOULCH, P., LIM, A., OSBORNE, C. S., PAWLIUK, R., MORILLON, E., SORENSEN, R., FORSTER, A., FRASER, P., COHEN, J. I., DE SAINT BASILE, G., ALEXANDER, I., WINTERGERST, U., FREBOURG, T., AURIAS, A., STOPPA-LYONNET, D., ROMANA, S., RADFORD-WEISS, I., GROSS, F., VALENSI, F., DELABESSE, E., MACINTYRE, E., SIGAUX, F., SOULIER, J., LEIVA, L. E., WISSLER, M., PRINZ, C., RABBITTS, T. H., LE DEIST, F., FISCHER, A. & CAVAZZANA-CALVO, M. 2003. LMO2-associated clonal T cell

proliferation in two patients after gene therapy for SCID-X1. *Science,* 302**,** 415-9.

HAJ, M., LEVON, A., FREY, Y., HOURVITZ, N., CAMPISI, J., TZFATI, Y., ELKON, R., ZIV, Y. & SHILOH, Y. 2023. Accelerated replicative senescence of ataxia-telangiectasia skin fibroblasts is retained at physiologic oxygen levels, with unique and common transcriptional patterns. *Aging Cell,* 22**,** e13869.

HANSON, G. & COLLER, J. 2018. Codon optimality, bias and usage in translation and mRNA decay. *Nat Rev Mol Cell Biol,* 19**,** 20-30.

HARIGAYA, Y. & PARKER, R. 2016. Analysis of the association between codon optimality and mRNA stability in Schizosaccharomyces pombe. *BMC Genomics,* 17**,** 895.

HASLER, D. & MEISTER, G. 2016. From tRNA to miRNA: RNA-folding contributes to correct entry into noncoding RNA pathways. *FEBS Lett,* 590**,** 2354-63.

HAYFLICK, L. & MOORHEAD, P. S. 1961. The serial cultivation of human diploid cell strains. *Exp Cell Res,* 25**,** 585-621.

HELM, M. 2006. Post-transcriptional nucleotide modification and alternative folding of RNA. *Nucleic Acids Res,* 34**,** 721-33.

HENDERSON, J. M., UJITA, A., HILL, E., YOUSIF-ROSALES, S., SMITH, C., KO, N., MCREYNOLDS, T., CABRAL, C. R., ESCAMILLA-POWERS, J. R. & HOUSTON, M. E. 2021. Cap 1 Messenger RNA Synthesis with Co-transcriptional CleanCap((R)) Analog by In Vitro Transcription. *Curr Protoc,* 1**,** e39.

HILLS, M. & LANSDORP, P. M. 2009. Short telomeres resulting from heritable mutations in the telomerase reverse transcriptase gene predispose for a variety of malignancies. *Ann N Y Acad Sci,* 1176**,** 178-90.

HOMBACH-KLONISCH, S., PANIGRAHI, S., RASHEDI, I., SEIFERT, A., ALBERTI, E., POCAR, P., KURPISZ, M., SCHULZE-OSTHOFF, K., MACKIEWICZ, A. & LOS, M. 2008. Adult stem cells and their trans-differentiation potential--perspectives and therapeutic applications. *J Mol Med (Berl),* 86**,** 1301-14.

HOWE, S. J., MANSOUR, M. R., SCHWARZWAELDER, K., BARTHOLOMAE, C., HUBANK, M., KEMPSKI, H., BRUGMAN, M. H., PIKE-OVERZET, K., CHATTERS, S. J., DE RIDDER, D., GILMOUR, K. C., ADAMS, S., THORNHILL, S. I., PARSLEY, K. L., STAAL, F. J., GALE, R. E., LINCH, D. C., BAYFORD, J., BROWN, L., QUAYE, M., KINNON, C., ANCLIFF, P., WEBB, D. K., SCHMIDT, M., VON KALLE, C., GASPAR, H. B. & THRASHER, A. J. 2008. Insertional mutagenesis combined with acquired somatic mutations causes leukemogenesis following gene therapy of SCID-X1 patients. *J Clin Invest*, 118**,** 3143-50.

JENVEY, C. J. & STABEL, J. R. 2017. Autofluorescence and Nonspecific Immunofluorescent Labeling in Frozen Bovine Intestinal Tissue Sections: Solutions for Multicolor Immunofluorescence Experiments. *J Histochem Cytochem,* 65**,** 531-541.

JEON, B. G., KUMAR, B. M., KANG, E. J., OCK, S. A., LEE, S. L., KWACK, D. O., BYUN, J. H., PARK, B. W. & RHO, G. J. 2011. Characterization and comparison of telomere length, telomerase and reverse transcriptase activity and gene expression in human mesenchymal stem cells and cancer cells of various origins. *Cell Tissue Res,* 345**,** 149-61.

JIA, L. & QIAN, S. B. 2021. Therapeutic mRNA Engineering from Head to Tail. *Acc Chem Res,* 54**,** 4272-4282.

JIAO, X., DOAMEKPOR, S. K., BIRD, J. G., NICKELS, B. E., TONG, L., HART, R. P. & KILEDJIAN, M. 2017. 5' End Nicotinamide Adenine Dinucleotide Cap in

Human Cells Promotes RNA Decay through DXO-Mediated deNADding. *Cell,* 168**,** 1015-1027 e10.

KACZMAREK, J. C., KOWALSKI, P. S. & ANDERSON, D. G. 2017. Advances in the delivery of RNA therapeutics: from concept to clinical reality. *Genome Med,* 9**,** 60.

KANEGANE, H., KASAHARA, Y., OKAMURA, J., HONGO, T., TANAKA, R., NOMURA, K., KOJIMA, S. & MIYAWAKI, T. 2005. Identification of DKC1 gene mutations in Japanese patients with X-linked dyskeratosis congenita. *Br J Haematol,* 129**,** 432-4.

KELLAND, L. R. 2005. Overcoming the immortality of tumour cells by telomere and telomerase based cancer therapeutics--current status and future prospects. *Eur J Cancer,* 41**,** 971-9.

KHATTAR, E., KUMAR, P., LIU, C. Y., AKINCILAR, S. C., RAJU, A., LAKSHMANAN, M., MAURY, J. J., QIANG, Y., LI, S., TAN, E. Y., HUI, K. M., SHI, M., LOH, Y. H. & TERGAONKAR, V. 2016. Telomerase reverse transcriptase promotes cancer cell proliferation by augmenting tRNA expression. *J Clin Invest,* 126**,** 4045-4060.

KIM, J., EYGERIS, Y., GUPTA, M. & SAHAY, G. 2021. Self-assembled mRNA vaccines. *Adv Drug Deliv Rev,* 170**,** 83-112.

KIM, T. K. & EBERWINE, J. H. 2010. Mammalian cell transfection: the present and the future. *Anal Bioanal Chem,* 397**,** 3173-8.

KIM, Y. K. 2022. RNA therapy: rich history, various applications and unlimited future prospects. *Exp Mol Med,* 54**,** 455-465.

KORBLING, M. & ESTROV, Z. 2003. Adult stem cells for tissue repair - a new therapeutic concept? *N Engl J Med,* 349**,** 570-82.

KOWALSKI, P. S., RUDRA, A., MIAO, L. & ANDERSON, D. G. 2019. Delivering the Messenger: Advances in Technologies for Therapeutic mRNA Delivery. *Mol Ther,* 27**,** 710-728.

KOZAK, M. 1991. Structural features in eukaryotic mRNAs that modulate the initiation of translation. *Journal of Biological Chemistry,* 266**,** 19867-19870.

KOZAK, M. 2002. Pushing the limits of the scanning mechanism for initiation of translation. *Gene,* 299**,** 1-34.

KWON, H., KIM, M., SEO, Y., MOON, Y. S., LEE, H. J., LEE, K. & LEE, H. 2018. Emergence of synthetic mRNA: In vitro synthesis of mRNA and its applications in regenerative medicine. *Biomaterials,* 156**,** 172-193.

LAI, F., DAMLE, S. S., LING, K. K. & RIGO, F. 2020. Directed RNase H Cleavage of Nascent Transcripts Causes Transcription Termination. *Mol Cell,* 77**,** 1032-1043 e4.

LEI, M., LI, K., LI, B., GAO, L. N., CHEN, F. M. & JIN, Y. 2014. Mesenchymal stem cell characteristics of dental pulp and periodontal ligament stem cells after in vivo transplantation. *Biomaterials,* 35**,** 6332-43.

LEMONNIER, J. & LEMONNIER, N. 2023. Messenger RNA (mRNA): From Transcription to Protein Translation. *The Marathon of the Messenger.*

LENASI, T. & BARBORIC, M. 2013. Mutual relationships between transcription and pre-mRNA processing in the synthesis of mRNA. *Wiley Interdiscip Rev RNA,* 4**,** 139-54.

LEPPEK, K., DAS, R. & BARNA, M. 2018. Functional 5' UTR mRNA structures in eukaryotic translation regulation and how to find them. *Nat Rev Mol Cell Biol,* 19**,** 158-174.

LI, H., WANG, B., LI, D., LI, J., LUO, Y. & DAN, J. 2021. Roles of telomeres and telomerase in age-related renal diseases (Review). *Mol Med Rep,* 23.

LI, N., CAI, Y., ZOU, M., ZHOU, J., ZHANG, L., ZHOU, L., XIANG, W., CUI, Y. & LI, H. 2023. CFIm-mediated alternative polyadenylation safeguards the development of mammalian pre-implantation embryos. *Stem Cell Reports,* 18, 81-96.

LIAO, M. L., DONG, Y. W. & SOMERO, G. N. 2021. Thermal adaptation of mRNA secondary structure: stability versus lability. *Proc Natl Acad Sci U S A,* 118.

LINDROSE, A. R., MCLESTER-DAVIS, L. W. Y., TRISTANO, R. I., KATARIA, L., GADALLA, S. M., EISENBERG, D. T. A., VERHULST, S. & DRURY, S. 2021. Method comparison studies of telomere length measurement using qPCR approaches: A critical appraisal of the literature. *PLoS One,* 16, e0245582.

LIVAK, K. J. & SCHMITTGEN, T. D. 2001. Analysis of relative gene expression data using real-time quantitative PCR and the 2(-Delta Delta C(T)) Method. *Methods,* 25, 402-8.

LYTLE, J. R., YARIO, T. A. & STEITZ, J. A. 2007. Target mRNAs are repressed as efficiently by microRNA-binding sites in the 5' UTR as in the 3' UTR. *Proc Natl Acad Sci U S A,* 104, 9667-72.

MAMAGHANI, S., PENNA, R. R., FREI, J., WYSS, C., MELLETT, M., LOOK, T., WEISS, T., GUENOVA, E., KUNDIG, T. M., LAUCHLI, S. & PASCOLO, S. 2024. Synthetic mRNAs Containing Minimalistic Untranslated Regions Are Highly Functional In Vitro and In Vivo. *Cells,* 13.

MARRELLI, M., CODISPOTI, B., SHELTON, R. M., SCHEVEN, B. A., COOPER, P. R., TATULLO, M. & PADUANO, F. 2018. Dental Pulp Stem Cell Mechanoresponsiveness: Effects of Mechanical Stimuli on Dental Pulp Stem Cell Behavior. *Front Physiol,* 9, 1685.

MARTIN, N. A., MCLESTER-DAVIS, L. W. Y., ROY, T. R., MAGRUDER, M. G., HASTINGS, W. J. & DRURY, S. S. 2024. Monochrome Multiplex Quantitative PCR Telomere Length Measurement. *J Vis Exp*.

MARTINEZ-NEGRO, M., GUERRERO-MARTINEZ, A., GARCIA-RIO, L., DOMENECH, O., AICART, E., TROS DE ILARDUYA, C. & JUNQUERA, E. 2018. Multidisciplinary Approach to the Transfection of Plasmid DNA by a Nonviral Nanocarrier Based on a Gemini-Bolaamphiphilic Hybrid Lipid. *ACS Omega,* 3, 208-217.

MATOULKOVA, E., MICHALOVA, E., VOJTESEK, B. & HRSTKA, R. 2012. The role of the 3' untranslated region in post-transcriptional regulation of protein expression in mammalian cells. *RNA Biol,* 9, 563-76.

MAZUMDER, B., SESHADRI, V. & FOX, P. L. 2003. Translational control by the 3'-UTR: the ends specify the means. *Trends Biochem Sci,* 28, 91-8.

MINO, T. & TAKEUCHI, O. 2021. Regnase-1-related endoribonucleases in health and immunological diseases. *Immunol Rev,* 304, 97-110.

MISCHO, H. E. & PROUDFOOT, N. J. 2013. Disengaging polymerase: terminating RNA polymerase II transcription in budding yeast. *Biochim Biophys Acta,* 1829, 174-85.

MOKRY, J., SOUKUP, T., MICUDA, S., KARBANOVA, J., VISEK, B., BRCAKOVA, E., SUCHANEK, J., BOUCHAL, J., VOKURKOVA, D. & IVANCAKOVA, R. 2010. Telomere attrition occurs during ex vivo expansion of human dental pulp stem cells. *J Biomed Biotechnol,* 2010, 673513.

MULLIGAN, M. J., LYKE, K. E., KITCHIN, N., ABSALON, J., GURTMAN, A., LOCKHART, S., NEUZIL, K., RAABE, V., BAILEY, R., SWANSON, K. A., LI, P., KOURY, K., KALINA, W., COOPER, D., FONTES-GARFIAS, C., SHI, P. Y.,

TURECI, O., TOMPKINS, K. R., WALSH, E. E., FRENCK, R., FALSEY, A. R., DORMITZER, P. R., GRUBER, W. C., SAHIN, U. & JANSEN, K. U. 2021. Publisher Correction: Phase I/II study of COVID-19 RNA vaccine BNT162b1 in adults. *Nature,* 590**,** E26.

MURAKAMI, K. S., MASUDA, S. & DARST, S. A. 2002. Structural basis of transcription initiation: RNA polymerase holoenzyme at 4 A resolution. *Science,* 296**,** 1280-4.

NAGPAL, N., WANG, J., ZENG, J., LO, E., MOON, D. H., LUK, K., BRAUN, R. O., BURROUGHS, L. M., KEEL, S. B., REILLY, C., LINDSLEY, R. C., WOLFE, S. A., TAI, A. K., CAHAN, P., BAUER, D. E., FONG, Y. W. & AGARWAL, S. 2020. Small-Molecule PAPD5 Inhibitors Restore Telomerase Activity in Patient Stem Cells. *Cell Stem Cell,* 26**,** 896-909 e8.

NISHIO, Y., NAKANISHI, K., OZEKI, Y., JIANG, S. X., KAMEYA, T., HEBISAWA, A., MUKAI, M., TRAVIS, W. D., FRANKS, T. J. & KAWAI, T. 2007. Telomere length, telomerase activity, and expressions of human telomerase mRNA component (hTERC) and human telomerase reverse transcriptase (hTERT) mRNA in pulmonary neuroendocrine tumors. *Jpn J Clin Oncol,* 37**,** 16-22.

O'CALLAGHAN, N. J. & FENECH, M. 2011. A quantitative PCR method for measuring absolute telomere length. *Biol Proced Online,* 13**,** 3.

OH, S. & KESSLER, J. A. 2018. Design, Assembly, Production, and Transfection of Synthetic Modified mRNA. *Methods,* 133**,** 29-43.

OHNO, H., AKAMINE, S., MOCHIZUKI, M., HAYASHI, K., AKICHIKA, S., SUZUKI, T. & SAITO, H. 2023. Versatile strategy using vaccinia virus-capping enzyme to synthesize functional 5' cap-modified mRNAs. *Nucleic Acids Res,* 51**,** e34.

ORIMOTO, A., KYAKUMOTO, S., EITSUKA, T., NAKAGAWA, K., KIYONO, T. & FUKUDA, T. 2020. Efficient immortalization of human dental pulp stem cells with expression of cell cycle regulators with the intact chromosomal condition. *PLoS One,* 15**,** e0229996.

PARDI, N., HOGAN, M. J., PORTER, F. W. & WEISSMAN, D. 2018. mRNA vaccines - a new era in vaccinology. *Nat Rev Drug Discov,* 17**,** 261-279.

PATEL, R., KAKI, M., POTLURI, V. S., KAHAR, P. & KHANNA, D. 2022. A comprehensive review of SARS-CoV-2 vaccines: Pfizer, Moderna & Johnson & Johnson. *Hum Vaccin Immunother,* 18**,** 2002083.

PETUSHKOV, I., ESYUNINA, D. & KULBACHINSKIY, A. 2023. Effects of natural RNA modifications on the activity of SARS-CoV-2 RNA-dependent RNA polymerase. *FEBS J,* 290**,** 80-92.

PHUA, K. K., LEONG, K. W. & NAIR, S. K. 2013. Transfection efficiency and transgene expression kinetics of mRNA delivered in naked and nanoparticle format. *J Control Release,* 166**,** 227-33.

PILBAUEROVA, N., SOUKUP, T., SUCHANKOVA KLEPLOVA, T., SCHMIDT, J. & SUCHANEK, J. 2021. The Effect of Cultivation Passaging on the Relative Telomere Length and Proliferation Capacity of Dental Pulp Stem Cells. *Biomolecules,* 11.

POYNTER, S. J. & DEWITTE-ORR, S. J. 2018. Understanding Viral dsRNA-Mediated Innate Immune Responses at the Cellular Level Using a Rainbow Trout Model. *Front Immunol,* 9**,** 829.

PRENTICE, D. A. 2019. Adult Stem Cells. *Circ Res,* 124**,** 837-839.

PRESNYAK, V., ALHUSAINI, N., CHEN, Y. H., MARTIN, S., MORRIS, N., KLINE, N., OLSON, S., WEINBERG, D., BAKER, K. E., GRAVELEY, B. R. & COLLER, J.

2015. Codon optimality is a major determinant of mRNA stability. *Cell,* 160**,** 1111-24.

RACHEZ, C., LEGENDRE, R., COSTALLAT, M., VARET, H., YI, J., KORNOBIS, E. & MUCHARDT, C. 2021. HP1gamma binding pre-mRNA intronic repeats modulates RNA splicing decisions. *EMBO Rep,* 22**,** e52320.

RAMANATHAN, A., ROBB, G. B. & CHAN, S. H. 2016. mRNA capping: biological functions and applications. *Nucleic Acids Res,* 44**,** 7511-26.

ROCCA, M. S., FORESTA, C. & FERLIN, A. 2019. Telomere length: lights and shadows on their role in human reproduction. *Biol Reprod,* 100**,** 305-317.

ROTH, A., DURIG, J., HIMMELREICH, H., BUG, S., SIEBERT, R., DUHRSEN, U., LANSDORP, P. M. & BAERLOCHER, G. M. 2007. Short telomeres and high telomerase activity in T-cell prolymphocytic leukemia. *Leukemia,* 21**,** 2456-62.

SAHIN, U., MUIK, A., DERHOVANESSIAN, E., VOGLER, I., KRANZ, L. M., VORMEHR, M., BAUM, A., PASCAL, K., QUANDT, J., MAURUS, D., BRACHTENDORF, S., LORKS, V., SIKORSKI, J., HILKER, R., BECKER, D., ELLER, A. K., GRUTZNER, J., BOESLER, C., ROSENBAUM, C., KUHNLE, M. C., LUXEMBURGER, U., KEMMER-BRUCK, A., LANGER, D., BEXON, M., BOLTE, S., KARIKO, K., PALANCHE, T., FISCHER, B., SCHULTZ, A., SHI, P. Y., FONTES-GARFIAS, C., PEREZ, J. L., SWANSON, K. A., LOSCHKO, J., SCULLY, I. L., CUTLER, M., KALINA, W., KYRATSOUS, C. A., COOPER, D., DORMITZER, P. R., JANSEN, K. U. & TURECI, O. 2020. COVID-19 vaccine BNT162b1 elicits human antibody and T(H)1 T cell responses. *Nature,* 586**,** 594-599.

SAKURAI, Y., WATANABE, H., NISHIO, K., HASHIMOTO, K., HARADA, A., GOMI, M., SUZUKI, M., OYAMA, R., HANDA, T., SATO, R., TAKEUCHI, H., TAIRA, R., TEZUKA, K., TANGE, K., NAKAI, Y., AKITA, H. & UCHIDA, Y. 2022. pH-Responsive Lipid Nanoparticles Achieve Efficient mRNA Transfection in Brain Capillary Endothelial Cells. *Pharmaceutics,* 14.

SELB, J., OSOLNIK, K., KERN, I., KOROSEC, P. & RIJAVEC, M. 2022. Utility of Telomerase Gene Mutation Testing in Patients with Idiopathic Pulmonary Fibrosis in Routine Practice. *Cells,* 11.

SHUKLA, S., SCHMIDT, J. C., GOLDFARB, K. C., CECH, T. R. & PARKER, R. 2016. Inhibition of telomerase RNA decay rescues telomerase deficiency caused by dyskerin or PARN defects. *Nat Struct Mol Biol,* 23**,** 286-92.

SMIETANSKI, M., WERNER, M., PURTA, E., KAMINSKA, K. H., STEPINSKI, J., DARZYNKIEWICZ, E., NOWOTNY, M. & BUJNICKI, J. M. 2014. Structural analysis of human 2'-O-ribose methyltransferases involved in mRNA cap structure formation. *Nat Commun,* 5**,** 3004.

SOKOLOWSKA, E. & BLACHNIO-ZABIELSKA, A. U. 2019. A Critical Review of Electroporation as A Plasmid Delivery System in Mouse Skeletal Muscle. *Int J Mol Sci,* 20.

SON, S., PARK, M., KIM, J. & LEE, K. 2024. ACE mRNA (Additional Chimeric Element incorporated IVT mRNA) for Enhancing Protein Expression by Modulating Immunogenicity. *Adv Sci (Weinh),* 11**,** e2307541.

SVITKIN, Y. V., CHENG, Y. M., CHAKRABORTY, T., PRESNYAK, V., JOHN, M. & SONENBERG, N. 2017. N1-methyl-pseudouridine in mRNA enhances translation through eIF2alpha-dependent and independent mechanisms by increasing ribosome density. *Nucleic Acids Res,* 45**,** 6023-6036.

SVITKIN, Y. V., GINGRAS, A. C. & SONENBERG, N. 2022. Membrane-dependent relief of translation elongation arrest on pseudouridine- and N1-methyl-pseudouridine-modified mRNAs. *Nucleic Acids Res,* 50**,** 7202-7215.

TAHERI, M., GHAFOURI-FARD, S., NAJAFI, S., KALLENBACH, J., KERAMATFAR, E., ATRI ROOZBAHANI, G., HEIDARI HORESTANI, M., HUSSEN, B. M. & BANIAHMAD, A. 2022. Hormonal regulation of telomerase activity and hTERT expression in steroid-regulated tissues and cancer. *Cancer Cell Int,* 22**,** 258.

TEDONE, E., HUANG, E., O'HARA, R., BATTEN, K., LUDLOW, A. T., LAI, T. P., AROSIO, B., MARI, D., WRIGHT, W. E. & SHAY, J. W. 2019. Telomere length and telomerase activity in T cells are biomarkers of high-performing centenarians. *Aging Cell,* 18**,** e12859.

TENCHOV, R., BIRD, R., CURTZE, A. E. & ZHOU, Q. 2021. Lipid Nanoparticles horizontal line From Liposomes to mRNA Vaccine Delivery, a Landscape of Research Diversity and Advancement. *ACS Nano,* 15**,** 16982-17015.

THAM, C. Y., POON, L., YAN, T., KOH, J. Y. P., RAMLEE, M. K., TEOH, V. S. I., ZHANG, S., CAI, Y., HONG, Z., LEE, G. S., LIU, J., SONG, H. W., HWANG, W. Y. K., TEH, B. T., TAN, P., XU, L., KOH, A. S., OSATO, M. & LI, S. 2023. High-throughput telomere length measurement at nucleotide resolution using the PacBio high fidelity sequencing platform. *Nat Commun,* 14**,** 281.

TORABI, S. F., VAIDYA, A. T., TYCOWSKI, K. T., DEGREGORIO, S. J., WANG, J., SHU, M. D., STEITZ, T. A. & STEITZ, J. A. 2021. RNA stabilization by a poly(A) tail 3'-end binding pocket and other modes of poly(A)-RNA interaction. *Science,* 371.

TRYBEK, T., KOWALIK, A., GOZDZ, S. & KOWALSKA, A. 2020. Telomeres and telomerase in oncogenesis. *Oncol Lett,* 20**,** 1015-1027.

VAHIDI, S. & SAMADANI, A. A. 2021. TERRA Gene Expression in Gastric Cancer: Role of hTERT. *J Gastrointest Cancer,* 52**,** 431-447.

VAN DEN HOOGENHOF, M. M., PINTO, Y. M. & CREEMERS, E. E. 2016. RNA Splicing: Regulation and Dysregulation in the Heart. *Circ Res,* 118**,** 454-68.

VERHULST, S., SUSSER, E., FACTOR-LITVAK, P. R., SIMONS, M. J., BENETOS, A., STEENSTRUP, T., KARK, J. D. & AVIV, A. 2015. Commentary: The reliability of telomere length measurements. *Int J Epidemiol,* 44**,** 1683-6.

VIRIJEVIC, M., MARJANOVIC, I., ANDJELKOVIC, M., JAKOVIC, L., MICIC, D., BOGDANOVIC, A. & PAVLOVIC, S. 2024. Novel telomerase reverse transcriptase gene mutation in a family with aplastic anaemia. *Fam Cancer*.

WANG, B., LEE, W. Y., HUANG, B., ZHANG, J. F., WU, T., JIANG, X., WANG, C. C. & LI, G. 2016. Secretome of Human Fetal Mesenchymal Stem Cell Ameliorates Replicative Senescen. *Stem Cells Dev,* 25**,** 1755-1766.

WANG, S., ZHAO, Y., HU, C. & ZHU, J. 2009. Differential repression of human and mouse TERT genes during cell differentiation. *Nucleic Acids Res,* 37**,** 2618-29.

WANG, W., CHEN, L., ZHANG, Y., WANG, H., DONG, D., ZHU, J., FU, W. & LIU, T. 2024. Adipose-derived stem cells enriched with therapeutic mRNA TGF-beta3 and IL-10 synergistically promote scar-less wound healing in preclinical models. *Bioeng Transl Med,* 9**,** e10620.

WANG, W., YAN, M., AARABI, G., PETERS, U., FREYTAG, M., GOSAU, M., SMEETS, R. & BEIKLER, T. 2022. Cultivation of Cryopreserved Human Dental Pulp Stem Cells-A New Approach to Maintaining Dental Pulp Tissue. *Int J Mol Sci,* 23.

WANG, Y., ZHANG, Z., LUO, J., HAN, X., WEI, Y. & WEI, X. 2021. mRNA vaccine: a potential therapeutic strategy. *Mol Cancer,* 20**,** 33.

WARMINSKI, M., MAMOT, A., DEPAIX, A., KOWALSKA, J. & JEMIELITY, J. 2023. Chemical Modifications of mRNA Ends for Therapeutic Applications. *Acc Chem Res,* 56**,** 2814-2826.

WASSARMAN, D. A. & STEITZ, J. A. 1993. A base-pairing interaction between U2 and U6 small nuclear RNAs occurs in > 150S complexes in HeLa cell extracts: implications for the spliceosome assembly pathway. *Proc Natl Acad Sci U S A,* 90**,** 7139-43.

WILSON, R., URRACA, N., SKOBOWIAT, C., HOPE, K. A., MIRAVALLE, L., CHAMBERLIN, R., DONALDSON, M., SEAGROVES, T. N. & REITER, L. T. 2015. Assessment of the Tumorigenic Potential of Spontaneously Immortalized and hTERT-Immortalized Cultured Dental Pulp Stem Cells. *Stem Cells Transl Med,* 4**,** 905-12.

WOJCIK, R., BARANOWSKI, M. R., MARKIEWICZ, L., KUBACKA, D., BEDNARCZYK, M., BARAN, N., WOJTCZAK, A., SIKORSKI, P. J., ZUBEREK, J., KOWALSKA, J. & JEMIELITY, J. 2021. Novel N7-Arylmethyl Substituted Dinucleotide mRNA 5' cap Analogs: Synthesis and Evaluation as Modulators of Translation. *Pharmaceutics,* 13.

YANG, Q., NAUSCH, L. W., MARTIN, G., KELLER, W. & DOUBLIE, S. 2014a. Crystal structure of human poly(A) polymerase gamma reveals a conserved catalytic core for canonical poly(A) polymerases. *J Mol Biol,* 426**,** 43-50.

YANG, X. & CAO, D. 2023. DXO gears mRNA with alternative NAD and m(7)G caps. *Trends Plant Sci,* 28**,** 1083-1085.

YANG, Z., WANG, Y., LI, Y., LIU, Q., ZENG, Q. & XU, X. 2014b. Options for tracking GFP-Labeled transplanted myoblasts using in vivo fluorescence imaging: implications for tracking stem cell fate. *BMC Biotechnol,* 14**,** 55.

ZANET, D. L., SABERI, S., OLIVEIRA, L., SATTHA, B., GADAWSKI, I. & COTE, H. C. 2013. Blood and dried blood spot telomere length measurement by qPCR: assay considerations. *PLoS One,* 8**,** e57787.

ZHANG, T., LI, C., ZHU, J., LI, Y., WANG, Z., TONG, C. Y., XI, Y., HAN, Y., KOIWA, H., PENG, X. & ZHANG, X. 2024. Structured 3' UTRs destabilize mRNAs in plants. *Genome Biol,* 25**,** 54.

ZHANG, X., LI, H., SUN, J., LUO, X., YANG, H., XIE, L., YANG, B., GUO, W. & TIAN, W. 2017. Cell-derived micro-environment helps dental pulp stem cells promote dental pulp regeneration. *Cell Prolif,* 50.

ZHU, K., QU, D., SAKAMOTO, T., FUKASAWA, I., HAYASHI, M. & INABA, N. 2008. Telomerase expression and cell proliferation in ovarian cancer cells induced by histone deacetylase inhibitors. *Arch Gynecol Obstet,* 277**,** 15-9.

ALAIDAROOS, N. Y. A., ALRAIES, A., WADDINGTON, R. J., SLOAN, A. J. & MOSELEY, R. 2021. Differential SOD2 and GSTZ1 profiles contribute to contrasting dental pulp stem cell susceptibilities to oxidative damage and premature senescence. *Stem Cell Res Ther,* 12**,** 142.

ALRAIES, A., ALAIDAROOS, N. Y., WADDINGTON, R. J., MOSELEY, R. & SLOAN, A. J. 2017. Variation in human dental pulp stem cell ageing profiles reflect contrasting proliferative and regenerative capabilities. *BMC Cell Biol,* 18**,** 12.

BAIRD, D. M. 2005. New developments in telomere length analysis. *Exp Gerontol,* 40**,** 363-8.

BARNES, R. P., FOUQUEREL, E. & OPRESKO, P. L. 2019. The impact of oxidative DNA damage and stress on telomere homeostasis. *Mech Ageing Dev,* 177**,** 37-45.

BERKOVITS, B. D. & MAYR, C. 2015. Alternative 3' UTRs act as scaffolds to regulate membrane protein localization. *Nature,* 522**,** 363-7.

CAWTHON, R. M. 2002. Telomere measurement by quantitative PCR. *Nucleic Acids Res,* 30**,** e47.

CHAI, Y., JIANG, X., ITO, Y., BRINGAS, P., JR., HAN, J., ROWITCH, D. H., SORIANO, P., MCMAHON, A. P. & SUCOV, H. M. 2000. Fate of the mammalian cranial neural crest during tooth and mandibular morphogenesis. *Development,* 127**,** 1671-9.

DE FARIAS, J. O., DA COSTA SOUSA, M. G., MARTINS, D. C. M., DE OLIVEIRA, M. A., TAKAHASHI, I., DE SOUSA, L. B., DA SILVA, I. G. M., CORREA, J. R., SILVA CARVALHO, A. E., SALDANHA-ARAUJO, F. & REZENDE, T. M. B. 2024. Senescence on Dental Pulp Cells: Effects on Morphology, Migration, Proliferation, and Immune Response. *J Endod,* 50**,** 362-369.

DEBATIN, K. M. & KRAMMER, P. H. 2004. Death receptors in chemotherapy and cancer. *Oncogene,* 23**,** 2950-66.

DUNN, E. A. & RADER, S. D. 2010. Secondary structure of U6 small nuclear RNA: implications for spliceosome assembly. *Biochem Soc Trans,* 38**,** 1099-104.

FENG, X., LI, L., WAGNER, E. J. & LI, W. 2018. TC3A: The Cancer 3' UTR Atlas. *Nucleic Acids Res,* 46**,** D1027-D1030.

FERRER, A., STEPHENS, Z. D. & KOCHER, J. A. 2023. Experimental and Computational Approaches to Measure Telomere Length: Recent Advances and Future Directions. *Curr Hematol Malig Rep,* 18**,** 284-291.

FULDA, S. 2013. Regulation of apoptosis pathways in cancer stem cells. *Cancer Lett,* 338**,** 168-73.

GRONTHOS, S., BRAHIM, J., LI, W., FISHER, L. W., CHERMAN, N., BOYDE, A., DENBESTEN, P., ROBEY, P. G. & SHI, S. 2002. Stem cell properties of human dental pulp stem cells. *J Dent Res,* 81**,** 531-5.

GRONTHOS, S., MANKANI, M., BRAHIM, J., ROBEY, P. G. & SHI, S. 2000. Postnatal human dental pulp stem cells (DPSCs) in vitro and in vivo. *Proc Natl Acad Sci U S A,* 97**,** 13625-30.

GRUDZIEN-NOGALSKA, E., STEPINSKI, J., JEMIELITY, J., ZUBEREK, J., STOLARSKI, R., RHOADS, R. E. & DARZYNKIEWICZ, E. 2007. Synthesis of anti-reverse cap analogs (ARCAs) and their applications in mRNA translation and stability. *Methods Enzymol,* 431**,** 203-27.

HACEIN-BEY-ABINA, S., VON KALLE, C., SCHMIDT, M., MCCORMACK, M. P., WULFFRAAT, N., LEBOULCH, P., LIM, A., OSBORNE, C. S., PAWLIUK, R., MORILLON, E., SORENSEN, R., FORSTER, A., FRASER, P., COHEN, J. I., DE SAINT BASILE, G., ALEXANDER, I., WINTERGERST, U., FREBOURG, T., AURIAS, A., STOPPA-LYONNET, D., ROMANA, S., RADFORD-WEISS, I., GROSS, F., VALENSI, F., DELABESSE, E., MACINTYRE, E., SIGAUX, F., SOULIER, J., LEIVA, L. E., WISSLER, M., PRINZ, C., RABBITTS, T. H., LE DEIST, F., FISCHER, A. & CAVAZZANA-CALVO, M. 2003. LMO2-associated clonal T cell proliferation in two patients after gene therapy for SCID-X1. *Science,* 302**,** 415-9.

HILLS, M. & LANSDORP, P. M. 2009. Short telomeres resulting from heritable mutations in the telomerase reverse transcriptase gene predispose for a variety of malignancies. *Ann N Y Acad Sci,* 1176**,** 178-90.

HOWE, S. J., MANSOUR, M. R., SCHWARZWAELDER, K., BARTHOLOMAE, C., HUBANK, M., KEMPSKI, H., BRUGMAN, M. H., PIKE-OVERZET, K., CHATTERS, S. J., DE RIDDER, D., GILMOUR, K. C., ADAMS, S., THORNHILL, S. I., PARSLEY, K. L., STAAL, F. J., GALE, R. E., LINCH, D. C., BAYFORD, J., BROWN, L., QUAYE, M., KINNON, C., ANCLIFF, P., WEBB, D. K., SCHMIDT, M., VON KALLE, C., GASPAR, H. B. &

THRASHER, A. J. 2008. Insertional mutagenesis combined with acquired somatic mutations causes leukemogenesis following gene therapy of SCID-X1 patients. *J Clin Invest,* 118**,** 3143-50.

INAGAKI, M., ABE, N., LI, Z., NAKASHIMA, Y., ACHARYYA, S., OGAWA, K., KAWAGUCHI, D., HIRAOKA, H., BANNO, A., MENG, Z., TADA, M., ISHIDA, T., LYU, P., KOKUBO, K., MURASE, H., HASHIYA, F., KIMURA, Y., UCHIDA, S. & ABE, H. 2023. Cap analogs with a hydrophobic photocleavable tag enable facile purification of fully capped mRNA with various cap structures. *Nat Commun,* 14**,** 2657.

KAWASHIMA, N. 2012. Characterisation of dental pulp stem cells: a new horizon for tissue regeneration? *Arch Oral Biol,* 57**,** 1439-58.

KELLAND, L. R. 2005. Overcoming the immortality of tumour cells by telomere and telomerase based cancer therapeutics--current status and future prospects. *Eur J Cancer,* 41**,** 971-9.

LAINO, G., GRAZIANO, A., D'AQUINO, R., PIROZZI, G., LANZA, V., VALIANTE, S., DE ROSA, A., NARO, F., VIVARELLI, E. & PAPACCIO, G. 2006. An approachable human adult stem cell source for hard-tissue engineering. *J Cell Physiol,* 206**,** 693-701.

LANSDORP, P. M., VERWOERD, N. P., VAN DE RIJKE, F. M., DRAGOWSKA, V., LITTLE, M. T., DIRKS, R. W., RAAP, A. K. & TANKE, H. J. 1996. Heterogeneity in telomere length of human chromosomes. *Hum Mol Genet,* 5**,** 685-91.

LEI, M., LI, K., LI, B., GAO, L. N., CHEN, F. M. & JIN, Y. 2014. Mesenchymal stem cell characteristics of dental pulp and periodontal ligament stem cells after in vivo transplantation. *Biomaterials,* 35**,** 6332-43.

LINDROSE, A. R., MCLESTER-DAVIS, L. W. Y., TRISTANO, R. I., KATARIA, L., GADALLA, S. M., EISENBERG, D. T. A., VERHULST, S. & DRURY, S. 2021. Method comparison studies of telomere length measurement using qPCR approaches: A critical appraisal of the literature. *PLoS One,* 16**,** e0245582.

MACHADO, C. V., PASSOS, S. T., CAMPOS, T. M., BERNARDI, L., VILAS-BOAS, D. S., NOR, J. E., TELLES, P. D. & NASCIMENTO, I. L. 2016. The dental pulp stem cell niche based on aldehyde dehydrogenase 1 expression. *Int Endod J,* 49**,** 755-63.

MARRELLI, M., CODISPOTI, B., SHELTON, R. M., SCHEVEN, B. A., COOPER, P. R., TATULLO, M. & PADUANO, F. 2018. Dental Pulp Stem Cell Mechanoresponsiveness: Effects of Mechanical Stimuli on Dental Pulp Stem Cell Behavior. *Front Physiol,* 9**,** 1685.

MARTIN-RUIZ, C. M., BAIRD, D., ROGER, L., BOUKAMP, P., KRUNIC, D., CAWTHON, R., DOKTER, M. M., VAN DER HARST, P., BEKAERT, S., DE MEYER, T., ROOS, G., SVENSON, U., CODD, V., SAMANI, N. J., MCGLYNN, L., SHIELS, P. G., POOLEY, K. A., DUNNING, A. M., COOPER, R., WONG, A., KINGSTON, A. & VON ZGLINICKI, T. 2015. Reproducibility of telomere length assessment: an international collaborative study. *Int J Epidemiol,* 44**,** 1673-83.

MULLIGAN, M. J., LYKE, K. E., KITCHIN, N., ABSALON, J., GURTMAN, A., LOCKHART, S., NEUZIL, K., RAABE, V., BAILEY, R., SWANSON, K. A., LI, P., KOURY, K., KALINA, W., COOPER, D., FONTES-GARFIAS, C., SHI, P. Y., TURECI, O., TOMPKINS, K. R., WALSH, E. E., FRENCK, R., FALSEY, A. R., DORMITZER, P. R., GRUBER, W. C., SAHIN, U. & JANSEN, K. U. 2021. Publisher Correction: Phase I/II study of COVID-19 RNA vaccine BNT162b1 in adults. *Nature,* 590**,** E26.

NAGATA, M., ONO, N. & ONO, W. 2021. Unveiling diversity of stem cells in dental pulp and apical papilla using mouse genetic models: a literature review. *Cell Tissue Res,* 383**,** 603-616.

NASSOUR, J., AGUIAR, L. G., CORREIA, A., SCHMIDT, T. T., MAINZ, L., PRZETOCKA, S., HAGGBLOM, C., TADEPALLE, N., WILLIAMS, A., SHOKHIREV, M. N., AKINCILAR, S. C., TERGAONKAR, V., SHADEL, G. S. & KARLSEDER, J. 2023. Telomere-to-mitochondria signalling by ZBP1 mediates replicative crisis. *Nature,* 614**,** 767-773.

NEL, S., DURANDT, C., MURDOCH, C. & PEPPER, M. S. 2022. Determinants of Dental Pulp Stem Cell Heterogeneity. *J Endod,* 48**,** 1232-1240.

O'CALLAGHAN, N. J. & FENECH, M. 2011. A quantitative PCR method for measuring absolute telomere length. *Biol Proced Online,* 13**,** 3.

ORIMOTO, A., KYAKUMOTO, S., EITSUKA, T., NAKAGAWA, K., KIYONO, T. & FUKUDA, T. 2020. Efficient immortalization of human dental pulp stem cells with expression of cell cycle regulators with the intact chromosomal condition. *PLoS One,* 15**,** e0229996.

PATEL, R., KAKI, M., POTLURI, V. S., KAHAR, P. & KHANNA, D. 2022. A comprehensive review of SARS-CoV-2 vaccines: Pfizer, Moderna & Johnson & Johnson. *Hum Vaccin Immunother,* 18**,** 2002083.

PILBAUEROVA, N., SCHMIDT, J., SOUKUP, T., DUSKA, J. & SUCHANEK, J. 2021a. Intra-Individual Variability of Human Dental Pulp Stem Cell Features Isolated from the Same Donor. *Int J Mol Sci,* 22.

PILBAUEROVA, N., SOUKUP, T., SUCHANKOVA KLEPLOVA, T., SCHMIDT, J. & SUCHANEK, J. 2021b. The Effect of Cultivation Passaging on the Relative Telomere Length and Proliferation Capacity of Dental Pulp Stem Cells. *Biomolecules,* 11.

PISCIOTTA, A., BERTONI, L., VALLAROLA, A., BERTANI, G., MECUGNI, D. & CARNEVALE, G. 2020. Neural crest derived stem cells from dental pulp and tooth-associated stem cells for peripheral nerve regeneration. *Neural Regen Res,* 15**,** 373-381.

RAIK, S., KUMAR, A., RATTAN, V., SETH, S., KAUR, A. & BHATTA CHARYYA, S. 2020. Assessment of Post-thaw Quality of Dental Mesenchymal Stromal Cells After Long-Term Cryopreservation by Uncontrolled Freezing. *Appl Biochem Biotechnol,* 191**,** 728-743.

REMOT, F., RONGET, V., FROY, H., REY, B., GAILLARD, J. M., NUSSEY, D. H. & LEMAITRE, J. F. 2022. Decline in telomere length with increasing age across nonhuman vertebrates: A meta-analysis. *Mol Ecol,* 31**,** 5917-5932.

SHANMUGASUNDARAM, M., SENTHILVELAN, A. & KORE, A. R. 2022. Recent Advances in Modified Cap Analogs: Synthesis, Biochemical Properties, and mRNA Based Vaccines. *Chem Rec,* 22**,** e202200005.

SONG, J., PERREAULT, J. P., TOPISIROVIC, I. & RICHARD, S. 2016. RNA G-quadruplexes and their potential regulatory roles in translation. *Translation (Austin),* 4**,** e1244031.

THESLEFF, I. & ABERG, T. 1999. Molecular regulation of tooth development. *Bone,* 25**,** 123-5.

WAJAHAT, M., BRACKEN, C. P. & ORANG, A. 2021. Emerging Functions for snoRNAs and snoRNA-Derived Fragments. *Int J Mol Sci,* 22.

WANG, W., YAN, M., AARABI, G., PETERS, U., FREYTAG, M., GOSAU, M., SMEETS, R. & BEIKLER, T. 2022. Cultivation of Cryopreserved Human Dental Pulp Stem Cells-A New Approach to Maintaining Dental Pulp Tissue. *Int J Mol Sci,* 23.

WARREN, L., MANOS, P. D., AHFELDT, T., LOH, Y. H., LI, H., LAU, F., EBINA, W., MANDAL, P. K., SMITH, Z. D., MEISSNER, A., DALEY, G. Q., BRACK, A. S., COLLINS, J. J., COWAN, C., SCHLAEGER, T. M. & ROSSI, D. J. 2010. Highly efficient reprogramming to pluripotency and directed differentiation of human cells with synthetic modified mRNA. *Cell Stem Cell,* 7**,** 618-30.

WASSARMAN, D. A. & STEITZ, J. A. 1993. A base-pairing interaction between U2 and U6 small nuclear RNAs occurs in > 150S complexes in HeLa cell extracts: implications for the spliceosome assembly pathway. *Proc Natl Acad Sci U S A,* 90**,** 7139-43.

WILLIAMS, S. G., SIM, S. & WOLIN, S. L. 2025. RNA sensing at the crossroads of autoimmunity and autoinflammation. *RNA*.

WILSON, R., URRACA, N., SKOBOWIAT, C., HOPE, K. A., MIRAVALLE, L., CHAMBERLIN, R., DONALDSON, M., SEAGROVES, T. N. & REITER, L. T. 2015. Assessment of the Tumorigenic Potential of Spontaneously Immortalized and hTERT-Immortalized Cultured Dental Pulp Stem Cells. *Stem Cells Transl Med,* 4**,** 905-12.

YU, J., JAMAL, M., GARCIA-GODOY, F. & HUANG, G. T. J. 2015. Dental Pulp Stem Cell Niche. *Tissue-Specific Stem Cell Niche*.

ZANET, D. L., SABERI, S., OLIVEIRA, L., SATTHA, B., GADAWSKI, I. & COTE, H. C. 2013. Blood and dried blood spot telomere length measurement by qPCR: assay considerations. *PLoS One,* 8**,** e57787.

ZHU, X., KUMAR, R., MANDAL, M., SHARMA, N., SHARMA, H. W., DHINGRA, U., SOKOLOSKI, J. A., HSIAO, R. & NARAYANAN, R. 1996. Cell cycle-dependent modulation of telomerase activity in tumor cells. *Proc Natl Acad Sci U S A,* 93**,** 6091-5.